Porous Nanocrystalline Silicon Membranes as Highly Permeable and Molecularly Thin Substrates for Cell Culture

by

Anant Akash Agrawal

Submitted in Partial Fulfillment of the

Requirements for the Degree

Master of Science

Supervised by

Professor James L. McGrath

Department of Biomedical Engineering

Arts, Sciences and Engineering

Edmund A. Hajim School of Engineering and Applied Sciences

University of Rochester

Rochester, New York

2009

CURRICULUM VITAE

The author was born in Raipur, India on January 18, 1984. He attended M. S. Ramaiah Institute of Technology, Bangalore, India under the Visveswaraiah Technological University from 2003 to 2007, and graduated with a Bachelor of Engineering (Biotechnology) degree in 2007. Anant began his graduate studies in Biomedical Engineering at the University of Rochester in Fall of 2007. He pursued his research in using recently discovered nanomembranes for cell culture under the direction of Professor James L. McGrath and received the Master of Science degree from the University of Rochester in 2009.

ACKNOWLEDGEMENTS

I thank my advisor Professor James McGrath for giving me the opportunity to work in a wonderful lab environment. His supportive, dedicated and compassionate guidance helped me grow my scientific insight during this research work and I wish to carry the lessons he has taught me through my life. I also thank my defense committee, Professors Philippe Fauchet and Harold Smith. I really appreciate the time and effort they have put in this process.

There are many people from the Nanomembrane Research Group that have helped me with their valuable inputs. I would like to start with thanking Karl Reisig, SiMPore Inc. co-op student and a friend, for helping significantly with the cell culture experiments. I thank Barrett Nehilla, a post-doctoral fellow in McGrath lab, for his immense support and guidance in lab as well as in preparing this thesis. I am grateful to Henry Chung and Jess Snyder for their contributions in diffusion experiments as well as their friendship and encouragement. I thank other past and present members of the McGrath lab, particularly Mort Ehrenberg, Tom Gaborski, Mike Hoffman, Rachel Twardowski, Derek Crowe for thoughtful discussions and general camaraderie. Importantly, I would like to thank Dave Fang, Chris Striemer and other employees of SiMPore Inc. for their role in nanomembrane fabrication and testing. I thank Loel Turpin at University of Rochester Medical Centre for providing human vascular cells used in this study. I appreciate all the help from the BME office staff, especially Donna Porcelli for her efforts in answering my queries.

Last but not the least; I thank my parents (Alka and Suresh) for their unconditional love, support and belief. I would like to thank my sister and brother-in-law (Avanti and Amit) for their affection and good wishes. I thank my circle of friends, from both here and back in India (Rajesh, Nakul, Shilpa, Dhiren, Ryan, Carlos, Dan, Manoj, Justin, Nate, Shikhir, Shail, Rahul, Vignesh, Chirag, Ritesh, Sunaina and more) for making me feel lucky. I particularly thank Vijaya, my best friend, for her undying encouragement and cooperation, not forgetting all the meals she cooked for me during this period.

ABSTRACT

Porous nanocrystalline silicon (pnc-Si) is a novel silicon based material with potential uses in lab-on-a-chip devices, drug delivery, cell culture, tissue engineering and biosensing. The pnc-Si material is an ultrathin (15 nm), free-standing, nanoporous membrane made with highly scalable semiconductor technology. Because pnc-Si membranes are approximately 1000 times thinner than any polymeric membrane, the permeability of pnc-Si to small solutes is orders-of-magnitude greater than conventional materials. As cell culture substrates, pnc-Si membranes could overcome the inadequacy of membrane materials used in conventional transwells and enable new types of culture devices for the precise control and manipulation of cellular microenvironments.

The objective of this thesis is to investigate the feasibility of pnc-Si as a cell culture substrate by comparing cell adhesion, spreading, growth kinetics and viability on pnc-Si to conventional tissue culture substrates. By each of these metrics, the behaviors of both immortalized cells (3T3-L1 fibroblast cell line) and primary vascular endothelial cells (HUVEC) were found to be highly similar on pnc-Si, tissue culture grade polystyrene and glass. Significantly, pnc-Si was found to degrade in cell culture media over several days without cytotoxic effects. Membrane stability could be tuned by modifying the density of a superficial native oxide layer through post production rapid thermal processing and additional surface treatment like amino-silanization. Pnc-Si was assembled in a custom designed tube to form a pnc-Si transwell device that could replace existing 24-well plate inserts. The adhesion of HUVEC to treated pnc-Si transwells was found to be comparable to commercial transwells. Collectively, the results establish pnc-Si as a viable new substrate for cell culture and a new type of degradable biomaterial. Pnc-Si membranes should find many uses in bioscience including the study of molecular transport through cell monolayers, as molecularly thin dividers for the study of cell-cell communication in co-cultures, and as biodegradable scaffolds for three-dimensional tissue constructs.

TABLE OF CONTENTS

TABLE OF CONTENTS (continued)

TABLE OF CONTENTS (continued)

TABLE OF CONTENTS (continued)

LIST OF FIGURES

LIST OF FIGURES (continued)

LIST OF FIGURES (continued)

LIST OF MOVIES (in Supplementary Compact Disk)

Movie 1: Phase-contrast movie of microparticle assay. Images (10X objective) of 15 μm polystyrene beads on top of pnc-Si membranes were acquired every 15 minutes for 30 hours at 25⁰C in serum-supplemented DMEM and then collected as a movie. The beads fell through the broken membrane and out of focus approximately halfway (~12-13 hours) through the movie.

Movie 2: Phase contrast movie of 3T3-L1 cells spreading on a glass cover slip. Spherical cells were present at the start of the movie. As cells attached to the glass surface, they extended cell processes and spread across the substrate. By the end of the 5-hour movie, cell morphologies were elongated and similar to mature fibroblasts. Non-adhered spherical cells can be seen moving across the field of view.

Movie 3: Phase contrast movie of 3T3-L1 cells spreading on two ~100 μm wide pnc-Si membrane windows. Similar to their behavior on glass, 3T3-L1 cells were spherical until they adhered to pnc-Si and began to spread across this substrate. After 5 hours, the 3T3-L1 cells had spread almost across the entire pnc-Si membrane windows.

Movie 4: Phase contrast movie of HUVEC spreading on a glass cover slip. The cells exhibited spherical morphology immediately after seeding. Over 5 hours, HUVEC attached to the glass surface and began to spread across the substrate.

Movie 5: Phase-contrast movie of HUVEC spreading on two ~100 μm wide pnc-Si membrane windows. Immediately after seeding, HUVEC exhibited a spherical morphology. The cells quickly spread across the pnc-Si membrane windows over 5 hours until nearly the entire window area was covered by HUVEC.

Chapter 1

Introduction

Porous nanocrystalline silicon (pnc-Si) is an ultrathin nanoporous membrane with tunable pores that has been developed for molecular separations. In this thesis, it has been shown that pnc-Si is a viable cell culture substrate with numerous advantages over currently available nanoporous membranes. Nanoporous membranes are used in cell biology research to setup *in vitro* models to produce an environment that resembles the *in vivo* system as closely as possible and for applications in drug delivery and tissue engineering. Pnc-Si is a novel degradable biomaterial that can find uses in numerous such biological applications.

This introductory chapter will provide an overview of nanoporous membrane technologies and membrane based cell culture applications. There are three primary topics focused in different sections of this chapter. The first is a review of what is known about nanoporous membranes and different nanoporous materials used to make membranes commercially. Porous silicon is described as a potential biomaterial in one of the sections. This literature is covered in Sections 1.2 and 1.3. The next focus is on a newly discovered porous nanocrystalline material which is introduced in Section 1.4. We will see that these ultrathin membranes have extraordinarily high permeability and could overcome shortcomings of commercial transwell membranes for setting up *in vitro* models of *in vivo* systems. The third focus of this chapter covered in Section 1.5 is to explore the use and limit of existing nanoporous membranes for membrane based cell culture. Finally, with an understanding of the current state of knowledge, the research objectives of the thesis work are presented in Section 1.6. Before beginning a detailed look into nanoporous membrane technology, a brief overview on nanotechnology and its importance in the modern world is covered in the following section.

1.1 Nanotechnology

Nanotechnology is a broad field that encompasses the creation and application of functional systems and materials through engineering of matter at molecular to atomic scales. Nanomaterials have at least one dimension of the order of about one to few hundred nanometers and often exhibit novel properties that enable new applications. For example, nanomaterials have a higher surface area to volume ratio than larger materials[*], which gives greater absorption, adsorption, reaction/catalysis, conduction, transport, etc [1]. Also, at the nanoscale, the mechanical, thermal, electrical and optical properties of materials change. For instance, opaque substances become transparent (Cu) [2], stable materials turn combustible (Al) [3], solids turn into colloids at room temperature (Au) and inert materials become reactive (Au) [4]. The carbon nanotube (CNT), a well-known nanomaterial, is essentially a rolled tube of an atomic sheet of carbon called graphene. Carbon nanotubes can have high electrical conductivity and mechanical strength as compared to bulk carbon [5-7]. In going from macro to micro dimensions, such effects do not prominently come into play. However, the effect becomes dominant when the nanometer size range is reached.

Because of the unique properties of nanomaterials, nanotechnology has the potential to create many new materials and devices using new approaches and possessing wide-ranging applications in medicine, electronics, and energy production [8]. As a sub-discipline of nanotechnology, nanobiotechnology is a rapidly advancing area of scientific opportunity that applies the tools and processes of micro to nanofabrication to build devices for studying biosystems, as well as to use biosystems for non-biological modeling purposes.

Many technologies descending from conventional solid-state silicon methods for fabricating microprocessors are now capable of creating features in the nanoscale regime, thus falling

---

[*] The volume of an object decreases as the third power of its linear dimensions, but the surface area only decreases as its second power. Hence surface area to volume ratio will increase as the first power of the linear dimension.

under the definition of nanotechnology [9]. Two main approaches are used in such nanofabrication: first, in the "bottom-up" approach, materials and devices are built from molecular components which assemble themselves chemically by principles of molecular recognition and, second, in the "top-down" approach, nano-objects are constructed from larger entities without atomic-level control. Combination of top-down (lithographic) and bottom-up (self assembly) techniques will be employed for efficient manufacturing of future nanostructures and systems.

Like any other new technology, nanotechnology raises concerns about the health and environmental impact of nanomaterials. Because of small size and increased chemical and biological activity, nanomaterials can more readily gain entry into the human body and may result in toxicity [10-12]. For example, slowly degradable or non degradable nanoparticles can accumulate in the body and affect the regulatory mechanisms of enzymes and other proteins by adsorbing them on to their large surface area. The waste generated by the manufacturing of nanodevices and nanomaterials can become airborne or get into water supplies [13]. As nanotechnology progresses, it may become a challenge to deal with 'nanopollution', and thus we need to call for proper regulation of nanotechnological applications.

The first generation of nanotechnology belonged to nanostructures and nanomaterials designed to perform at higher efficiency than conventional materials. This dissertation will focus on a silicon-based nanoporous material manufactured through a combination of top-down and bottom-up approaches.

1.2 Nanoporous Membrane Technology

1.2.1 Overview of Membrane Technology

As an important area of nanomaterial research, nanomembranes are thin films with pores ranging anywhere up to 100 nm in diameter. Nanoporous materials exist naturally, for example, the biological cell wall is nanoporous with many proteins embedded and floating around [14, 15], whereas, zeolites are naturally occurring minerals that are used as catalysts in the petroleum industry [16]. In addition to naturally occurring nanomembranes, synthetic nanomembranes are engineered using advanced semiconductor manufacturing technologies[17].

Different porous materials are utilized in the form of membranes that act as semi permeable barriers and are used to control transport from one side to other. There are materials which are not porous but are used to develop membranes through various techniques and directed design, as reviewed later in this section. Either way, membrane technology can be used for almost any kind of separation with relatively low energy consumption, reduced cost and less waste compared to other chemical industry processes [18, 19]. Membrane processes can be continuous with scale up/down being comparatively simpler as compared to other separation processes like distillation, extraction, fractionation, chromatography, etc.

The success of a membrane process will depend heavily on the properties and structure of the membrane. Membrane surface chemistry is important because interfacial interactions between the surface and the surrounding fluid and solutes will impact the transport characteristics, selectivity, biocompatibility and fouling propensity of the membrane. The structure of the membrane is also vital to its performance. The shape, density and size of the membrane pores along with the membrane thickness contribute significantly to its effectiveness.

Recent developments in the ability to observe, understand and manipulate matter at nanoscale level have transformed the process of nanomaterials discovery from being opportunistic to a

more directed design. This transformation is evident in the area of nanoporous membranes where pores can be designed to specific sizes and physical-chemical properties that match selection needs for advanced applications [17]. Before discussing advanced membrane technology, an overview of the conventional membrane materials and manufacturing techniques is presented in the following sections.

1.2.2 Polymeric Membranes

Polymers are used for manufacturing open porous membrane structures for microfiltration and ultrafiltration, as well as to create dense nonporous membranes for applications such as gas separation and pervaporation [20]. Polymer membranes are most commonly used as low cost disposable filters.

1.2.2.1 Materials

The polymeric material selected for a membrane process will depend on the flux, selectivity, fouling tendency, chemical and thermal properties that the process requires [18, 20]. Polymers such as polytetrafluoroethylene (PTFE), poly(vinylidene-fluoride) (PVDF), polystyrene (PS), polyethylene (PE) and polypropylene (PP) exhibit good thermal and chemical stability but need to be pre-wetted because of their hydrophobicity. Polycarbonate (PC) and polyester like polyethylene terephthalate (PET) have outstanding mechanical properties and are therefore used for making membranes through track-etching [21]. Hydrophilic polymers are useful because of their low adsorption tendencies which help in increasing flux and are easier to clean. Natural polymers like cellulose esters and ethers such as cellulose acetate, cellulose nitrate, ethyl cellulose and other mixed esters are crystalline and hydrophilic materials but are sensitive to thermal, chemical and biological degradation. Polyamide (PA), polyimide (PI), polyacrylonitrile (PAN) and poly (ether sulfone) (PES) are other popular membrane materials with high chemical and thermal stability [18, 20].

1.2.2.2 Methods

The type of technique used to make membranes depends on the polymer used and desired membrane structure. There are a number of conventional techniques to prepare polymer based porous membranes, such as, sintering, stretching, track-etching and phase inversion [18] [19]. Other advanced techniques involving exposure, deposition and molding are discussed later in this section.

Sintering: The process involves compressing a powder of particles of given size and sintering at elevated temperatures (Figure 1.1). Sintering causes the interfaces between the contacting particles to disappear and a pore is formed in between the fused particles. Different thermally and chemically resistant polymers such as polyethylene, polypropylene and PTFE can be used [18].
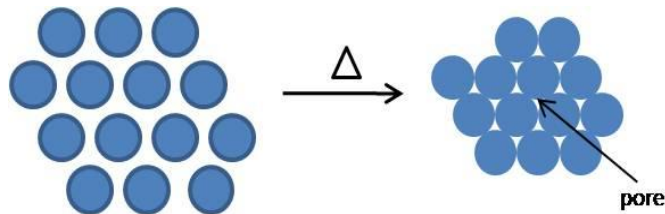
Figure 1.1 Schematic drawing illustrating the sintering process to make porous membranes: under suitable heating conditions particles fuse together to form pores between them.

Stretching: Semi-crystalline polymeric materials like polyethylene, polypropylene, polycaprolactone (PCL) and PTFE films or foils can be stretched so that small ruptures occur due to the mechanical stress and a porous structure is obtained [18].

Track-etching: Track-etched membranes are produced by exposing dense polycarbonate (PC) or polyester (PET) films to a high energy ion bombardment or gamma particle radiation. The bombardment causes small 'tracks' to be formed due to fractures made in the polymeric chains of the dense film (Figure 1.2). Chemical etching is done along the damaged track to digest the polymer strands and open parallel cylindrical pores [21]. Energy of the particles, radiation time

and etching time determine the thickness of the membrane, porosity and pore diameter respectively.
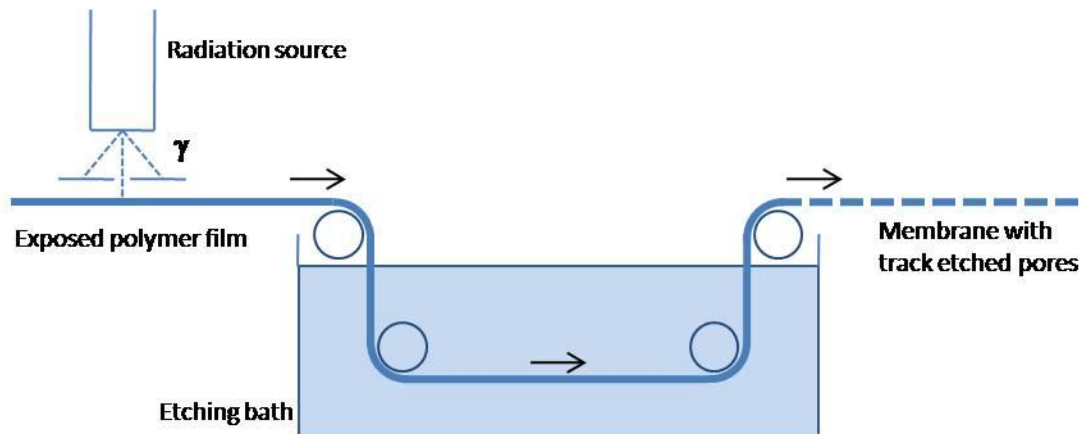
Figure 1.2 Schematic drawing of the preparation of porous membrane by track-etch method: ionic radiations form tracks in the polymer film which are further etched to form open pores.

Phase inversion: Phase inversion is a popular process in which a polymer is transformed in a controlled manner from a liquid to a solid state. Phase inversion converts one-phase polymer casting liquid solution into at least two separate phases: a solid polymer rich phase that forms the porous structure of the membrane and a polymer poor phase that gets removed from the membrane *via* precipitation and dissolution respectively [22]. Phase inversion membranes can be prepared from a wide variety of polymers but the widely used ones are polyethersulfone (PES), polystyrene, cellulose acetate and cellulose mixed esters.

Membrane morphology can be controlled by controlling the initial stage of phase transition. The change in the casting solution composition, temperature and pressure leads to the solidification of the polymer and pore formation [22]. Different phase separation processes are categorized depending on the cause of change in the casting solution composition: vapor induced (air casting), liquid induced (immersion or solvent casting), temperature induced (melt casting), pressure induced, reaction induced or colloidal induced [20]. The majority of phase inversion membranes are prepared by immersion precipitation or solvent casting [18]. In solvent casting,

a polymer solution (polymer in suitable solvent like DMSO or acetone) is cast on a suitable support and immersed in a coagulation bath containing a non solvent (water). Exchange occurs between the solvent and the non solvent leading to precipitation of the polymer (Figure 1.3). The membrane morphology results from combination of mass transfer and phase separation. High mutual affinity between the solvent and non-solvent and low polymer concentration helps to produce high porosity membranes [18].

The normal thickness (20-200 µm) of dense polymer membranes leads to low permeation rates. The membrane thicknesses cannot be reduced because this would compromise membrane strength. So, the phase inversion process is typically combined with solution coating, grafting or in-situ polymerization techniques to develop asymmetric and composite membranes which have a thin dense selective layer supported by a porous sub-layer of same or different material [23].
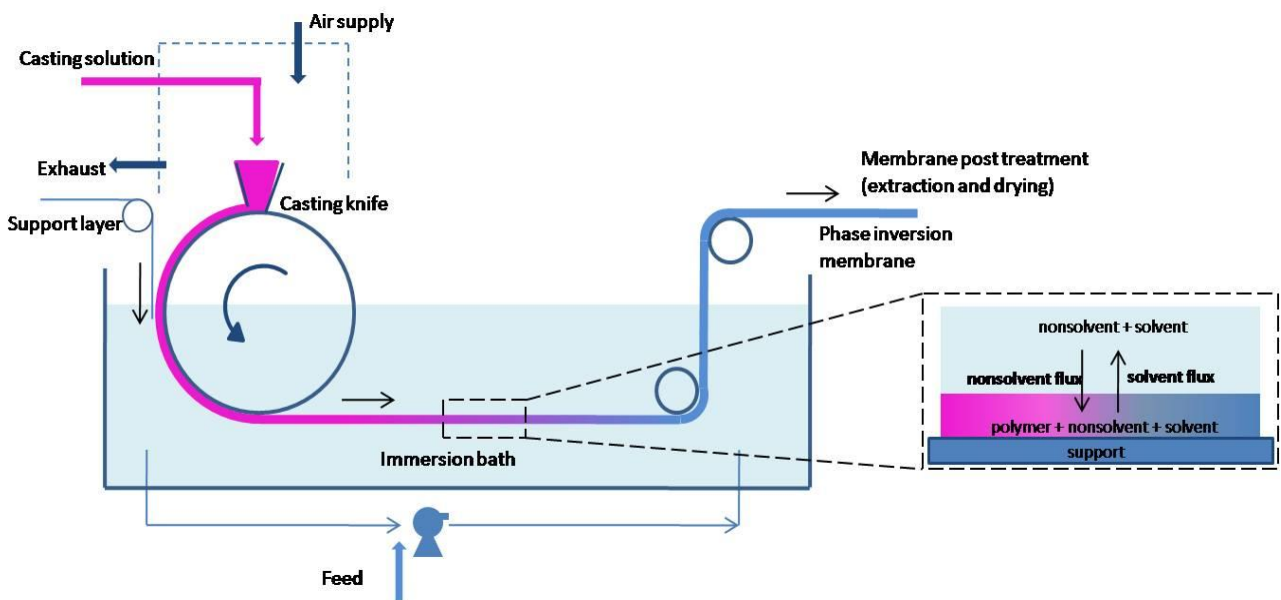
Figure 1.3 Schematic drawing depicting the preparation of phase inversion membranes: during solvent or immersion casting the dissolved polymer solution is spread onto a moving belt and run through a bath. Exchange between the solvent in the casting solution and the non-solvent in the bath takes place leading to pore formation.

1.2.2.3 Characteristics

Membranes developed by sintering methods have pore sizes of about 0.1 to 10 μm with wide pore size distributions and low porosity (10-20%). Through stretching processes, high porosities of up to 90% and wide pore size distribution with pore sizes ranging from 0.1 to 3 μm can be obtained. Both these methods produce membranes suitable for microfiltration since they cannot form pores smaller than 0.1 μm [18].

Phase inversion is the most common manufacturing process for polymer membranes. Most of the synthetic membranes produced by processes like phase inversion have a 10-100 μm thick inner sponge like structure that gives additional fluid resistance and reduced operational flux at a given trans-membrane pressure. Particles, proteins and other coagulates can be retained/adsorbed in the tortuous spongy structure with a high internal surface area (10-200 μm^2 per μm^2 of frontal surface) leading to sample loss, fouling or contamination [24]. Though they have high porosity (up to 70%), wide pore distributions with a high size cut-off prevents polymeric membrane from sharp size based separations.

Polymer membranes contain fixed pores in the range of 0.1 to 10 μm for microfiltration and 2 to 100 nm for ultrafiltration, nanofiltration, gas separation etc. Ultrafiltration membranes are prepared by phase inversion since other techniques lead to pores with minimum size of about 0.05-0.1 μm which is useful for microfiltration. Ultrafiltration membranes are asymmetric membranes with 0.1-1 μm thin selective layer and 50-100 μm thick support layer formed by coating on phase inversion membranes [23]. Asymmetric membranes offer high selectivity and flux through the thin top layer and mechanical strength to the thin film through the strong macroporous support with negligible transport resistance. Though efficient enough, microns thick opaque asymmetric polymeric membranes are not ideal for cell culture applications as discussed in Section 1.5.

Track-etched membranes are thick (20 µm) but highly controlled membranes traditionally used for high-precision size filtration in laboratory applications. Pore size distribution of track-etched membranes is comparatively narrower than dense spongy polymeric membranes with pore sizes ranging from 0.02 to 10 µm and the maximum porosity is up to 10% [20]. Porosity depends on the radiation intensity and if radiation is increased in order to increase the porosity, there are chances of overlapping pores being formed compromising the pore regularity. Although the track-etched membranes overcome the problem of sponge-like structure that leads to imprecise fractionations, they lack the possibility of achieving high porosity or precisely tunable pore sizes. Apart from relatively sophisticated fabrication, track-etched membranes have adsorption problems and because they are hydrophobic, they need to be pre-treated. Since PET is translucent and PC is opaque, these pose problems in applications requiring visualization (like membrane based cell culture applications, as discussed later in Section 1.5). However, track-etched membranes have extensively been used for cell culture based applications since they have controllable pore sizes and are comparatively thinner and efficient than the spongy, tortuous polymeric membranes made *via* phase inversion process.
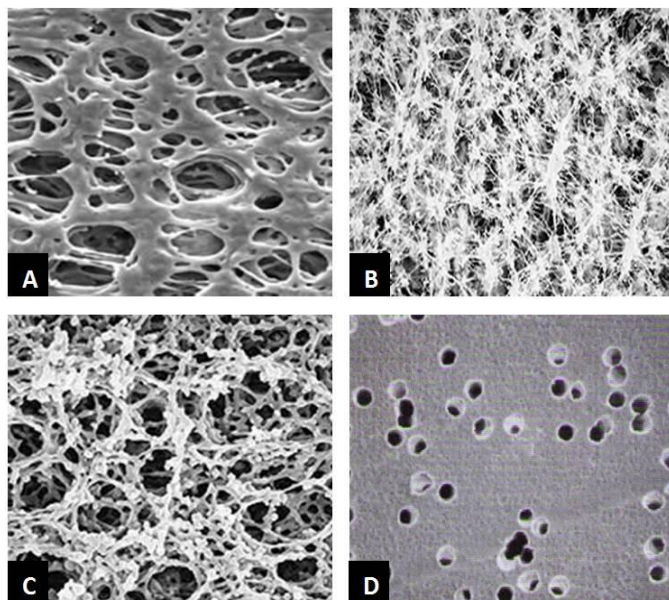
Figure 1.4 Different kinds of polymeric membranes: A) polyethersulfone (PES) membrane made from phase inversion (pore sizes: 0.03 to 20 µm), B) polytetrafluoroethylene (PTFE) membrane made by stretching (pore sizes: 0.2 to 100 µm), C) cellulose acetate membrane (pore sizes: 0.22 to 5.0 µm), D) polycarbonate (PC) membrane made by track etching (pore sizes: 0.01 to 30 µm). *(Courtesy: www.sterlitech.com)*

1.2.3 Inorganic Membranes

Inorganic membranes are not as popular as cheaper polymer membranes but possess higher durability and superior chemical and thermal properties. Due to their structural integrity, the pore sizes in these membranes can be better controlled than polymeric membranes, leading to relatively narrow pore size distribution [25]. Inorganic membranes are used in the field of microfiltration, ultrafiltration, gas separation and membrane reactors under harsh conditions [18, 19].

1.2.3.1 Materials

Important inorganic materials used for membrane manufacture include: ceramics (including glass), metals (including carbon/graphite) and zeolite minerals. Ceramics are a combination of metal (Al, Ti, Si, Zr) with a non metal in form of oxide, nitride or carbide), like alumina (Al_2O_3), titania (TiO_2), zirconia (ZrO_2), silica (SiO_2), silicon carbide (SiC), silicon nitride (Si_3N_4). Metallic membranes are made of stainless steel, palladium (Pd), tungsten (W), molybdenum (Mo) or silver (Ag) [25].

1.2.3.2 Methods

Some of the techniques used for polymeric membranes are also used in the production of inorganic membranes. The other membrane fabrication methods discussed below are template leaching, sol-gel process and anodic oxidation [18, 19].

Sintering: The method is similar as in case of polymers and powders of different thermally and chemically resistant materials such as metals (stainless steel, tungsten), ceramics (alumina, zirconia), graphite and glass can be used.

Template leaching: The process of selective leaching is mainly for manufacturing inorganic porous glass membranes. A homogeneous three component system (for example, Na_2O-B_2O_3-

SiO_2) separates into two phases, one phase consisting mainly of SiO_2 which is not soluble whereas the other phase is soluble. This second phase is leached out by an acid or base and wide range of pore diameters can be obtained as low as 5 nm [25]. Porous glass membranes have poor mechanical and chemical stability but can be obtained in wide range of pore diameters.

Sol-gel process: Ceramic membranes in the nanometer range can be prepared using sol-gel techniques [26, 27]. The sol-gel process involves two different routes: the colloidal suspension route and the polymeric gel route [18]. Both routes use precursors which may be hydrolyzed and polymerized. A colloidal dispersion of particles or an inorganic polymer in a liquid called 'sol' is formed. The precursor alkoxide yields a hydroxide on hydrolysis which undergoes polymerization to form a 'gel' [28]. This three dimensional sol-gel network structure needs to be sintered after which the final morphology of the membrane is stabilized. Densification of the membrane can be achieved through internal deposition of pores by a monolayer or multilayer, by pore plugging using nanoparticles, by coating a layer of inorganic polymeric gel on top of the membrane or by depositing constrictions in the pore sites [18]. New routes for sol-gel processes to form non-shrinking composite materials have also been pursued [29].

Anodic oxidation: Alumina membranes are formed as result of a self structuring process that induces aligned and mono-dispersed pores during the anodization of aluminum [30]. The lattice expansion due to anodic oxidation of Al, the potential distribution and heat formation during anodization leads to formation of long pores with uniform pore sizes [31]. Nanoporous aluminum oxide membranes have been used as a template in the fabrication of nanostructures [32]. Recently, high porosity nanoporous aluminum oxide membranes have been fabricated with mean pore sizes of ~0.2 μm and thickness of 1-10 μm [33].

1.2.3.3 Characteristics

Inorganic membranes have several advantages over polymer membranes. One of the important advantages is its superior chemical and thermal stability. This can be useful in separation processes at high temperatures and, chemically and physically harsh conditions like in membrane reactors and gas separations [34, 35].

Ceramic membranes do not absorb water and do not swell which could have led to change in pore sizes, retention and thereby the selectivity [36]. These materials are also wear resistant making them reusable and less vulnerable to corrosion and abrasion. Because flat disc shaped ceramic membranes are brittle, the preferred shape for ceramic membranes is a rod. Ceramics can also provide high flux rates compared to polymer membranes due to a thickness smaller than the pore size [37]. Although they are relatively expensive, they undergo less fouling, because of their smooth surface and short pore channels. They can be operated at very low trans-membrane pressures during cross flow filtration [37].

Ceramic membranes generally have asymmetrical membrane structure with pore size between 1-5 µm [31]. This size can be further regulated by depositing layers, for example, a typical alpha-alumina membrane has a pore size of 110-180 nm and for finer membrane a gamma-alumina layer can be applied on top of the alpha-alumina layer to give a final pore size of 3-7 nm. For even finer pore sizes, an ultrathin silica layer can be applied [38]. However, these additional layers tend to lower flux as multilayer inorganic membranes with micrometer thick top layer having pore sizes as low as 1 nm have total membrane thickness in 100's of microns [24, 31].

Zeolites are natural porous minerals which act as molecular sieves and comprise highly crystalline alumino silicate frameworks. They have a defined pore structure with typical channel sizes roughly between 0.3 to 1 nm. Zeolites are made synthetically by a crystallization process

using a template that by self assembly together with the Si, Al and O atoms forms the structure [24]. The template is removed by heating, leaving behind small channels in the zeolite structure. They can be used as chemical reaction catalysts along with oxidation and reduction reactions. Zeolites are useful in fuel synthesis, gas separation and pervaporation [39]. Metallic membranes such as thin metal plates of palladium, silver and their alloys are dense membranes which are used for hydrogen, oxygen, ammonia and carbon dioxide gas separations [40].
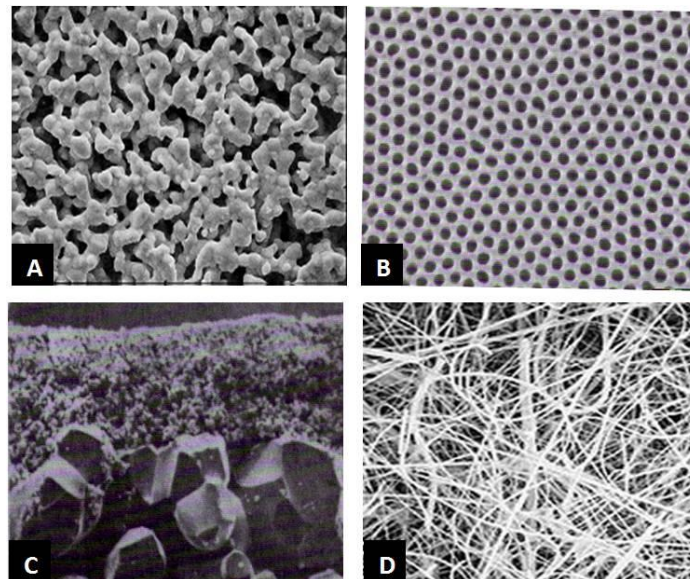
Figure 1.5 Types of inorganic membranes: A) Silver membrane filters (pore size: 0.2 to 5.0 μm), B) Anodized alumina membrane (pore size: 50 nm), C) Ceramic sintered membrane, D) Glass fiber membrane (pore sixe: 1 μm). *(Courtesy: C.J.M. van Rijn [24] and Sterlitech Corp. Reprint permission granted by Elsevier.)*

In addition to polymeric and ceramic membranes, nanocomposite membranes have received attention recently. Nanocomposite membranes combine two or more phases containing different compositions or structures with at least one in the nanoscale regime. Such a combination helps achieve high molecular sieving selectivities while maintaining easy polymer processing conditions. For example, polyimide-silica hybrid membranes, polymer-zeolite nanocomposite membranes, silica nanoparticle embedded carbon based membranes, polymer or silicon nitride encapsulated carbon nanotube membranes [39, 41-43] . Nanocomposite membranes are useful

for air and gas filtrations. They are also used in processes such as biomolecular purification, sensing, environmental remediation, desalination and petrochemical production [44].

1.2.4 Advanced Membrane Technology: Microsieves and Nanosieves

Most of the previously discussed membranes have dense spongy-like tortuous and long pore channel structure which leads to poor selectivity and inefficient transfer of materials from one side to other. High internal surface area also leads to sample loss and increased fouling as particles, proteins and coagulates are retained in the dead-end pores, grooves and cavities. Until recently, the best sieve structures are track-etched and anodized alumina membranes [20]. However, track-etched can only be made with polymeric material (which is not chemically resistant) and lack the possibility of achieving high porosity or tunable pore sizes, while the alumina membrane is relatively brittle, available in limited pore sizes and has low flux performance. These conventional membranes give a trade-off which leads to increase in product flux causing loss in perm selectivity and vice versa [45]. With the advent of the semiconductor technology and its integration with membrane technology, investigators have developed new approaches for making more ideal membrane structures [9, 17, 20].

Nano and micro engineered membrane technology typically requires top-down approaches such as patterning, deposition, and etching to fabricate membrane structures [24]. An additional possibility for discrete nanoscale structure formations however, is bottom-up self assembly where molecular recognition helps in assembling the building components (atoms or molecules or colloidal particles) to form larger and complex structures analogous to biological systems. Combinations of top-down (lithographic) and bottom-up (self assembly) techniques might be employed for efficient manufacturing of future membrane structures and systems [9]. Bottom-up approaches involve formation of self-assembled-monolayers (SAMs) supported by suitable substrates. For example, oriented zeolite or silicalite monolayers supported by a silicon nitride

membrane gives a free standing zeolite membrane that with pores between 0.3 to 1 nm, and can be used for molecular separations [24]. An example that involves a combination of bottom-up and top-down approaches is the fabrication of pnc-Si, a novel material that is the focus of this thesis.

1.2.4.1 Micro and Nanoengineered Membranes

Nano and microengineering techniques like thin layer deposition, photolithography and high resolution etching methods originating from semiconductor technology have been used to fabricate membranes [46]. These engineered membranes ranging from silicon-based to polymeric and the techniques used to fabricate them are briefly reviewed below.
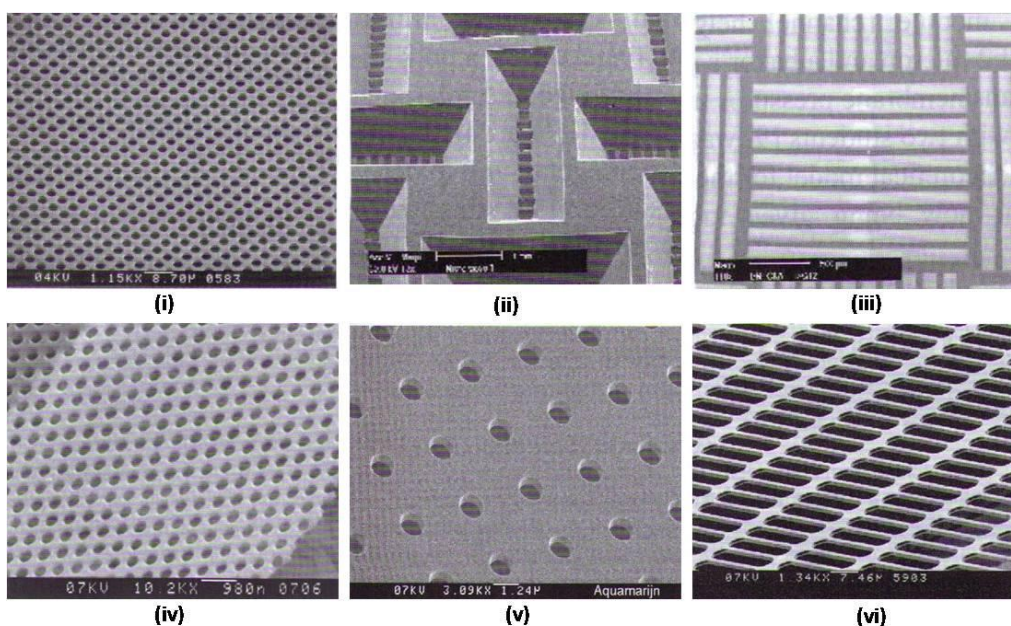
Figure 1.6 SEM (scanning electron microscopy) images of various membranes made by microelectronic fabrication techniques: overview of microsieves and their different pore patterns. *(Courtesy: C. J. M. van Rijn [24]. Reprint permission granted by Elsevier.)*

Precision shaped membrane perforations can be made with two dominant top-down techniques that include photolithography and scanning/particle beam lithography. Photolithography uses light-based tools such as photoresist masks and etchants to make precise patterns on

substrates. A photoresist is an organic material that, upon exposure to high energy short wavelength light (like, UV light), either cross-links to become insoluble or transforms chemically to become more soluble in a basic solution [47]. A mask is used for patterned exposure of the photoresist to the light. The photoresist is immersed in solvents that dissolve the exposed (positive photoresist) or unexposed (negative photoresist) regions of the photoresist. The patterned photoresist masks the underlying substrate during a subsequent step of chemically etching the exposed regions of the substrate to form the membrane pattern. The etching could be either done in liquid phase (wet) or plasma phase (dry). Etching methods like wet etching (with $FeCl_3$, HF, HNO_3, KOH or EDP), reactive ion etching (with Argon) or plasma etching (with CCl_4, CHF_3 or SF_6/O_2) are used. Electro forming is another technique involving the deposition of metal on a lithographic patterned conducting substrate, followed by separation of electroformed product from the substrate. Membranes produced by these methods have a thickness of at least 10-15 µm with pore sizes ranging from 5-15 µm. These membranes can be made from a wide array of microfabrication materials including Al, Cr, Cu, Ni, Au, Ag, Si, S_3N_4, SiO_2, Ti, Pt [24].

Photolithographic techniques have limitations such as minimum feature sizes that are overcome by sub-micron semiconductor lithography [24]. The lower limit of pore sizes that can be achieved using conventional photolithographic methods is 2-5 µm in a foil or sheet of thickness larger than 5 µm. A sub-wavelength environment such as in X-ray lithography can be used to pattern pore sizes of 0.25 µm to less than 0.1 µm, but requires very precise masks, optical sources and is thus quite expensive. Sub-micron semiconductor lithography like laser interference lithography can be used for even smaller feature sizes [9].

Laser interference lithography can produce simple patterns for micro and nanosieves without using a photo-mask or expensive projection optics [24]. Laser based interferometric lithography involves the constructive and destructive interference of multiple laser beams that pattern fringes at the surface of a photoresist [48-50]. Photoresist leads to the patterned exposure of the

17

underlying substrate (for example, silicon nitride) and the pattern is transferred by reactive ion etching (CHF_3/O_2) through plasma. With laser interference lithography it is possible to create nanosieves with pore size and thickness as low as 100 nm.

Scanning beam lithography is a mask-less serial technique classified as: (i) scanned laser beams, (ii) focused electron beams, and (iii) focused ion beams (FIB) [9]. In scanned laser drilling, a laser beam is used to form apertures (of sizes as low as 100 nm) with consistent accuracy. Electron beam lithography involves scanning a beam of electrons across a surface covered with a photoresist film, creating features in the sub-100 nm range. Electron beam lithography is mainly used for fabricating high resolution masks for photolithography or embossing masters for soft lithography [51]. Both laser and electron beam lithography are at least an order of magnitude slower than optical lithography and have high manufacturing costs.

Focused ion beam (FIB) lithography has higher resolution (sub-50 nm feature size), whereas throughput, cost and complexity is on par with electron beam lithography. A focused ion beam is used to pattern a photoresist or directly the substrate by selectively removing material through ion bombardment [52]. FIB lithography can also create patterns by localized ion deposition or chemical vapor deposition leading to *in situ* doping [53]. The ion bombardment in this technique can damage the sample and thus cannot be used with a broad range of materials. Tong *et al* fabricated a nanosieve (with pore sizes ~10 nm) by direct FIB drilling and coating on an ultrathin Si_3N_4 membrane (Figure 1.7) [54].Recently, another group manufactured sub-10 nm pores on 45 nm thick Si_3N_4 membrane after ion beam induced deposition (IBID) of Pt and SiO_2 [55]. Such ultrathin nanostructured membranes, where the membrane is roughly as thick (10-45 nm) as the molecules being separated are close to being ideal, but membrane fragility and complex fabrication have prevented their use for molecular separations. Hence, the FIB nanomachining technique is primarily used in research.
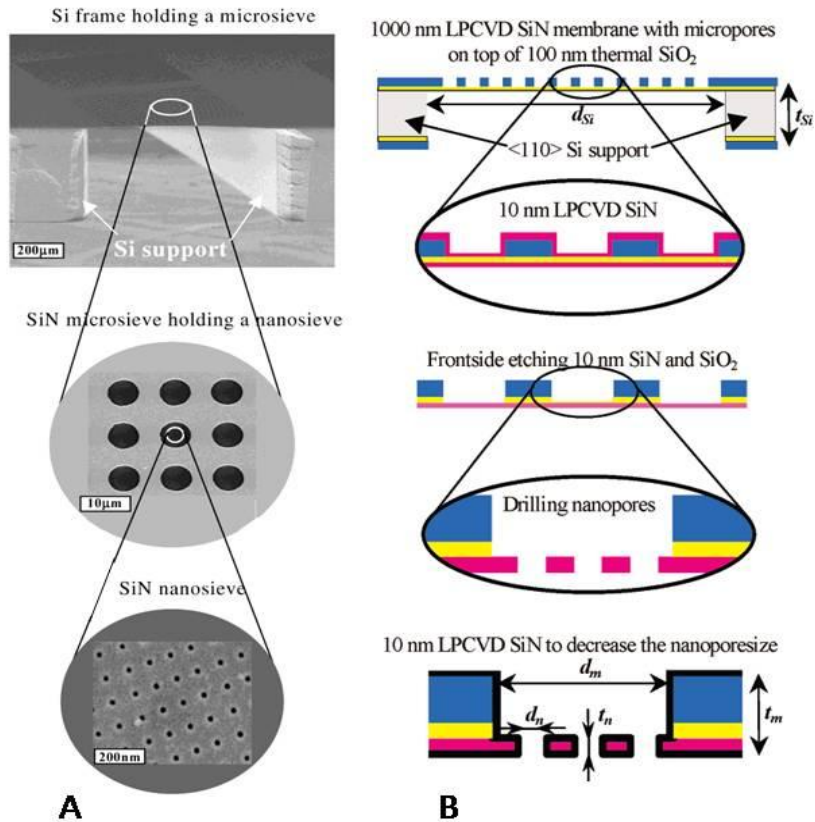
Figure 1.7 A) SEM overview with close-ups of the nanosieve membrane: A strong, thick silicon frame supports a thin SiN microsieve which supports a nanosieve, B) Simplified process flow of the nanosieve membrane: A silicon frame is etched to support a 1000 nm thin SiN microsieve which consists of an array of 5 μm circular perforations etched to support a 10 nm thin SiN nanomembrane. This nanomembrane is etched with FIB with an array of nanopores forming the nanosieve *(Courtesy: Tong et al [54]. Reprint permission requested from American Chemical Society.)*

The slow rate of patterning through laser, ion and electron beam tools restricts scanning beam lithography techniques to small areas or low densities of features. Hence, scanning beam lithography is most often used to produce high-resolution photomasks for projection lithography rather than for actual device fabrication. The high maintenance and operating costs also limits the utilization to research applications only.

Inorganic microsieves (for example, silicon based microsieves) are durable with outstanding chemical inertness, thermal resistance, hydrophilicity and low particle adsorption. Unfortunately, these high quality microsieves have elaborate fabrication techniques leading to high manufacturing costs and thus cannot be disposed of easily [54]. Though silicon nitride membranes have important advantages, polymeric microsieves can be suitable for large scale applications in medical and biological markets. By combining semiconductor technology precision to low cost polymer substrates, polymeric microsieves can be manufactured [20].

Polymeric microsieves are fabricated using conventional deposition and exposure techniques or unconventional approaches such as molding, embossing and printing [9, 20]. The unconventional methods are also referred as soft lithography [56]. Exposure techniques using UV radiation are used to make patterned membranes after spin coating of photosensitive polymer like polyimide on a suitable substrate. The exposed area polymerizes and the unexposed polymer is dissolved in solvents such as cyclopentanone. The membrane obtained is generally 1-2 µm thick with pore size as low as 4 µm [24]. Deposition techniques on patterned substrate structures also form microsieves. Polymeric material is deposited on the substrate and is removed after curing.

Unconventional methods like molding (using silicon molds) and hot embossing/imprinting (using nickel stamps or molds) are used for thermoplastic polymers like polyethylene, polycarbonate and polyester to manufacture polymeric microsieves [20, 57, 58]. The thermoplastic polymer is placed between a flat disc and the desired pattern is transferred onto the polymer using a mold that is pressurized against the flat disc. During molding or hot embossing, a thermoplastic polymer is heated above the glass transition temperature so that it can be shaped mechanically without damaging the mold [24]. But, it is difficult to obtain a fully micro perforated product because mechanical fragility of the membrane leads to distortion and anchoring of material during release from the molds [24].

Phase separation micromolding (PSµM) or soft embossing combines the microsieve molding process with the vapor and liquid induced phase separation process of polymers [20, 59]. After casting the polymer solution onto the mold, phase separation is initiated through exchange between the solvent and the non solvent. As the polymer micro/nano sized structure solidifies, the material shrinks and thus is easy to be removed from the mold. Phase separated polymeric microsieves can be made in a broad range of pore sizes and from many different polymers like polysulfones, polyimide, polypropylene, polyamide, teflon, polyurethane, etc. Flat sheet, tubular polymeric structures as well as hollow fiber and capillary polymeric structures can be made using this process [60]. Polymer microsieves are better than conventional polymer membranes for applications like molecular filtration and renal dialysis as they have comparatively low flow resistances and higher pore uniformities. But, polymer microsieves cannot replace costly silicon microsieves in certain applications where durability, hydrophilicity, chemical inertness, thermal resistance and low adsorption are essential.

Comparisons between different membrane structures [18, 19, 24]*:*

Microsieve/nanosieve filters consist of thin membrane with well defined uniform pores, and a macroporous support structure. On the other hand, inorganic membranes particularly ceramic membranes have advantages over polymeric (organic) membranes like high thermal and wear resistance, chemical inertness, easy sterilization and recyclable. But inorganic membranes are expensive and at the same time have relatively poor control on pore size distributions. Also the active membrane layer is very thick in comparison to the mean pore size which results in reduced flow rates. Whereas, microsieves having a relatively thin filtration or sieving layer with a high pore density and a narrow pore distribution will show better separation behavior at high flow rates. The pore depth in microsieves is as small as the pore size which leads to low flow resistance. Nanoporous membranes with nanometer thicknesses will be of use in gas separation processes in which the flux should be very high with minimal permeation resistance.

This should enable gas molecules to ballistically pass the membrane without colliding with the walls inside the membrane layer [17].
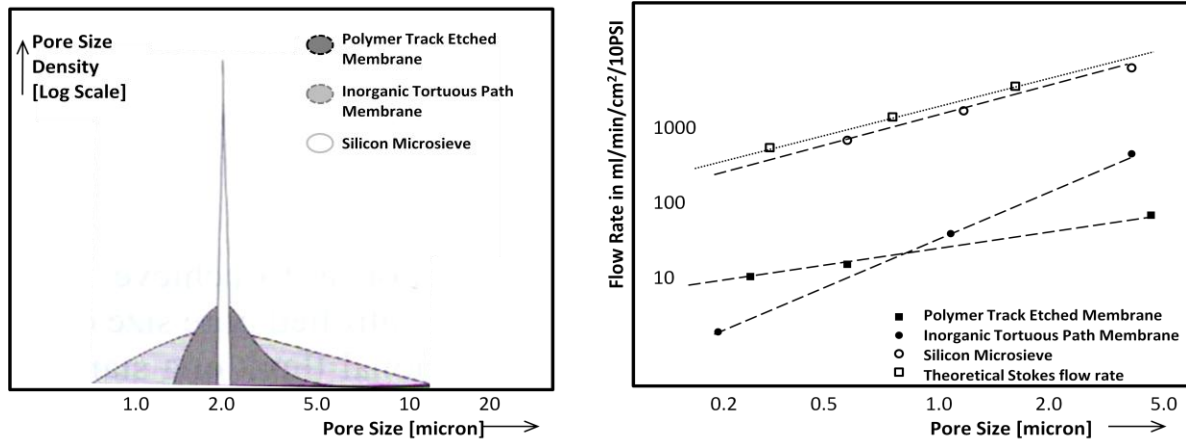
Figure 1.8 Left: Pore size distributions of different types of porous membranes, Right: water flow rates through these membrane filters. *(Courtesy: C.J.M. van Rijn [24]. Reprint permission granted by Elsevier.)*

The water flux through such microsieves is at least 30 times higher than organic membranes such as track-etched PC and stretched PTFE membranes, and 100 times higher than inorganic anodic membranes.

1.2.4.2 Carbon Nanotube Membranes

Carbon nanotube (CNT) membranes have significantly contributed to membrane science with their potential for highly efficient and precise separations. The uniform and smooth pores present in CNT membranes allow researchers to conduct studies of nanometer scale mass transport [42, 43].

Carbon nanotubes are hollow cylindrical constructs made out of graphene sheets and have inner diameters smaller than 100 nm [61]. A CNT can have one or more concentric shells based on which they are referred as single-walled (SWCNT), double-walled CNT (DWCNT) or multi-walled CNT (MWCNT). Because of their small dimensions, CNTs have extremely high aspect

ratio (~1000 or larger) [62]. These nanotubes have smooth and straight channel morphology due to the atomic planarity and high rigidity of graphene. The CNT walls are hydrophobic and chemically inert which makes the CNT useful in a wide variety of applications especially those involving high-flux mass transport [63]. High quality CNTs are produced by catalytic chemical vapor deposition (CVD) in presence of ethylene at 850°C [64, 65]. Filtration membranes and microsieves can be used for nanomaterial synthesis and transformed into nanotubular structures by deposition of appropriate materials in their pores or channels [32]. Such a structure has been produced in past by Martin *et al*, where they fabricated amorphous CNTs within porous alumina membrane templates through chemical vapor deposition [66]. A dense parallel array of CNTs encapsulated in a sheet of support material results in a CNT membrane.

The most successful approach to make CNT membranes are by growing aligned array of CNTs on a substrate, followed by penetration of impermeable filler material in between the CNTs to form the membrane support structure. The substrate can be removed to open the ends of the CNTs on either side of the membrane and form smooth straight functional pores perpendicular to the membrane surface. The filler material can either be a polymer or dense silicon nitride (Si_3N_4). Polymer encapsulation of CNT arrays was pioneered by Hinds *et al* [42]. Polystyrene is generally used for infiltration and then cured to produce high density MWCNT membrane with pore sizes ~7 nm. The problem in using such elaborate procedures in liquid phase is the possibility of CNTs aggregating together during solvent evaporation. Holt *et al* developed a process for the encapsulation of CNTs in low-stress silicon nitride (Si_3N_4) by CVD (Figure 1.9) [43]. Silicon nitride forms a uniform coating around the CNTs without any nano or microvoids. Etching is done to remove excess silicon nitride, remove silicon substrate and to open the CNTs from both ends, producing a robust membrane that can withstand differential pressure in excess of 1 atm. Pores sizes of 1-2 nm (DWNT) and ~6.5 nm (MWNT) were demonstrated by this

group. The thicknesses of such CNT membranes is close to the length of the CNTs i.e. 5-10 µm [43].
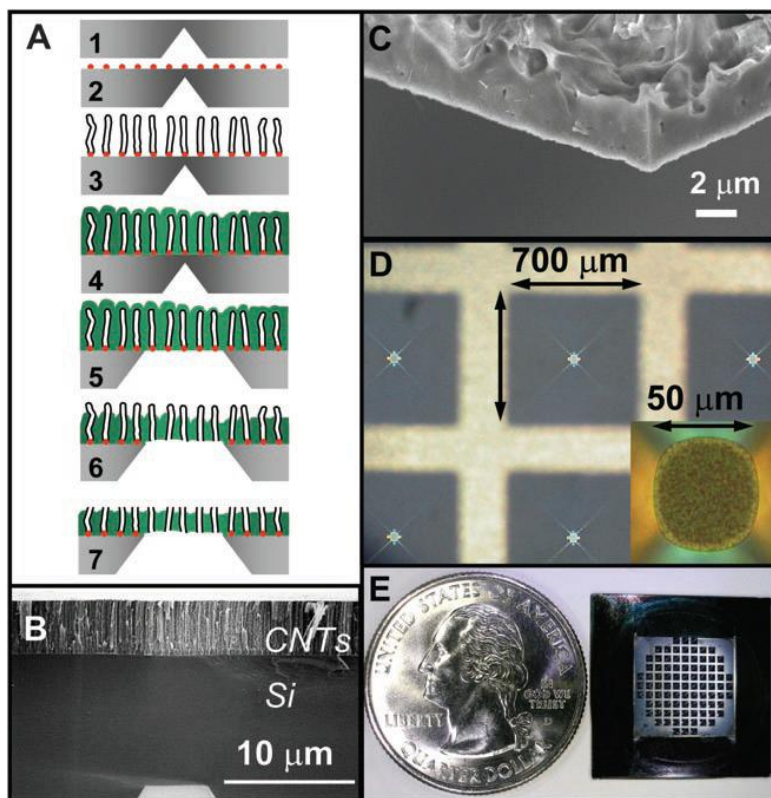
Figure 1.9 A) DWNT membrane fabrication process, B) SEM cross section of DWNTs, C) SEM cross section of the membrane: silicon nitride matrix around CNTs, D) photograph of open membrane areas; the inset is a close up of one membrane, E) photograph of a membrane chip with 89 windows. *(Courtesy: Holt et al [67]. Reprint permission requested from AAAS.)*

An alternative approach to produce CNT membranes with polymer filler material has been described by Marand *et al* [68]. Instead of growing aligned CNTs on a substrate, the alignment of dispersed SWCNTs can be assisted through filtration across membrane with pores bigger than the CNT diameter. CNT suspension in tetrahydrofuran is filtered through PTFE membrane (0.2 µm pores) which helps assembling the CNTs in an array. A thin film of polymer solution (polysulfone or polydimethylsiloxane (PDMS)) is spin coated on the CNT array to form a membrane with CNT ends opening on either side (pore size ~1.2 nm) [68]. This filtration

assisted assembly is more scalable than a CVD process but the nanotube pore density produced is much smaller.

CNT membranes with filler material have low porosities (less than 3%). Yu *et al* have devised a new method to fabricate CNT membranes by getting rid of filler material and just packing the nanotubes together, leading to increased porosity (as high as 80%) and flow rates [69]. The high density array of SWCNTs is created by collapsing together CNTs through solvent evaporation. The spaces between the CNTs are very similar to the pores sizes and all measure ~3 nm. The thickness is 750 μm and the CNT membrane is further supported on a bigger microporous filter. This process is uncontrolled and the membrane quality and pore sizes are quite variable.

CNT composite membranes have narrow pore size distributions with ultra narrow molecular pipe-like pores. The smooth and straight pore walls offer extremely efficient gas and water transport [42, 67-70]. Control of transport involves size exclusion and chemical modifications of the membrane. Though size exclusion transport is possible through CNT membranes, enhancing selectivity by chemically modifying CNTs is a big challenge. There has been progress in this area with the use of carbodiimide chemistry at the opening of the CNTs to attach range of biological molecules. The combination of transport efficiency and selectivity could be used to study nanofluidics and theoretically for large scale applications such as water purification and gas separation [71, 72]. However, CNT membranes face a fabrication challenge involving elaborate procedures and advanced microfabrication facilities not conducive for mass production.

1.2.5 Membrane Processes and Applications

Membranes are primarily used for separations for concentration, purification and fractionation where a certain size of molecule is allowed to pass through the membrane whereas anything

above that size is retained [18]. However, membrane technology is expanding and finding its use in other fields like microfluidics, cell biology, optics, electronics and energy conversion [18, 19, 24, 73, 74]. In this section we review various membrane separation processes and applications.

1.2.5.1 *Separation Processes*

a) Size Exclusion Filtration

Size exclusion filtration involves separation of different species of particles, macromolecules, proteins, extracts, cells and other fragments based on their size (hydrodynamic radius). Feed containing molecules is filtered through the porous membrane across a pressure gradient. Large molecules are retained from flowing through the pores because of steric hindrance, but the solution itself can flow across. Depending on the cut off capability and specificity of the separation, size exclusion filtration/membrane chromatography can be classified as microfiltration, ultrafiltration or nanofiltration [18, 19].

Microfiltration: Microfiltration processes involve pressure driven transport across 10-150 μm thick membranes with pores ranging from 100 nm to 10 μm in diameter [75]. It is useful for retention of larger particles like bacteria, protozoa and colloids. Open symmetric membrane structure with high porosity and low resistance requires small driving forces (< 2 bar pressure difference) to obtain high fluxes in microfiltration. Materials ranging from polymers to ceramics are utilized to make microfiltration membranes. Microfiltration is typically used in beverage clarification, sterile filtration, water treatment, pharmaceutical and dye industry [76, 77].

Ultrafiltration: Ultrafiltration processes employ membranes with pores ranging from 10 to 100 nm and pressure gradients as the driving force [19]. Macromolecules with molecular weights between 10 - 1000 kD can be retained. The ultrafiltration membranes are denser with increased hydrodynamic resistance and therefore require greater pressure (1-10 bar) than microfilters [75].

Ultrafiltration membranes are typically asymmetric membranes with a 1 μm thick, dense, top layer made of polymers (PES, cellulose esters, polyimides, polyamides). Although inorganic materials like alumina or zirconia are also used. Ultrafiltration is typically used in water treatment and food, textile and pharmaceutical industries [73, 76].

Nanofiltration: Membranes with pore sizes ranging from 1 to 10 nm are used for nanofiltration processes. Through nanofiltration, retention of low molecular weight organics ranging from 0.2 - 20 kD is allowed resulting in separation from a mixture and thereby extending the range of membrane filtration [76, 78]. Nanofiltration employs asymmetric (dense top layer is of the same material as the bulk support layer) as well as composite (top layer is of different material than the support layer) membranes. Due to increased membrane resistance, higher pressure difference of 10-30 bar is applied during nanofiltration. In nanofiltration, intrinsic membrane properties are very important: the membrane material should have high affinity for solvent and low affinity for the solute. Materials such as cellulose esters and polyamides are commonly used to manufacture nanofiltration membranes. Typical applications of nanofiltration include water treatment, desalination, product concentration, separation of salts from dye solutions or acids from sugar solutions.

b) Solution Diffusion Separations

Solution diffusion separations involve a two step process. First, the molecule has to dissolve into the membrane by finding a pore on the surface of the membrane. Second, the molecule diffuses across the pore channel under a driving force to the other side. The separation takes place due to differences in the solubility of the components into the membrane material and the diffusion velocities across the membrane. Hence, the properties associated are the intrinsic material properties of the membrane as much as the geometric properties of their pores. Modifying the functionality of the material helps develop the specificity of the membrane

material. For example, polycarbonate track etched membranes containing 10 nm pores can be lined with gold and thiols to increase affinity for gold [79]. There are four important solution diffusion separation processes, namely, reverse osmosis, gas separation, dialysis and pervaporation [80].

In solution diffusion separations, asymmetric, composite as well as non porous membranes are used. Polymeric membranes made of polyimides, polysulfones, PDMS are applicable in hydrogen and helium recovery, CO_2/CH_4 separation, O_2/N_2 separation [18]. Dialysis uses a concentration gradient as the driving force and hydrophilic polymers like cellulose esters as membrane materials. Molecular sieves with sub-nanometer pores between 0.3 to 1 nm are used for precise separations between molecules based on their molecular structure (for example, isomeric separations) [24]. Zeolites are common molecular sieves helpful in fuel synthesis and gas separations [39].

c) Separation by Charge

Membrane materials can carry intrinsic charge that influences their permeability for charged substances. The membrane fixed charge creates an equilibrium potential difference with respect to the surrounding solution. The strength of the electrostatic interaction between the analyte and the sieving structure dictates the molecular transport behavior. The charge-selective nanopores restrict the co-ions (with the same polarity as the surface charges) and allow the counter-ions (with the opposite polarity as the surface charges). Such perm-selectivity can be an essential function for desalination and fuel cells [17]. The potential across the membrane can also be used for electro-modulating transport of ions or charged molecules [81, 82]. This also presents a well-suited mechanism for the separation of similarly sized biomolecules based on their charge density (pI values or isoelectric point). Depending on the pI value of the protein and the pH condition of the solution, partitioning across the perm-selective nanofilter would be charge

dependent [83, 84].Semi permeable membranes that allow selective passage of cations or anions are called as ion exchange or ion selective membranes and can be used to study electrokinetic phenomena such as electro dialysis and electro osmosis [19, 85].

1.2.5.2 *Other Applications*

Apart from numerous filtration and separation applications, porous membranes can be put into plethora of other industrial and research applications. Membrane based reactors and bioreactors are made possible for higher productivity and bioconversion to form antibiotics, vitamins, amino acids, alcohols etc. Membranes can be employed in template based synthesis of nanomaterials and act as nanostencils for building photonic crystals and nanostructures like nanotubes [32, 66, 86]. Membranes can be integrated into microfluidic lab-on-chip systems as separating components of an in-line miniature perfusion bioreactor [87] or used as a nanoporous platform for biosensing, drug screening and delivery [88, 89]. Membrane based cell culture [90] is prevalent in cell biology research to develop *in vitro* tissue models for drug testing [91] and for cell-to-cell signaling experiments [92, 93] . Membranes can be used as a scaffold to study particles, proteins, microorganisms, cells etc. Allowing molecules like DNA to pass through a membrane pore can help in determining their sequence under specific conditions [94] [95]. Membranes can also be employed in tissue engineering as biodegradable scaffolds or medical implants for structural or drug delivery purposes [96]. In the near future, nanoporous membranes can also be used as a substrate to cultivate biomembranes, as discussed below.

Nanoengineered biomembranes: The engineering of biomembranes involves the creation of artificial membranes at nanometer scale that mimic natural membranes [97, 98]. Natural biomembranes such as the cell's plasma membrane have important function in biological molecular exchange and signal transduction processes taking place by trans-membrane channels and pores. The plasma membrane has a nanoporous crystalline surface layer (S-

layer) composed of proteins/glycoproteins and repetitive physiochemical properties close in range of nanofiltration membranes [14, 15]. Hence, S-layer proteins can be self assembled or S-layer carrying cell wall fragments can be deposited on synthetic porous membranes and modified through immobilization or functionalization to manipulate the pore permeation properties. Such membranes can be used to immobilize biological macromolecules like enzymes, ligands, antibodies which in turn can be applied in affinity filtration of hybridoma cell culture supernatants [99, 100] and in immunoassays [101].

1.3 Porous Silicon: A Biomaterial

The previous section discussed a wide array of nanoporous materials that can be used in filtration, sensing, catalytic and biological applications. One important material that is yet to be mentioned is porous silicon. Porous silicon is known for its biocompatibility and non-toxic, controllable dissolution in biological fluids. This thesis focuses on a novel silicon based nanoporous and biodegradable material (pnc-Si) with characteristics similar to those of porous silicon.

1.3.1 Formation of Porous Silicon

Porous Silicon (P-Si), as the name suggests, is a porous form of silicon having a microstructure with a large surface to volume ratio on the order of 10^6 cm^2/cm^3. Anodization or stain etching of a silicon wafer using hydrofluoric acid (HF) leads to formation of porous silicon [102]. The etching results in a system of disordered pores with silicon crystals remaining in the inter-pore regions. Depending on the rate of etching, the current density, HF concentration and sample thickness, porous silicon can have wide ranging porosities and is classified as macroporous (Pore size greater than 50nm), mesoporous (Pore size of 5-50nm) or nanoporous/microporous (Pore size less than 5nm) (Figure 1.10) [103].
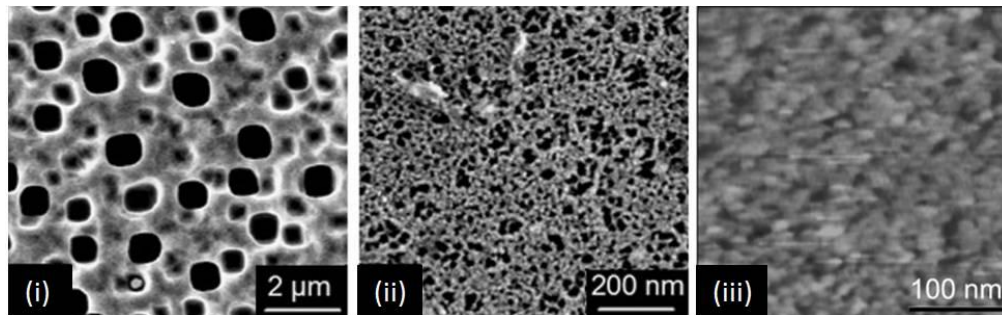
Figure 1.10 Images of the surface morphology of three forms of P-Si. i) Macroporous P-Si: straight pores with openings close to 1 µm (scanning electron microscopy (SEM)). ii) Mesoporous P-Si: branching pores with pore openings of 50 nm (SEM). iii) Nanoporous P-Si: spongy porous structure with pore sizes less than 15 nm (atomic force microscopy (AFM)). *(Courtesy: Sun et al [104]. Reprint permission granted by Wiley & Co.)*

1.3.2 Biocompatibility of Porous Silicon

A material is biocompatible if it can interact with a living system without provoking a harmful response. The success of any medical implant depends on the behavior of cells in the vicinity of the interface between the host and the biomaterial used in the device [105]. An effective biomaterial must bond to living tissues after adsorption of a layer of protein. Besides allowing protein adsorption, a biocompatible material should also be amenable to the unique environment that the tissue creates. The large surface area of porous silicon enables bio-organic molecules to adhere well. The absorption of human serum albumin (HSA) and fibrinogen has been measured for nanostructured silicon and found to be comparable to other biomaterials [96, 106, 107]. The first evidence that porous silicon is a biocompatible material was reported in 1995 [108] . In this study, it was found that hydroxyapatite growth was occurring on porous silicon which indicates its potential for bone implantation. It was then suggested by author L.T. Canham that hydrated microporous Si could be a bioactive form of the semiconductor and should be considered for development as a biomaterial for widespread *in vivo* applications such as tissue implantation. Following this, *in vitro* studies have been conducted to evaluate the interaction of cells with porous silicon. One group in 1995 studied the

interaction of B50 rat hippocampal cells with porous silicon and found that B50 cells had clear preference for adhesion to porous silicon over other surfaces [109]. Apart from providing larger surface area for adhesion, a porous substrate allows the cells easy access to media nutrients through its pores.

1.3.3 Biodegradation of Porous Silicon

Another positive attribute of porous silicon is its controllable degradation into non toxic monomeric silicic acid (orthosilicic acid, H_4SiO_4) [108, 110].

$$Si + O_2 \rightarrow SiO_2 \quad ; \quad SiO_2 + 2H_2O \rightarrow H_4SiO_4$$

Silicon is essential to biological systems as it affects both morphological development and metabolic processes [111]. Silicic acid is reputed to be the most natural form of silicon in the body and is readily removed by kidneys without any harmful effects [112]. However, silicon-induced toxicity may occur if a system is exposed to more silicon than is needed physiologically. The human blood plasma contains monomeric silicic acid at levels of less than 1 mg Si/l, corresponding to the average dietary intake of 10-50 mg/day [113, 114]. Hence, it was proposed that the small thickness of a silicon implant presents minimal risk [114]. Even though the porous silicon substrate degrades and produces silicic acid, cells growing on the material are viable in terms of structure and metabolism [115]. P-Si wafers are not fatally toxic to the cells and present an acceptable surface for growth [115, 116]. Therefore, P-Si is a form of silicon that is tolerated by the body's immune system and cellular cultures. P-Si has potential applications in medicine such as biosensors, tissue engineering and medical implants [104, 117, 118].

The rate of degradation of P-Si is proportional to its porosity. In studies by Canham *et al* (1995), it was found that high porosity mesoporous layers were completely dissolved by simulated body fluids within a day. In contrast, low to medium porosity microporous layers displayed more stable configurations and induced hydroxyapatite growth [108]. The increase in porosity means

increase in the surface area to volume ratio, which gives more area for the fluid to attack the material. Hence, nature of porous silicon can be altered in between bio-inert and bioactive by varying its porosity. These events may take place for other silicon-based porous materials.

Degradation of porous silicon is related to the amount of contamination after its production. After formation of porous silicon, the surface contains impurities such as covalently bonded fluorine and oxygen from the air and the etching process. Although the hydrogen coated surface is sufficiently stable when exposed to atmosphere for a short period of time, prolonged exposures render the surface prone to oxidation by atmospheric oxygen and hydroxylation by atmospheric water [119]. Over a few days Si-O-Si, Si-O-H and O_3-Si-H groups are formed. Irregular atmospheric oxidation and hydroxylation promotes instability of porous silicon in simulated biological fluids and is undesirable for long term applications [102].

1.3.4 Enhancing Stability in Physiological Fluids

Several methods have been developed to control the surface stability by improving the quality of oxide layer formed or by passivating the surface through derivatization [120-122]. Thermal oxidation can be used to create a high quality oxide layer and reduce P-Si instability in biological fluids [123]. This process generally involves heating the porous silicon to a temperature above 1000°C for around 10 minutes to promote full oxidation of sub-oxide species to form a stable oxide layer. The large amount of energy provided in a short period of time during Rapid thermal processing (RTP) resulted in superior photoluminescence of porous silicon, which indicates improvement in the surface oxide quality [124]. In other work with porous silicon, the growth of an oxide layer *via* ozone oxidation considerably slowed silicon degradation in PBS [125]. Additionally, UV-ozone cleaning of the substrate has been reportedly used to remove organic impurities from its surface or create a hydrophilic and oxidized/hydroxylized layer [126-130].

In addition to improving the surface oxide quality, derivatization of the porous silicon also helps in improving porous silicon stability. Thermal dissociation of acetylene is exploited to carbonize porous silicon films; the carbon atoms from acetylene bind to the Si atoms of porous silicon substrate. The surface is washed in acetylene at high temperature to deposit a layer of carbon. Carbonization leaves porous silicon with improved stability due to SiC residues on its surface [131]. Other treatments like thermal nitridation and dodecene derivatization have also shown improved stability of porous silicon in simulated biological fluids [121, 122].

Surface functionalization can stabilize P-Si and additionally be used to promote cell adhesion [132, 133]. It is known that a dense oxide layer provides protection to the underlying P-Si. Similarly, a layer of a different chemistry could be used to enhance the stability. Silanization, a form of functionalization that links silanols to the silicon by a dehydration reaction, has been found to be effective in stabilizing porous silicon in aqueous environments [134]. Depending on the silane monolayer's terminal functional group, silanization can promote or hinder cell attachment [135]. The mammalian cell lines such as PC12 cells and Human Lens Epithelial (HLE) cells have been cultured on the modified surfaces of porous silicon [125]. This research concluded that amino-silanization and coating the P-Si surface with proteins such as collagen enhanced cell attachment and spreading

Summary: Although porous silicon is not a free standing material that could be used in biological separations or membrane based cell culture applications, the topological features of porous silicon are similar to a porous membrane. Cells are sensitive to topological, chemical and electrical properties of substrates on which they are grown [136]. They have been found to grow normally on porous silicon or silicon surfaces covered with microelectrode arrays, as well as on microperforated silicon membranes [106]. This indicates that cells can be cultivated on a nanoporous topology. Nanostructured porous silicon (P-Si) has properties that make it a very

promising biomaterial and allow it to be exploited in tissue engineering and drug delivery research [137-140].

1.4 Porous Nanocrystalline Silicon (Pnc-Si): A Novel Material

Most of the conventional membranes discussed thus far have broad or logarithmic pore size distributions [24], high internal surface area or are over 1000 times thicker than the molecules they are designed to separate [141]. This leads to poor size cut off, loss of sample within the membrane, and inefficient transport across the membrane. Besides the traditional membranes made of polymers and ceramics, there are others that are made from advanced nanofabrication techniques. Nanostructured membranes have been fabricated with thickness close to the size of molecules being separated (~10 nm) using focused ion-beam lithography in silicon nitride membranes, but these have limitations such as mechanical fragility and complicated nanolithography process [54].

List of important nanoporous membranes with their advantages and disadvantages:

1. Polymeric Membranes: *These are inefficient and microns-thick membranes with long size cut-off tail, but have facile fabrication techniques.*

2. Alumina Membranes: *These are microns-thick membranes with low transport rates, but have high chemical and heat resistance.*

3. Silicon Nitride Membranes: *These are fragile, ultrathin membranes requiring elaborate and expensive fabrication technique.*

4. Carbon Nanotube Membranes: *These are membranes with uniform pores and high flow rates, but are difficult to fabricate and are available in limited pore sizes.*

1.4.1 Characteristics of Pnc-Si Membranes

Recently, a novel ultrathin nanoporous membrane based on nanocrystalline silicon was discovered at the University of Rochester [142]. This porous nanocrystalline silicon (pnc-Si) membrane was developed using standard silicon fabrication techniques. These membranes are nearly as thick as biological membranes (7-50 nm) and consist of through pores with tunable pore distributions ranging from 5-100 nm in diameter and porosities as high as 15%. Pnc-Si membranes have ~0.04 μm^2 of internal surface area per um^2 of frontal surface, which lowers resistance to intramembrane transport (~0.04 μm^2 per μm^2 of frontal surface for pnc-Si vs. 10-200 μm^2 per μm^2 for polymer-based membranes). Pnc-Si membranes are mechanically robust and can sustain an atmosphere of differential pressure without exhibiting plastic deformation and maintaining their structural integrity over a free standing area of 0.2 x 0.2 mm (Figure 1.12 B).
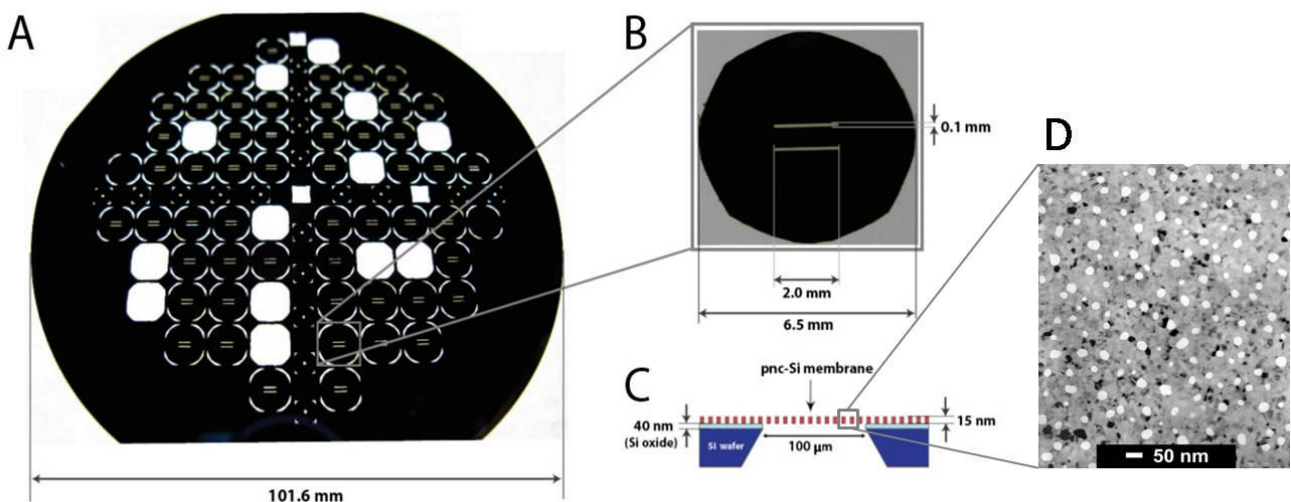
Figure 1.11 A) Photolithographically patterned silicon wafer designed to yield approximately 80 samples, some of which are missing from this wafer, B) Each sample contains two approximately 2 mm x 100 μm slits with freely suspended 15 nm thin pnc-Si membranes, C) Cross sectional schematic diagram of the chip showing the 15 nm thin pnc-Si and 40 nm sputter-deposited thermal silicon dioxide on the silicon wafer, D) TEM (Transmission electron microscopy) image of the membrane with pores in white and nanocrystals in black.

1.4.2 Thermodynamically Driven Fabrication of Pnc-Si

The pore formation process in pnc-Si is a thermodynamically driven bottom-up approach. The fabrication process is shown schematically in figure 1.12 and is described in detail in the methods section of following chapter.
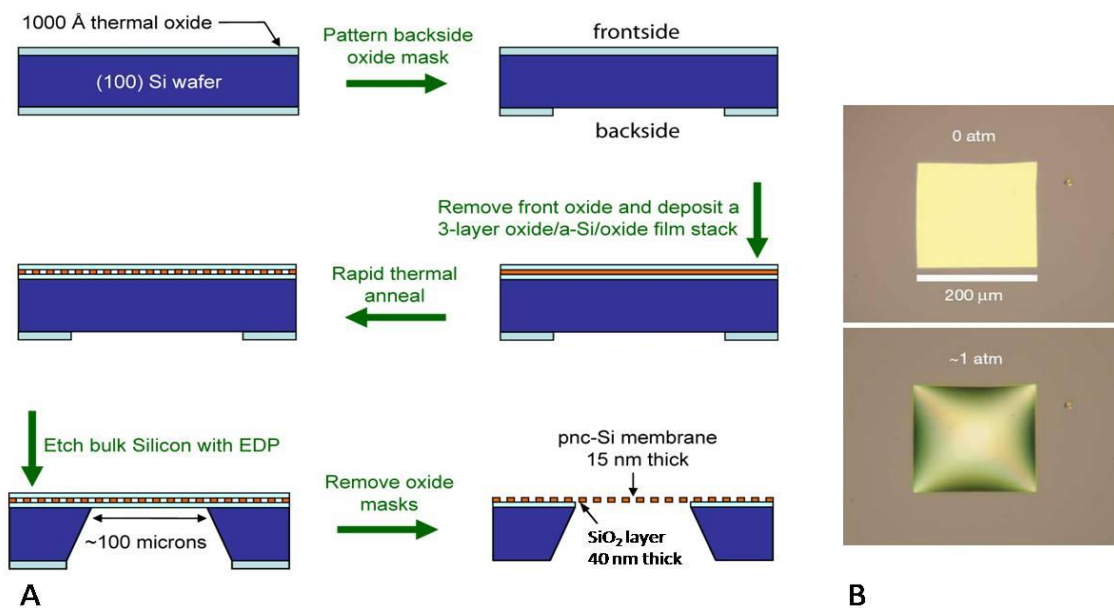
Figure 1.12 A) Fabrication steps of porous nanocrystalline silicon membrane using standard silicon deposition and etching techniques. A thermal annealing step induces pore formation. B) Mechanical testing of 200 μm x 200 μm membrane shows that intact membrane can sustain a differential pressure of ~1 atm. Image taken through reflection microscopy. *(Courtesy: Striemer et al [142]. Reprint permission requested from Nature Publishing Group)*

Succinctly, precision silicon deposition and etching techniques are used for the ultrathin membrane development [142]. Unlike the nanolithographic approaches where the pores are directly patterned on the substrate [54], here the pores self-form due to a phase transition of the material. During rapid thermal annealing, a thin (7-50 nm) deposited layer of amorphous silicon (a-Si) at temperatures greater than the threshold crystallization temperature of ~700°C for 30 seconds, voids are formed spontaneously among the nucleating silicon nanocrystals. As the a-Si layer is molecularly thin, voids span the layer to form the porous structure of the membrane

material. This membrane is held free standing over a rigid crystalline silicon frame with slits of several hundred micrometers in dimensions created by back etching and removing the oxide barriers from the three layer film initially deposited. The active area of the free standing membrane can be of desired formats, such as, 200 x 200 µm squares, 2000 x 100 µm slits, 2000 x 200 µm slits, etc (Figure 1.13). The pore sizes are tunable in the range of 5 to 100 nm depending on the annealing temperature [142]. The thermodynamically driven fabrication allows tunable pore distribution by controlling temperature, ramp speed, thickness etc. Although the pore size distribution of pnc-Si is not mono-dispersed, it has no tail at larger pore sizes. This sharp cut-off in pore size is what allows precise separations. On the other hand, nanofabricated pores created through top-down approaches have mono-dispersed distributions, but involve more expense and effort which may prohibit mass production. Unlike other nanomembranes, pnc-Si fabrication involves a combination of bottom-up and top-down techniques.
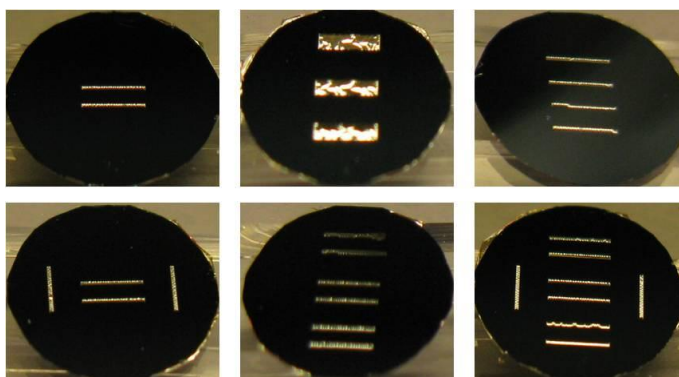
Figure 1.13 Formats of pnc-Si chip with different active areas of the free standing membrane.

1.4.3 Molecular Separations using Pnc-Si

In aqueous solutions, pnc-Si allows highly efficient biomolecular filtration, outperforming the conventional ultrafiltration membranes with an order of magnitude faster diffusive transport [143]. Pnc-Si membranes have a native negative charge because of a thin oxide layer spontaneously formed after exposure to atmosphere. Proteins of different sizes and similarly sized molecules with different charges can be separated with minimal loss using this material.

Due to its molecular thinness and minimal material surface area, pnc-Si offers low resistance for precise molecular sieving, and thereby optimizes flux and selectivity simultaneously. In conventional dialysis and other diffusion based separations, diffusion through the commercial membrane is the rate-limiting step. In the case of pnc-Si membranes, diffusion through the bulk solution is rate-limiting. Substantial improvement of transport rate is expected in systems that implement active mixing or forced flow (pressure or voltage-driven). A recently submitted manuscript shows extraordinarily high gas and water permeability through pnc-Si under pressure (Gaborski *et al*, Science 2009, submitted). Another significant advantage of the standard silicon fabrication technique presented by Striemer *et al,* is that, pnc-Si membranes can be easily integrated as separation elements into 'lab-on-a-chip' microfluidics systems that have growing potential for medical diagnostics, drug discovery and chemical synthesis [144].

Various biomolecules, including proteins and DNA, fall in the nanometer regime and their efficient separation from a mixture requires a membrane with pores and thickness in the same regime. The tunability of pore size in this range makes pnc-Si membranes apt for size-selective separation of biomolecules. Striemer *et al* demonstrated efficient size-based diffusive separation of two proteins, bovine serum albumin and immunoglobulin G, which differ in molecular weight by a factor of ~2.2X [142]. Manufacturers of conventional polymer membranes recommend a factor of 10X as the minimum for effective separation. Charge based separation was demonstrated when flow of molecules was regulated using different salt concentrations in positively or negatively charged pnc-Si membranes [142]. Further, since silicon is easily functionalized, it can be adapted for affinity-based separations of similarly sized macromolecules. Due to its molecular thinness, direct imaging of membrane pores is possible with transmission electron microscopy [142]. Additionally, the material as a whole is nearly transparent in visible light and can be used as a platform for electron imaging, spectroscopy and fluorescent imaging.

In conclusion, pnc-Si is a truly revolutionary platform for molecular separations. The unique structure of pnc-Si makes it orders-of-magnitude more permeable than other membrane materials and allows for precise fractionation of mixtures by size or charge. The silicon platform with planar geometry and mechanical strength of pnc-Si makes membranes practical to manufacture and use. Pnc-Si membrane can be utilized in desirable formats like centrifuge tubes, transwells and microfluidic systems. If biocompatible, these characteristics are relevant to membrane cell culture research because through its high permeability, molecular thinness, and a capacity for device integration, pnc-Si can enable new discoveries in cell biology.

1.5 Membranes for Cell Biology Research

Biocompatible membranes can be used as growth substrates in cell biology research and biotechnological applications. In this thesis, porous nanocrystalline silicon (pnc-Si) is investigated as a potential cell culture substrate. Permeable membranes allow passage of nutrients, drugs and signaling molecules through their pores. Cell culture on permeable membranes enhances the analysis techniques to improve the basic understanding of cellular mechanisms and helps identify the signaling pathways involved in a development or disease. Numerous studies using membrane based cell culture have been performed to investigate cell monolayer integrity and transport to drugs, toxins [145-148], organotyping or organ-culture [149, 150], co-culturing cells for studying cell-cell interactions [93, 151], *in vitro* toxicology [152], angiogenesis, chemotaxis [153, 154], *in vitro* fertilization and immunohistochemistry detection.

1.5.1 Three Dimensional Transwell Cell Culture as In Vitro Models

In a traditional membrane cell biology experiment, a nanoporous polymer membrane sits at the base of a cup-like plastic device, which is suspended in a culture well. The device divides the well into two compartments: upper (apical; donor) and lower (basolateral; receiver) chambers

(Figure 1.14). This arrangement is referred to as 'transwell' and creates a cellular microenvironment for facile testing.
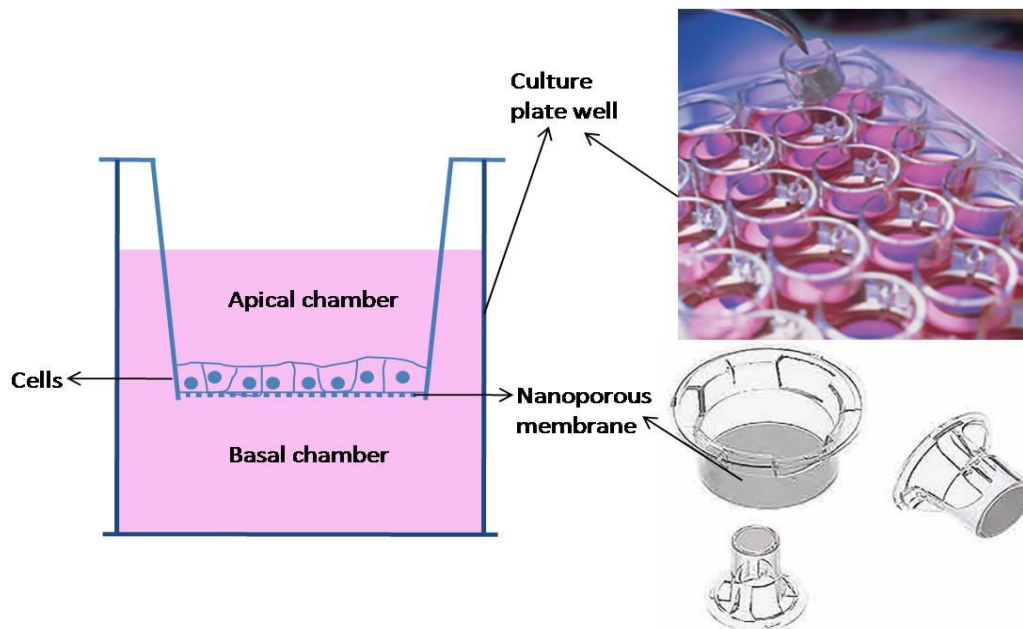
Figure 1.14 Schematic of a transwell assembly with membrane dividing the well into apical and basal compartment and with cells on the upper side of the membrane. Some of the common transwell devices by Millipore and Cole Palmer are also shown.

Cells grown on plastic tissue culture plates can only be nourished with media from their apical side. Porous membrane inserts nurture cells in a three dimensional environment, in which they can access media from both the apical and basolateral sides, resulting in improved cell morphology that mimics *in vivo* growth [155]. In addition, membrane-based cell culture allows researchers discrete access to both the apical and basolateral cell surfaces in their experimental designs. Cell growth on membranes has been shown to improve cell differentiation, increase the presence of intracellular organelles, and allow higher viable cell densities [156]. One comparison between cells grown on plastic and on a Millipore membrane, demonstrated that cells grown on the Millipore membrane formed characteristic tall columnar monolayers with ovoid or pyramidal nuclei [157].

Transwell cell culture techniques apart from promoting natural cell growth incorporate unique design features to improve flexibility in carrying out research. Using transwells procedures like cell seeding, feeding, washing, fixation, staining and visualization are easily supported in a single device. Depending on the type of membrane, fixed and stained cells can be visualized by stereoscopic microscopy, phase contrast microscopy, or fluorescent methods. Several different types of membranes are commercially available in the transwell format for cell culture based applications, such as, polystyrene (PS), hydrophilic polytetrafluoroethylene (PTFE), polycarbonate (PC), polyethylene therephthalate (PET) and other mixed cellulose ester filters. These membranes are available in different formats for different cell culture system devices; for example, single well, 6-well, 12-well, 24-well and 96-well standing and hanging plate inserts.

Advancements in *in vitro* cell culture have given researchers a viable alternative to live animal testing. Long term *in vitro* models offer a number of ethical and economic advantages [158, 159], in cases like toxicity testing to determine risk assessment and/or set up controls. Additionally, *in vitro* models give researchers an advantage in understanding the biological process involved in a toxic response to metals, cosmetics, drugs and pharmaceutical therapies [152]. The combination of lower-cost and high throughput can help bring products to market faster [160]. Pnc-Si based transwells can provide a better *in vitro* model than conventional membrane transwells by more closely matching the physiological arrangement as discussed later in this section.

1.5.2 In Vitro Cell Culture Based Assays

Cell based assays are valuable tools in basic research applications and drug screening techniques. The complexity of cell-to-cell and even cell-to-extracellular matrix interactions require simple, yet accurate methods to understanding cellular responses and communication under user-defined conditions [161-163]. There are two main applications for membranes in cell

biology research. First, membranes serve as semi-permeable substrates in assays of monolayer barrier function. In these applications, a confluent cell monolayer is grown in the transwell format (Figure 1.15). The presence of adherens junctions, tight junctions and gap junctions can be verified by immunofluorescence. The ability of cell monolayers to regulate transport between upper and lower chambers of a transwell device can be determined with trans-monolayer electrical resistance measurements or by measuring the flux of small, fluorescent or radiolabeled molecules. In the second application of transwell devices, filters are used to physically separate different cell types. This involves growing two or more cell types in culture simultaneously (Figure 1.15). Cell types can be co-cultured in direct contact with each other on the membrane or indirectly where one cell line is cultured on the apical side of the membrane and the other is cultured on either the underside of the membrane (basolateral) or on the surface of the plastic feeder or receiver trays. Such arrangements are employed in the study of cell-cell communication, for three-dimensional tissue models and in the creation of bioreactors requiring 'feeder' cells to support the growth of a second cell type [90].
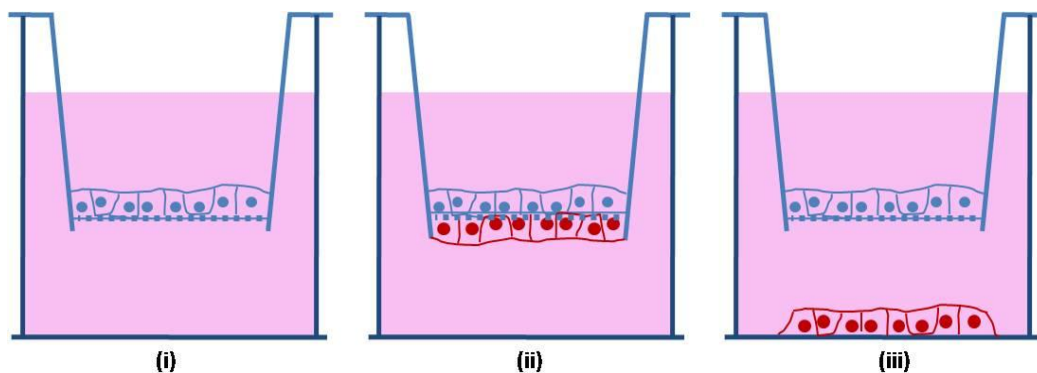
Figure 1.15 Different types of cell culture experiments using transwells. (i) Cell monolayer is formed on the upper side of the membrane support for drug permeability assays, (ii) two different populations of cells are cultured on either side of the membrane as a co-culture to study cell-cell interactions or signaling, (iii) one cell type is plated on bottom of the well and second cell type is plated on the membrane for a 'feeder' layer type co-culture.

Transswell systems are compatible with fluorescent imaging, as well as all tests for cell viability and monolayer integrity. Cell monolayer integrity is examined through transepithelial/endothelial electrical resistance (TEER) and passage of small molecules such as luciferase yellow, sodium fluorescein or paracellular drugs such as atenolol or mannitol. A maximal electrical resistance combined with minimal luciferase yellow passage or a paracellular drug transport indicates optimum monolayer integrity [164]. For drug transport analysis, the growth, integrity and differentiation of the cell monolayers need to be carefully monitored. Both, the tight junction formation and polarized expression of membrane proteins are crucial [165]. For example, Caco2 or MDCK monolayer differentiation is evaluated by the transport of compounds that are effluxed, such as digoxin and vinblastine [164]. This is a reliable indirect measure of expression and localization of P-glycoprotein to the apical plasma membrane.

1.5.3 Transswell Membrane Properties Affect Assay Sensitivity

Membrane properties are crucial for the accuracy and sensitivity of cell culture based assay measurements. During transport of molecules across a membrane supported cell monolayer, the resistance offered to the passage from one side to other is a sum of resistances of the membrane filter and the confluent cell monolayer formed on it. For accurate measurement of cell barrier function decoupling of these resistances is imperative. The resistance to transport should have significantly low contribution from the membrane that separates the two chambers as compared to the cell monolayer itself [91]. In cell-cell interaction studies, often cell types separated by transwell filters do not exhibit the signaling that occurs *in vivo*, while cells plated together on the same side of the surface do   [92, 93, 151, 166]. While such results could indicate that physical contact between the two cell types is necessary to reconstitute communication pathways, they may also be due to the loss of low concentration signaling molecules to spongy polymeric membranes [167]. *In vivo* cell-cell communication is often mediated by secreted soluble factors that diffuse freely over sub-cellular distances [132, 133]

and so the commercial transwell device is a poor *in vitro* model of *in vivo* system. Examples of which are, the signaling between T-cells and T-regulatory cells [167, 168] and the endothelium-astrocyte models of blood brain barrier [169, 170].

1.5.4 Potential Advantages of Pnc-Si Membranes over Traditional Membranes

In the case of both barrier function measurements and co-culture studies, pnc-Si offers potential advantages over microns-thick polymer membranes used in commercial transwell devices. As molecularly thin filters, pnc-Si membranes exhibit permeabilities to small solutes that are orders-of-magnitude higher than nanoporous polymer membranes [143]. Thus, pnc-Si membranes are superior substrates for monolayer permeability studies because their resistances will be negligible compared to cell monolayer resistances. The high permeability of pnc-Si will allow investigation of the most efficient cellular mechanisms for small molecule transport and more detailed looks at the ability of inflammatory signals to regulate vascular permeability. Additionally, cell monolayers on pnc-Si are easily characterized by bright-field and epifluorescence microscopy because the 15 nm thick membrane is optically transparent. This is in contrast to polymer nanoporous membranes which are opaque (PC) or translucent (PET) and exhibit high background fluorescence. In co-culture applications, pnc-Si should overcome concerns about the loss and dilution of soluble signals in transwell devices. Indeed if pnc-Si membranes support cell adhesion and growth, they will allow cells to be plated on their either side while allowing efficient chemical communication resembling *in vivo* arrangement. Because the internal surface area of pnc-Si membranes is 2-3 orders lower than that of nanoporous polymer membranes, low abundance signals are far less likely to be lost through membrane adsorption to pnc-Si. In conclusion, if biocompatible, pnc-Si membranes are expected to offer unique opportunities for discovery in membrane supported cell biology research.

1.6 Thesis Outline and Research Objectives

The goal of this thesis is to establish porous nanocrystalline silicon (pnc-Si) membranes as a molecularly thin, nanoporous and viable substrate for cell culture experiments. Additionally, the stability of pnc-Si in physiological conditions and the control over its biodegradation are also investigated. The work is divided into following three smaller objectives. The successful completion of these objectives will establish pnc-Si as a platform for answering questions that cannot be addressed with current commercial devices.

1.6.1 Investigate and control biodegradation of pnc-Si membranes in physiological media:

Porous silicon films dissolve in physiological media and produce soluble silicic acid compounds. Pnc-Si being a silicon-based material can undergo similar type of degradation. In chapter 2, methods are developed to monitor membrane stability in culture media. Also, methods for enhancing membrane stability are investigated, such as post production rapid thermal processing and amino-silanization. As a result of this work, pnc-Si can now be used for short term as well as long term cell culture applications.

1.6.2 Demonstrate that pnc-Si membranes are biocompatible and support cell culture growth:

To establish that pnc-Si is a viable substrate, cell adhesion, cell spreading, cell growth kinetics and cell viability will be investigated for both immortalized robust fibroblasts (3T3-L1) and environmentally sensitive primary human umbilical vein endothelial cells (HUVEC). In chapter 3, comparisons will be made to standard cell culture substrates such as glass and tissue culture grade plastic. The results show that pnc-Si performed comparably to common cell culture substrates in each of these metrics.

1.6.3 Demonstrate pnc-Si membrane performance in three dimensional transwell format:

The final aim of this thesis is to develop a pnc-Si - transwell hybrid that closely resembles the commercial transwell inserts. This transwell format will be used in the future for different cell culture applications like drug permeability assay and cellular co-culture. In chapter 4, membrane stability and cell adhesion for treated pnc-Si in three dimensional format are examined. Also, long term stability is achieved in the transwell configuration.

1.7 References

1.   Buzea, C., Pacheco, I.I., and Robbie, K. (2007). Nanomaterials and nanoparticles: Sources and toxicity. Biointerphases *2*, MR17-MR71.

2.   Zong, R.L., Zhou, J., Li, B., Fu, M., Shi, S.K., and Li, L.T. (2005). Optical properties of transparent copper nanorod and nanowire arrays embedded in anodic alumina oxide. The Journal of Chemical Physics *123*, 094710.

3.   Kenneth K. Kuo, G.A.R., Brian J. Evans, and Eric Boyer (2003). Potential Usage of Energetic Nano-sized Powders for Combustion and Rocket Propulsion. In Materials Research Society Conference Volume 800, N.T. Ronald Armstrong, William Wilson, John Gilman, Randall Simpson ed. (Boston, MA: MRS Publications).

4.   Hutchings, G.J. (2008). Nanocrystalline gold and gold-palladium alloy oxidation catalysts: a personal reflection on the nature of the active sites. Dalton Transactions, 5523-5536.

5.   Hong, S., and Myung, S. (2007). Nanotube Electronics: A flexible approach to mobility. Nat Nano *2*, 207-208.

6.   Zhang, M., Fang, S., Zakhidov, A.A., Lee, S.B., Aliev, A.E., Williams, C.D., Atkinson, K.R., and Baughman, R.H. (2005). Strong, Transparent, Multifunctional, Carbon Nanotube Sheets. Science *309*, 1215-1219.

7.   Kis, A., and Zettl, A. (2008). Nanomechanics of carbon nanotubes. Philosophical Transactions of the Royal Society A: Mathematical, Physical and Engineering Sciences *366*, 1591-1611.

8.   George M. Whitesides (2005). Nanoscience, Nanotechnology, and Chemistry. Small *1*, 172-179.

9.   Gates, B.D., Xu, Q., Stewart, M., Ryan, D., Willson, C.G., and Whitesides, G.M. (2005). New Approaches to Nanofabrication: Molding, Printing, and Other Techniques. Chemical Reviews *105*, 1171-1196.

10.   Oberdorster, G., Oberdorster, E., and Oberdorster, J. (2005). Nanotoxicology: an emerging discipline evolving from studies of ultrafine particles. Environ Health Perspect *113*, 823-839.

11.   Elder, A., Gelein, R., Silva, V., Feikert, T., Opanashuk, L., Carter, J., Potter, R., Maynard, A., Ito, Y., Finkelstein, J., et al. (2006). Translocation of inhaled ultrafine

manganese oxide particles to the central nervous system. Environ Health Perspect *114*, 1172-1178.

12.   Elder, A., and Oberdorster, G. (2006). Translocation and effects of ultrafine particles outside of the lung. Clin Occup Environ Med *5*, 785-796.

13.   Oberdorster, G., Maynard, A., Donaldson, K., Castranova, V., Fitzpatrick, J., Ausman, K., Carter, J., Karn, B., Kreyling, W., Lai, D., et al. (2005). Principles for characterizing the potential human health effects from exposure to nanomaterials: elements of a screening strategy. Part Fibre Toxicol *2*, 8.

14.   Sara, M., and Sleytr, U.B. (1996). Crystalline bacterial cell surface layers (S-layers): from cell structure to biomimetics. Prog Biophys Mol Biol *65*, 83-111.

15.   Messner, P., and Sleytr, U.B. (1992). Crystalline bacterial cell-surface layers. Adv Microb Physiol *33*, 213-275.

16.   Mumpton, F.A. (1999). La roca magica: Uses of natural zeolites in agriculture and industry. Proceedings of the National Academy of Sciences of the United States of America *96*, 3463-3470.

17.   Han, J., Fu, J., and Schoch, R.B. (2008). Molecular sieving using nanofilters: past, present and future. Lab Chip *8*, 23-33.

18.   Mulder, M. (1996). Basic principles of membrane technology, 2 Edition, (Springer).

19.   Baker, R.W. (2000). Membrane technology and applications, (New York: McGraw-Hill).

20.   Ulbricht, M. (2006). Advanced functional polymer membranes. Polymer (Guildf) *47*, 2217-2262.

21.   Apel, P. (2001). Track etching technique in membrane technology. Radiation Measurements *34*, 559-566.

22.   Kesting, R.E. (1971). Synthetic polymeric membranes, (New York,: McGraw-Hill).

23.   D. M. Koenhen, M.H.V.M., C. A. Smolders, (1977). Phase separation phenomena during the formation of asymmetric membranes. Journal of Applied Polymer Science *21*, 199-215.

24.   Rijn, C.J.M.v. (2004). Nano and micro engineered membrane technology, 1st Edition, (Amsterdam ; Boston: Elsevier).

25.   Bhave, R.R. (1991). Inorganic membranes synthesis, characteristics, and applications, (New York: Van Nostrand Reinhold).

26. Kim, J., and Lin, Y.S. (1998). Sol-gel synthesis and characterization of yttria stabilized zirconia membranes. Journal of Membrane Science *139*, 75-83.

27. Larbot, A., Julbe, A., Guizard, C., and Cot, L. (1989). Silica Membranes by the Sol-Gel Process. Journal of Membrane Science *44*, 289-303.

28. Pierre, A.C. (1998). Introduction to sol-gel processing, (Boston: Kluwer Academic Publishers).

29. Ellsworth, M.W., and Novak, B.M. (2002). Mutually interpenetrating inorganic-organic networks. New routes into nonshrinking sol-gel composite materials. Journal of the American Chemical Society *113*, 2756-2758.

30. Hsieh, H.P., Bhave, R.R., and Fleming, H.L. (1988). Microporous Alumina Membranes. Journal of Membrane Science *39*, 221-241.

31. Verweij, H. (2003). Ceramic membranes: Morphology and transport. Journal of Materials Science v. 38 no. 23 (December 1 2003) p. 4677-95.

32. Martin, C.R. (1994). Nanomaterials: A Membrane-Based Synthetic Approach. Science *266*, 1961-1966.

33. Thormann, A., Teuscher, N., Pfannmoller, M., Rothe, U., and Heilmann, A. (2007). Nanoporous aluminum oxide membranes for filtration and biofunctionalization. Small *3*, 1032-1040.

34. Wang, Y.H., Tian, T.F., Liu, X.Q., and Meng, G.Y. (2006). Titania membrane preparation with chemical stability for very hash environments applications. Journal of Membrane Science *280*, 261-269.

35. Van Gestel, T., Kruidhof, H., Blank, D.H.A., and Bouwmeester, H.J.M. (2006). ZrO2 and TiO2 membranes for nanofiltration and pervaporation: Part 1. Preparation and characterization of a corrosion-resistant ZrO2 nanofiltration membrane with a MWCO < 300. Journal of Membrane Science *284*, 128-136.

36. Larbot, A., Fabre, J.P., Guizard, C., Cot, L., and Gillot, J. (1989). New Inorganic Ultrafiltration Membranes - Titania and Zirconia Membranes. Journal of the American Ceramic Society *72*, 257-261.

37. Kuiper, S., van Rijn, C.J.M., Nijdam, W., and Elwenspoek, M.C. (1998). Development and applications of very high flux microfiltration membranes. Journal of Membrane Science *150*, 1-8.

38. de Lange, R.S.A., Hekkink, J.H.A., Keizer, K., and Burggraaf, A.J. (1995). Formation and characterization of supported microporous ceramic membranes prepared by sol-gel modification techniques. Journal of Membrane Science *99*, 57-75.

39. Katsuki Kusakabe, T.K.a.S.M. (1998). Separation of carbon dioxide from nitrogen using ion-exchanged faujasite-type zeolite membranes form. Journal of membrane science *148*.

40. F.C. Gielensa, H.D.T., C.J.M. van Rijn, M.A.G. Vorstman and J.T.F. Keurentjes (2004). Microsystem technology for high-flux hydrogen separation membranes. Journal of Membrane Science *243*, 203-213.

41. Joly, C., Goizet, S., Schrotter, J.C., Sanchez, J., and Escoubes, M. (1997). Sol-gel polyimide-silica composite membrane: gas transport properties. Journal of Membrane Science *130*, 63-74.

42. Hinds, B.J., Chopra, N., Rantell, T., Andrews, R., Gavalas, V., and Bachas, L.G. (2004). Aligned multiwalled carbon nanotube membranes. Science *303*, 62-65.

43. Holt, J.K., Noy, A., Huser, T., Eaglesham, D., and Bakajin, O. (2004). Fabrication of a carbon nanotube-embedded silicon nitride membrane for studies of nanometer-scale mass transport. Nano Letters *4*, 2245-2250.

44. Merkel, T.C., Freeman, B.D., Spontak, R.J., He, Z., Pinnau, I., Meakin, P., and Hill, A.J. (2002). Ultrapermeable, Reverse-Selective Nanocomposite Membranes. Science *296*, 519-522.

45. Robeson, L. (1991). Correlation of separation factor versus permeability for polymeric membranes. Journal of membrane science *62*.

46. Rijn, C.J.M.v., Nijdam, W., Kuiper, S., Veldhuis, G.J., Wolferen, H.v., and Elwenspoek, M. (1999). Microsieves made with laser interference lithography for micro-filtration applications. Journal of Micromechanics and Microengineering *9*, 170-172.

47. Michael D. Stewart, K.P., Mark H. Somervell, C. Grant Willson, (2000). Organic imaging materials: a view of the future. Journal of Physical Organic Chemistry *13*, 767-774.

48. Zaidi, S.H., and Brueck, S.R.J. (1993). Multiple-exposure interferometric lithography. Journal of Vacuum Science & Technology B: Microelectronics and Nanometer Structures *11*, 658-666.

49. Brueck, S.R.J., Zaidi, S.H., Chen, X., and Zhang, Z. (1998). Interferometric lithography - from periodic arrays to arbitrary patterns. Microelectron. Eng. *41-42*, 145-148.

50. Hoffnagle, J.A., Hinsberg, W.D., Sanchez, M., and Houle, F.A. (1999). Liquid immersion deep-ultraviolet interferometric lithography. Volume 17. (AVS), pp. 3306-3309.

51. L. J. Heyderman, B.K., D. Bächlea, F. Glausa, B. Haasa, H. Schifta, K. Vogelsanga, J. Gobrechta, L. Tiefenauera, O. Dubochetb, P. Surbledb and T. Hessler (2003). High volume fabrication of customised nanopore membrane chips. Microelectron. Eng. *67-68*, 208-213.

52. Gamo, K. (1993). Focused ion beam technology. Semiconductor Science and Technology *8*, 1118-1123.

53. Morita, T., Kometani, R., Watanabe, K., Kanda, K., Haruyama, Y., Hoshino, T., Kondo, K., Kaito, T., Ichihashi, T., Fujita, J.(2003). Free-space-wiring fabrication in nano-space by focused-ion-beam chemical vapor deposition. Journal of Vacuum Science & Technology B: Microelectronics and Nanometer Structures *21*, 2737-2741.

54. Tong, H.D., Jansen, H.V., Gadgil, V.J., Bostan, C.G., Berenschot, E., van Rijn, C.J.M., and Elwenspoek, M. (2004). Silicon Nitride Nanosieve Membrane. Nano Letters *4*, 283-287.

55. Chen, P., Wu, M.Y., Salemink, H.W., and Alkemade, P.F. (2009). Fast single-step fabrication of nanopores. Nanotechnology *20*, 15302.

56. Xia, Y., and Whitesides, G.M. (1998). Soft Lithography. Annual Review of Materials Science *28*, 153-184.

57. Xia, Y., Kim, E., Zhao, X.-M., Rogers, J.A., Prentiss, M., and Whitesides, G.M. (1996). Complex Optical Surfaces Formed by Replica Molding Against Elastomeric Masters. Science *273*, 347-349.

58. Chou, S.Y., Krauss, P.R., and Renstrom, P.J. (1996). Imprint Lithography with 25-Nanometer Resolution. Science *272*, 85-87.

59. L. Vogelaar, J.N.B., C.J.M. van Rijn, W. Nijdam, M. Wessling, (2003). Phase Separation Micromolding - PSµM. Advanced Materials *15*, 1385-1389.

60. Gironès, M., Akbarsyah, I.J., Nijdam, W., van Rijn, C.J.M., Jansen, H.V., Lammertink, R.G.H., and Wessling, M. (2006). Polymeric microsieves produced by phase separation micromolding. Journal of Membrane Science *283*, 411-424.

61. Terrones, M. (2003). Science and technology of the twenty-first century: Synthesis, properties and applications of carbon nanotubes. Annual Review of Materials Research *33*, 419-501.

62. Dresselhaus, M.S. (1998). Nanotechnology - New tricks with nanotubes. Nature *391*, 19-20.

63. Dresselhaus, M.S. (1998). Carbon nanotubes - Introduction. Journal of Materials Research *13*, 2355-2356.

64. Puretzky, A.A., Geohegan, D.B., Jesse, S., Ivanov, I.N., and Eres, G. (2005). In situ measurements and modeling of carbon nanotube array growth kinetics during chemical vapor deposition. Applied Physics a-Materials Science & Processing *81*, 223-240.

65. Franklin, N.R., Li, Y.M., Chen, R.J., Javey, A., and Dai, H.J. (2001). Patterned growth of single-walled carbon nanotubes on full 4-inch wafers. Applied Physics Letters *79*, 4571-4573.

66. Che, G., Lakshmi, B.B., Martin, C.R., Fisher, E.R., and Ruoff, R.S. (1998). Chemical Vapor Deposition Based Synthesis of Carbon Nanotubes and Nanofibers Using a Template Method. Chemistry of Materials *10*, 260-267.

67. Holt, J.K., Park, H.G., Wang, Y., Stadermann, M., Artyukhin, A.B., Grigoropoulos, C.P., Noy, A., and Bakajin, O. (2006). Fast Mass Transport Through Sub-2-Nanometer Carbon Nanotubes. Science *312*, 1034-1037.

68. Kim, S., Jinschek, J.R., Chen, H., Sholl, D.S., and Marand, E. (2007). Scalable Fabrication of Carbon Nanotube/Polymer Nanocomposite Membranes for High Flux Gas Transport. Nano Letters *7*, 2806-2811.

69. Yu, M., Funke, H.H., Falconer, J.L., and Noble, R.D. (2009). High Density, Vertically-Aligned Carbon Nanotube Membranes. Nano Letters *9*, 225-229.

70. Majumder, M., Chopra, N., Andrews, R., and Hinds, B.J. (2005). Nanoscale hydrodynamics: enhanced flow in carbon nanotubes. Nature *438*, 44.

71. Henk Verweij, Melissa C.S., Ju Li, (2007). Fast Mass Transport Through Carbon Nanotube Membranes. Small *3*, 1996-2004.

72. Noy, A., Park, H.G., Fornasiero, F., Holt, J.K., Grigoropoulos, C.P., and Bakajin, O. (2007). Nanofluidics in carbon nanotubes. Nano Today *2*, 22-29.

73. Wang, W.K. (2001). Membrane separations in biotechnology, 2nd Edition, (New York: M. Dekker).

74. de Jong, J., Lammertink, R.G., and Wessling, M. (2006). Membranes and microfluidics: a review. Lab Chip *6*, 1125-1139.

75. Zeman, L.J., and Zydney, A.L. (1996). Microfiltration and ultrafiltration : principles and applications, (New York: M. Dekker).

76. Cheryan, M. (1998). Ultrafiltration and microfiltration handbook, (Lancaster, Pa.: Technomic Pub. Co.).

77. Wang, L.K. (2004). Handbook of industrial and hazardous wastes treatment, 2nd Edition, (New York: Marcel Dekker, Inc.).

78. Eriksson, P. (1988). Nanofiltration extends the range of membrabne filtration. Environmental progress *7*, 58-62.

79. Jirage, K.B., Hulteen, J.C., and Martin, C.R. (1997). Nanotubule-Based Molecular-Filtration Membranes. Science *278*, 655-658.

80. Wijmans, J.G., and Baker, R.W. (1995). The solution-diffusion model: a review. Journal of Membrane Science *107*, 1-21.

81. Lee, S.B., and Martin, C.R. (2002). Electromodulated Molecular Transport in Gold-Nanotube Membranes. Journal of the American Chemical Society *124*, 11850-11851.

82. Nishizawa, M., Menon, V.P., and Martin, C.R. (1995). Metal Nanotubule Membranes with Electrochemically Switchable Ion-Transport Selectivity. Science *268*, 700-702.

83. Ku, J.-R., and Stroeve, P. (2004). Protein Diffusion in Charged Nanotubes: "On-Off" behavior of molecular transport. Langmuir *20*, 2030-2032.

84. Pujar, N.S., and Zydney, A.L. (1994). Electrostatic and Electrokinetic Interactions during Protein-Transport through Narrow Pore Membranes. Industrial & Engineering Chemistry Research *33*, 2473-2482.

85. van Reis, R., Brake, J.M., Charkoudian, J., Burns, D.B., and Zydney, A.L. (1999). High-performance tangential flow filtration using charged membranes. Journal of Membrane Science *159*, 133-142.

86. Martin, C.R. (1996). Membrane-Based Synthesis of Nanomaterials. Chemistry of Materials *8*, 1739-1746.

87. Ostrovidov, S., Jiang, J., Sakai, Y., and Fujii, T. (2004). Membrane-based PDMS microbioreactor for perfused 3D primary rat hepatocyte cultures. Biomed Microdevices *6*, 279-287.

88. Jiang, Y., Wang, P.-C., Locascio, L.E., and Lee, C.S. (2001). Integrated Plastic Microfluidic Devices with ESI-MS for Drug Screening and Residue Analysis. Analytical Chemistry *73*, 2048-2053.

89. Pen-Cheng Wang, D.L.D., Cheng S. Lee, (2001). Integration of polymeric membranes with microfluidic networks for bioanalytical applications. Electrophoresis *22*, 3857-3867.

90. Kim, S., Ahn, S.E., Lee, J.H., Lim, D.S., Kim, K.S., Chung, H.M., and Lee, S.H. (2007). A novel culture technique for human embryonic stem cells using porous membranes. Stem Cells *25*, 2601-2609.

91. Avdeef, A., Artursson, P., Neuhoff, S., Lazorova, L., Grasjo, J., and Tavelin, S. (2005). Caco-2 permeability of weakly basic drugs predicted with the double-sink PAMPA pKa(flux) method. Eur J Pharm Sci *24*, 333-349.

92. Schramm, C.A., Reiter, R.S., and Solursh, M. (1994). Role for short-range interactions in the formation of cartilage and muscle masses in transfilter micromass cultures. Dev Biol *163*, 467-479.

93. Kornyei, Z., Szlavik, V., Szabo, B., Gocza, E., Czirok, A., and Madarasz, E. (2005). Humoral and contact interactions in astroglia/stem cell co-cultures in the course of glia-induced neurogenesis. Glia *49*, 430-444.

94. Kasianowicz, J.J., Brandin, E., Branton, D., and Deamer, D.W. (1996). Characterization of individual polynucleotide molecules using a membrane channel. Proc Natl Acad Sci U S A *93*, 13770-13773.

95. Chen, P., Gu, J., Brandin, E., Kim, Y.-R., Wang, Q., and Branton, D. (2004). Probing Single DNA Molecule Transport Using Fabricated Nanopores. Nano Letters *4*, 2293-2298.

96. Canham, L.T., Reeves, C.L., King, D.O., Branfield, P.J., Crabb, J.G., and Ward, M.C.L. (1996). Bioactive polycrystalline silicon. Advanced Materials *8*, 850.

97. Winterhalter, M., Hilty, C., Bezrukov, S.M., Nardin, C., Meier, W., and Fournier, D. (2001). Controlling membrane permeability with bacterial porins: application to encapsulated enzymes. Talanta *55*, 965-971.

98. Bezrukov, S.M., Vodyanoy, I., and Parsegian, V.A. (1994). Counting polymers moving through a single ion channel. Nature *370*, 279-281.

99. Weiner, C., Sara, M., Dasgupta, G., and Sleytr, U.B. (1994). Affinity cross-flow filtration: Purification of IgG with a novel protein a affinity matrix prepared from two-dimensional protein crystals. Biotechnol Bioeng *44*, 55-65.

100. Weiner, C., Sara, M., and Sleytr, U.B. (1994). Novel protein a affinity matrix prepared from two-dimensional protein crystals. Biotechnol Bioeng *43*, 321-330.

101. Breitwieser, A., Kupcu, S., Howorka, S., Weigert, S., Langer, C., Hoffmann-Sommergruber, K., Scheiner, O., Sleytr, U.B., and Sara, M. (1996). 2-D protein crystals as an immobilization matrix for producing reaction zones in dipstick-style immunoassays. Biotechniques *21*, 918-925.

102. Canham, L.T. (1997). Properties of Porous Silicon, Volume 18, (INSPEC PUBLICATION).

103. Foell H, C.M., Carstensen J, Hasse G. (2002). Formation and application of porous silicon. Mater Sci Eng R Rep *39*, 93-141.

104. Sun, W., Puzas, J.E., Sheu, T.J., Liu, X., and Fauchet, P.M. (2007). Nano- to microscale porous silicon as a cell interface for bone-tissue engineering. Advanced Materials *19*, 921-924.

105. Bayliss, S.C., Buckberry, L.D., Harris, P.J., and Tobin, M. (2000). Nature of the silicon-animal cell interface. Journal of Porous Materials *7*, 191-195.

106. Bayliss, S.C., Heald, R., Fletcher, D.I., and Buckberry, L.D. (1999). The culture of mammalian cells on nanostructured silicon. Advanced Materials *11*, 318-321.

107. Bayliss, S.C., Harris, P.J., Buckberry, L.D., and Rousseau, C. (1997). Phosphate and cell growth on nanostructured semiconductors. Journal of Materials Science Letters *16*, 737-740.

108. Canham, L.T. (1995). Bioactive silicon structure fabrication through nanoetching techniques. Advanced Materials *7*, 1033.

109. Sapelkin, A.V., Bayliss, S.C., Unal, B., and Charalambou, A. (2006). Interaction of B50 rat hippocampal cells with stain-etched porous silicon. Biomaterials *27*, 842-846.

110. S. H. C. Anderson, H.E., D. J. Wallis, L. T. Canham, J. J. Powell, (2003). Dissolution of different forms of partially porous silicon wafers under simulated physiological conditions. physica status solidi (a) *197*, 331-335.

111. Birchall, J.D. (1995). The essentiality of silicon in biology. Chemical Society Reviews *24*, 351-357.

112. Reffitt, D.M., Jugdaohsingh, R., Thompson, R.P., and Powell, J.J. (1999). Silicic acid: its gastrointestinal uptake and urinary excretion in man and effects on aluminium excretion. J Inorg Biochem *76*, 141-147.

113. Bellia, J.P., Birchall, J.D., and Roberts, N.B. (1994). Beer: a dietary source of silicon. Lancet *343*, 235.

114. Bellia, J.P., Birchall, J.D., and Roberts, N.B. (1994). The effect of silicon as silicic acid on superoxide dismutase activity. Clin Chim Acta *224*, 215-217.

115. Low, S.P., Voelcker, N.H., Canham, L.T., and Williams, K.A. (2009). The biocompatibility of porous silicon in tissues of the eye. Biomaterials *30*, 2873-2880.

116. Alvarez, S.D., Derfus, A.M., Schwartz, M.P., Bhatia, S.N., and Sailor, M.J. (2009). The compatibility of hepatocytes with chemically modified porous silicon with reference to in vitro biosensors. Biomaterials *30*, 26-34.

117. A.H. Mayne, S.C.B., P. Barr, M. Tobin, L.D. Buckberry, (2000). Biologically Interfaced Porous Silicon Devices. physica status solidi (a) *182*, 505-513.

118. Stewart, M.P., and Buriak, J.M. (2000). Chemical and biological applications of porous silicon technology. Advanced Materials *12*, 859-869.

119. Salonen, J., Lehto, V.P., and Laine, E. (1997). The room temperature oxidation of porous silicon. Applied Surface Science *120*, 191-198.

120. Salonen, J., and Lehto, V.P. (2008). Fabrication and chemical surface modification of mesoporous silicon for biomedical applications. Chemical Engineering Journal *137*, 162-172.

121. M. Björkqvist, J.S., E. Laine, L. Niinistö, (2003). Comparison of stabilizing treatments on porous silicon for sensor applications. physica status solidi (a) *197*, 374-377.

122. Canham, L.T., Reeves, C.L., Newey, J.P., Houlton, M.R., Cox, T.I., Buriak, J.M., and Stewart, M.P. (1999). Derivatized mesoporous silicon with dramatically improved stability in simulated human blood plasma. Advanced Materials *11*, 1505.

123. Salonen, J., Lehto, V.-P., and Laine, E. (1997). Thermal oxidation of free-standing porous silicon films. Applied Physics Letters *70*, 637-639.

124. Petrova-Koch, V., Muschik, T., Kux, A., Meyer, B.K., Koch, F., and Lehmann, V. (1992). Rapid-thermal-oxidized porous Si - The superior photoluminescent Si. Applied Physics Letters *61*, 943-945.

125. Low, S.P., Williams, K.A., Canham, L.T., and Voelcker, N.H. (2006). Evaluation of mammalian cell adhesion on surface-modified porous silicon. Biomaterials *27*, 4538-4546.

126. Chao, S.C., Pitchai, R., and Lee, Y.H. (1989). Enhancement in Thermal-Oxidation of Silicon by Ozone. Journal of the Electrochemical Society *136*, 2751-2752.

127. Baunack, S., and Zehe, A. (1989). A Study of Uv Ozone Cleaning Procedure for Silicon Surfaces. Physica Status Solidi a-Applied Research *115*, 223-227.

128. Cui, Z.J., Madsen, J.M., and Takoudis, C.G. (2000). Rapid thermal oxidation of silicon in ozone. Journal of Applied Physics *87*, 8181-8186.

129. Thompson, W.H., Yamani, Z., Hassan, L.H.A., Greene, J.E., Nayfeh, M., and Hasan, M.A. (1996). Room temperature oxidation enhancement of porous Si(001) using ultraviolet-ozone exposure. Journal of Applied Physics *80*, 5415-5421.

130. Kern, W. (1993). Handbook of Semiconductor wafer cleaning technology.

131. Torres-Costa, V., Martin-Palma, R.J., Martinez-Duart, J.M., Salonen, J., and Lehto, V.-P. (2008). Effective passivation of porous silicon optical devices by thermal carbonization. Journal of Applied Physics *103*, 083124.

132. Chin, V., Collins, B.E., Sailor, M.J., and Bhatia, S.N. (2001). Compatibility of primary hepatocytes with oxidized nanoporous silicon. Advanced Materials *13*, 1877.

133. Moxon, K.A., Hallman, S., Aslani, A., Kalkhoran, N.M., and Lelkes, P.I. (2007). Bioactive properties of nanostructured porous silicon for enhancing electrode to neuron interfaces. J Biomater Sci Polym Ed *18*, 1263-1281.

134. Li, H.-L., Fu, A.-P., Xu, D.-S., Guo, Gui, L.-L., and Tang, Y.-Q. (2002). In Situ Silanization Reaction on the Surface of Freshly Prepared Porous Silicon. Langmuir *18*, 3198-3202.

135. Faucheux, N., Schweiss, R., Lutzow, K., Werner, C., and Groth, T. (2004). Self-assembled monolayers with different terminating groups as model substrates for cell adhesion studies. Biomaterials *25*, 2721-2730.

136. Curtis, A.S., Casey, B., Gallagher, J.O., Pasqui, D., Wood, M.A., and Wilkinson, C.D. (2001). Substratum nanotopography and the adhesion of biological cells. Are symmetry or regularity of nanotopography important? Biophys Chem *94*, 275-283.

137. Whitehead, M.A., Fan, D., Mukherjee, P., Akkaraju, G.R., Canham, L.T., and Coffer, J.L. (2008). High-porosity poly(epsilon-caprolactone)/mesoporous silicon scaffolds: calcium phosphate deposition and biological response to bone precursor cells. Tissue Eng Part A *14*, 195-206.

138. Mukherjee, P., Whitehead, M.A., Senter, R.A., Fan, D., Coffer, J.L., and Canham, L.T. (2006). Biorelevant mesoporous silicon / polymer composites: directed assembly, disassembly, and controlled release. Biomed Microdevices *8*, 9-15.

139.   Anglin, E.J., Cheng, L., Freeman, W.R., and Sailor, M.J. (2008). Porous silicon in drug delivery devices and materials. Adv Drug Deliv Rev *60*, 1266-1277.

140.   Jarno Salonen, A.M.K., Jouni Hirvonen, Vesa-Pekka Lehto, (2008). Mesoporous silicon in drug delivery applications. Journal of Pharmaceutical Sciences *97*, 632-653.

141.   van den Berg, A., and Wessling, M. (2007). Nanofluidics: silicon for the perfect membrane. Nature *445*, 726.

142.   Striemer, C.C., Gaborski, T.R., McGrath, J.L., and Fauchet, P.M. (2007). Charge- and size-based separation of macromolecules using ultrathin silicon membranes. Nature *445*, 749-753.

143.   Kim, E., Xiong, H., Striemer, C.C., Fang, D.Z., Fauchet, P.M., McGrath, J.L., and Amemiya, S. (2008). A structure-permeability relationship of ultrathin nanoporous silicon membrane: A comparison with the nuclear envelope. Journal of the American Chemical Society *130*, 4230.

144.   Hayden, T. (2007). Thinking thin for molecular filtration. Ultrathin silicon membranes offer fast, effective sorting and separation. Anal Chem *79*, 3263.

145.   Ojakian, G.K. (1981). Tumor promoter-induced changes in the permeability of epithelial cell tight junctions. Cell *23*, 95-103.

146.   Misfeldt, D.S., and Sanders, M.J. (1981). Transepithelial transport in cell culture: D-glucose transport by a pig kidney cell line (LLC-PK1). J Membr Biol *59*, 13-18.

147.   Artursson, P., Palm, K., and Luthman, K. (2001). Caco-2 monolayers in experimental and theoretical predictions of drug transport. Adv Drug Deliv Rev *46*, 27-43.

148.   Artursson, P., and Karlsson, J. (1991). Correlation between oral drug absorption in humans and apparent drug permeability coefficients in human intestinal epithelial (Caco-2) cells. Biochem Biophys Res Commun *175*, 880-885.

149.   Donjacour, A.A., Thomson, A.A., and Cunha, G.R. (2003). FGF-10 plays an essential role in the growth of the fetal prostate. Dev Biol *261*, 39-54.

150.   Nilsson, E., Parrott, J.A., and Skinner, M.K. (2001). Basic fibroblast growth factor induces primordial follicle development and initiates folliculogenesis. Mol Cell Endocrinol *175*, 123-130.

151.   Ahn, S.E., Kim, S., Park, K.H., Moon, S.H., Lee, H.J., Kim, G.J., Lee, Y.J., Cha, K.Y., and Chung, H.M. (2006). Primary bone-derived cells induce osteogenic differentiation

without exogenous factors in human embryonic stem cells. Biochem Biophys Res Commun *340*, 403-408.

152. Toimela, T., Maenpaa, H., Mannerstrom, M., and Tahti, H. (2004). Development of an in vitro blood-brain barrier model-cytotoxicity of mercury and aluminum. Toxicol Appl Pharmacol *195*, 73-82.

153. Milks, L.C., Brontoli, M.J., and Cramer, E.B. (1983). Epithelial permeability and the transepithelial migration of human neutrophils. J Cell Biol *96*, 1241-1247.

154. Cramer, E.B., Milks, L.C., and Ojakian, G.K. (1980). Transepithelial migration of human neutrophils: an in vitro model system. Proc Natl Acad Sci U S A *77*, 4069-4073.

155. Geroski, D.H., and Hadley, A. (1992). Characterization of corneal endothelium cell cultured on microporous membrane filters. Curr Eye Res *11*, 61-72.

156. Abouelfetouh, A., Kondoh, T., Ehara, K., and Kohmura, E. (2004). Morphological differentiation of bone marrow stromal cells into neuron-like cells after co-culture with hippocampal slice. Brain Res *1029*, 114-119.

157. Byers, S.W., Hadley, M.A., Djakiew, D., and Dym, M. (1986). Growth and characterization of polarized monolayers of epididymal epithelial cells and Sertoli cells in dual environment culture chambers. J Androl *7*, 59-68.

158. Savage, C.R., Jr., and Bonney, R.J. (1978). Extended expression of differentiated function in primary cultures of adult liver parenchymal cells maintained on nitrocellulose filters. I. Induction of phosphoenolpyruvate carboxykinase and tyrosine aminotransferase. Exp Cell Res *114*, 307-315.

159. Xiang, Z., Hrabetova, S., Moskowitz, S.I., Casaccia-Bonnefil, P., Young, S.R., Nimmrich, V.C., Tiedge, H., Einheber, S., Karnup, S., Bianchi, R., et al. (2000). Long-term maintenance of mature hippocampal slices in vitro. J Neurosci Methods *98*, 145-154.

160. Arnold, D., Feng, L., Kim, J., and Heintz, N. (1994). A strategy for the analysis of gene expression during neural development. Proc Natl Acad Sci U S A *91*, 9970-9974.

161. Wha Kim, S., Lee, I.W., Cho, H.J., Cho, K.H., Han Kim, K., Chung, J.H., Song, P.I., and Chan Park, K. (2002). Fibroblasts and ascorbate regulate epidermalization in reconstructed human epidermis. J Dermatol Sci *30*, 215-223.

162. Cam, Y., Meyer, J.M., Staubli, A., and Ruch, J.V. (1986). Epithelial-mesenchymal interactions: effects of a dental biomatrix on odontoblasts. Arch Anat Microsc Morphol Exp *75*, 75-89.

163. Lee, D.Y., Ahn, H.T., and Cho, K.H. (2000). A new skin equivalent model: dermal substrate that combines de-epidermized dermis with fibroblast-populated collagen matrix. J Dermatol Sci *23*, 132-137.

164. Artursson, P. (1990). Epithelial transport of drugs in cell culture. I: A model for studying the passive diffusion of drugs over intestinal absorptive (Caco-2) cells. J Pharm Sci *79*, 476-482.

165. Garcia-Perez, A., and Smith, W.L. (1984). Apical-basolateral membrane asymmetry in canine cortical collecting tubule cells. Bradykinin, arginine vasopressin, prostaglandin E2 interrelationships. J Clin Invest *74*, 63-74.

166. Ichijo, H., and Bonhoeffer, F. (1998). Differential withdrawal of retinal axons induced by a secreted factor. J Neurosci *18*, 5008-5018.

167. Pandiyan, P., Zheng, L., Ishihara, S., Reed, J., and Lenardo, M.J. (2007). CD4+CD25+Foxp3+ regulatory T cells induce cytokine deprivation-mediated apoptosis of effector CD4+ T cells. Nat Immunol *8*, 1353-1362.

168. Sojka, D.K., Huang, Y.H., and Fowell, D.J. (2008). Mechanisms of regulatory T-cell suppression - a diverse arsenal for a moving target. Immunology *124*, 13-22.

169. Omidi, Y., Campbell, L., Barar, J., Connell, D., Akhtar, S., and Gumbleton, M. (2003). Evaluation of the immortalised mouse brain capillary endothelial cell line, b.End3, as an in vitro blood-brain barrier model for drug uptake and transport studies. Brain Res *990*, 95-112.

170. Lundquist, S., Renftel, M., Brillault, J., Fenart, L., Cecchelli, R., and Dehouck, M.P. (2002). Prediction of drug transport through the blood-brain barrier in vivo: a comparison between two in vitro cell models. Pharm Res *19*, 976-981.

Chapter 2

Stability of Porous Nanocrystalline Silicon (Pnc-Si) in Cell Culture Media[*] [1]

2.1 Introduction

Membranes are used in a range of cell biology research experiments for which their stability and biocompatibility is imperative. Due to their molecular thinness, pnc-Si membrane stability can be susceptible to the chemical and mechanical effects of cell culture. Hence, apart from being efficient and scalable, it is crucial that pnc-Si is stable for biological applications. Membranes are viable cell culture substrates if their stability can be regulated without affecting their biocompatibility and sensitivity. Moreover, they should undergo non-cytotoxic degradation. Chemically stable and intact pnc-Si membranes are important for co-cultures [2] and quantitative studies of cell-cell communication and drug permeability. However, less stable pnc-Si membranes are advantageous as biocompatible and biodegradable scaffolds for tissue engineering or controlled drug delivery applications [3, 4].

Most of the membrane based cell culture applications are long term [2-4], lasting ~6-7 weeks. Although there are some short term cell culture experiments as well (ranging from 4-5 hours to 3-4 days) [5]. For such experiments, the membrane needs to maintain its integrity over the required time periods sustaining all the environmental influences, like the chemical effects of the components of the growth media in which the membrane is incubated and the stress due to cells that are proliferating on the surface. A typical cell growth media is composed of glucose (carbon source), inorganic salts (sodium chloride, sodium bicarbonate, chlorides, sulphates), amino acids (nitrogen source), vitamins, serum proteins (growth factors), antibiotics (ampicillin,

---

[*] The material in this chapter is prepared for a manuscript and at the time of writing it is ready for submission to Journal of *American Chemical Society-Nano*.

streptomycin), and buffers [6]. The following table lists the Invitrogen™ formulation of a common cell growth media, Dulbecco's Modified Eagle Medium (DMEM).

COMPONENTS	Molecular Weight	Concentration	
		(mg/L)	mM
Amino Acids			
Glycine	75	30	0.4
L-Alanine	89	35.6	0.4
L-Arginine hydrochloride	211	84	0.398
L-Asparagine	132	60	0.455
L-Aspartic acid	133	53	0.398
L-Cystine 2HCl	313	63	0.201
L-Glutamic Acid	147	59	0.401
L-Glutamine	146	584	4
L-Histidine hydrochloride-H2O	210	42	0.2
L-Isoleucine	131	105	0.802
L-Leucine	131	105	0.802
L-Lysine hydrochloride	183	146	0.798
L-Methionine	149	30	0.201
L-Phenylalanine	165	66	0.4
L-Proline	115	46	0.4
L-Serine	105	42	0.4
L-Threonine	119	95	0.798
L-Tryptophan	204	16	0.0784
L-Tyrosine	181	72	0.398
L-Valine	117	94	0.803
Vitamins			
Choline chloride	140	4	0.0286
D-Calcium pantothenate	477	4	0.00839
Folic Acid	441	4	0.00907
Niacinamide	122	4	0.0328
Pyridoxine hydrochloride	204	4	0.0196
Riboflavin	376	0.4	0.00106
Thiamine hydrochloride	337	4	0.0119
i-Inositol	180	7.2	0.04
Inorganic Salts			
Calcium Chloride (CaCl2-2H2O)	147	264	1.8
Ferric Nitrate (Fe(NO3)3"9H2O)	404	0.1	0.0002
Magnesium Sulfate (MgSO4-7H2O)	246	200	0.813
Potassium Chloride (KCl)	75	400	5.33
Sodium Bicarbonate (NaHCO3)	84	3700	44.05
Sodium Chloride (NaCl)	58	6400	110.34
Sodium Phosphate monobasic (NaH2PO4-2H2O)	154	141	0.916
Other Components			
D-Glucose (Dextrose)	180	4500	25
Phenol Red	376.4	15	0.0399

Pnc-Si being an ultrathin nanoporous substrate [7], can come under a chemical attack by the media components. Hence, it is important to keep the membrane stable in conditions optimum for typical cell growth experiments. Pnc-Si is a silicon based material and hence should have some resemblance to porous silicon in terms of its chemical properties responsible for biocompatibility and biodegradation [8].

Porous silicon is made by electrochemical etching of silicon wafers using ethanolic hydrogen fluoride solutions. P-Si porosity can be adjusted from macroporous (> 50 nm) to mesoporous (5-50 nm) to nano/microporous (< 5 nm) by varying the etching conditions [9]. P-Si is a well known biocompatible nanoporous material applicable in tissue engineering, biomaterial scaffolds and drug delivery applications [4, 10, 11]. P-Si is biodegradable in biological fluids to form benign monomeric orthosilicic acid (H_4SiO_4) through hydrolysis and oxidation [9, 12]. In nature, silicon primarily exists as silicic acid, with the general formula $[SiO_x(OH)_{4-2x}]_n$. Orthosilicic acid (H_4SiO_4), the most common aqueous form of silicon, is predominantly absorbed by humans from the environment and is readily removed by kidneys without causing any harm to the body [13, 14].

In 1995, Canham *et al* showed that the bioactivity of porous silicon could be varied significantly by changing its porosity [9]. Low porosity microporous layers displayed more stable configurations of bioactivity inducing hydroxyapatite growth and hence potential *in vivo* bonding ability. High porosity mesoporous layers exhibited substantial dissolution, implying biodegradability *in vivo*. Hence, the porosity of porous silicon can be varied depending on its potential application areas. For some biomedical applications, for example, drug delivery, material degradation is desirable, whereas for others such as biosensing, a stable interface between the pores and their biological environment is generally favorable. The ability to tune bioactivity *via* surface chemistry will provide much better flexibility than that available by choice of microstructure alone [15-17].

After the formation of porous silicon, the surface contains impurities from the air and the etching process. Common impurities include covalently bonded hydrogen, fluorine and oxygen. The levels of hydrogen and fluorine decrease over time as they are replaced with hydroxyl groups on hydrolysis by atmospheric water. Although the hydrogen coated surface is sufficiently stable when exposed to inert atmosphere for a short period of time, prolonged exposure render the surface prone to oxidation by atmospheric oxygen [18]. As much as 1% oxygen is normally adsorbed within minutes of air drying. Over a few days Si-O-Si, Si-O-H and O_3-Si-H groups are formed. These oxides at the P-Si surface are thought to improve its biocompatibility. Thus, several methods were developed to promote the surface stability and improve biocompatibility of porous silicon by enhancing the surface oxide quality [15-17].

One of the methods for improving P-Si stability is thermal oxidation. Thermal oxidation involves heating P-Si to a temperature above 1000°C for around 10-20 minutes to promote full oxidation of sub-oxide species to form a stable oxide layer. Thermally treated surfaces show improvements in the stability against oxidation [19]. After production, the P-Si surface starts losing Si-H passivation through atmospheric oxidation. By bridging Si-O-Si or Si-OH terminations formed by atmospheric oxidation and other partially unbalanced valences through thermal treatment, the surface layer becomes more stable against further oxidation/hydrolytic degradation.

Higher amounts of energy supplied through a broad pulse of heat shock could also be helpful in rearranging the surface oxide film. Rapid thermal processing (RTP) provides thermal energy in a short period of time (few seconds) which induces a higher quality of oxide layer. This more uniform oxide layer keeps the substrate stable for longer. Improvement in surface oxide quality was found to be evident from the superior photoluminescence of P-Si after RTP [20]. The study shows that the treated P-Si is a material in which hydrogen has been totally replaced by oxygen even on the internal surfaces of the pores. After fabrication, porous silicon has a fairly

disordered surface with random bridging oxygen atoms, lattice defects in the Si (imperfect grain boundaries), and random adsorbed water. The low-density native layer formed spontaneously after fabrication offers little protection against dissolution in biological media. By heating the sample through rapid thermal processing, enough energy is supplied so that some of these atoms can rearrange themselves, possibly creating a more continuous film. In addition, if there is any extra oxygen around while the membrane is getting heated, the oxide layer can actually grow in thickness as surface Si atoms get oxidized [21-23]. Densification could also take place by getting rid of substantial amount of sub-oxide species and even through change in the Si-O-Si bond angles [24, 25]. Surface treatments like UV-ozone cleaning of the substrate removes any kind of organic impurity from its surface. This treatment also makes the surface more hydrophilic and oxidized/hydroxylized [26-30]. In other work with porous silicon, the growth of an oxide layer *via* ozone oxidation considerably slowed silicon degradation in PBS [5].

In addition to oxidation, thermal carbonization also helps in stabilizing P-Si. In this technique, thermal dissociation of acetylene is exploited to carbonize porous silicon films. The carbon atoms from acetylene bind to the Si atoms of porous silicon substrate leaving porous silicon with improved stability due to SiC residues on its surface [31]. Other treatments like thermal nitridation and dodecene derivatization have also shown improved stability of porous silicon in simulated biological fluids [15, 16].

Surface functionalization alters the P-Si surface chemistry. It is known that a dense oxide layer provides protection to the underlying P-Si. Similarly, a layer of different chemistry could be used to enhance the stability. Silanization of P-Si surface covers the surface with a monolayer of self assembled silane molecules that has been found to be effective in stabilizing P-Si in aqueous environments [32]. In another study, amino-silanization was found to improve the stability of P-Si in PBS buffer. Coating of proteins such as serum (FBS) and collagen also stabilize porous silicon but not as much as the other treatments [5, 13].

Comparisons between the different treatment therapies to improve stability are made by investigating the rate of degradation. The degradation causes a change in the surface chemistry, and also release of silicic acid into the environment due to silicon dissolution. Surface chemistry and optical thickness of P-Si have been examined *via* transmission Fourier transform infrared (FTIR) spectroscopy [5] or inductively coupled plasma optical emission spectroscopy (ICPOES) [12]. Concentration of silicic acid produced during P-Si degradation can be measured by means of ammonium molybdate solution based colorimetric assay [13]. FTIR spectroscopy was used to measure the degradation rate of the various P-Si samples in neutral pH PBS buffer. By means of FTIR, it was found that simple oxidation stabilized P-Si significantly and functionalization with silanes further reduced the rate of hydrolytic dissolution. The results showed that the resistance to degradation could be attributed to thermal oxidation and further stabilization of the oxidized membrane could be achieved by amino-silanization [13].

Pnc-Si being a silicon based substrate is expected to have similar degradation mechanism as P-Si. Thus, similar tests could be used to assess the rate of degradation of pnc-Si in biological media. But due the ultrathinness of pnc-Si (15 nm), it might be difficult to resolve any change in pnc-Si's optical thickness or surface chemistry using techniques like FTIR, ICPOES spectroscopy. Also the spectrophotometric analysis in the ammonium molybdate colorimetric assay should be highly sensitive to detect the low amount of silicic acid produced from dissolution of pnc-Si. Though the optical thickness is difficult to resolve, any change in optical thickness causes a change in the wavelength of light reflected off the surface. Porous silicon shows change in its optical properties due to its degradation and thereby compromises its biosensing capabilities. This is as a result of change in optical thickness which records as a shift in the frequencies of light reflected off the surface. The variation in optical interference brings about a change in its color. Similarly, absorption or desorption of molecules on to the pore walls alters its porosity and the effective refractive index. Such a phenomenon is the fundamental

operating principle behind porous silicon based chemical and biological sensors [33-35]. So, an easier way to detect degradation of pnc-Si could be from changes in its optical properties.

In this chapter, effects of cell culture media on pnc-Si membrane are observed. Methods are developed to monitor pnc-Si membrane stability in cell culture media. Qualitative visual color changes of pnc-Si chip are found to directly correlate to nanoporous membrane stability and its biodegradation *in vitro* through a microparticle assay. In an effort to resolve the degradation mechanism, AFM and TEM images show that pnc-Si degrades through pore dissolution rather than flaking or cracking. Also, methods for enhancing and controlling membrane stability are investigated. Post production rapid thermal processing (RTP) renders the surface glass-like and stable for short-term experiments. The biodegradation rates of pnc-Si are further slowed down for some long-term cell culture applications by surface treatments like UV-ozone oxidation followed by amino-silanization. As a result, pnc-Si can be used for short term as well as long term cell culture applications.

2.2 Material and Methods

2.2.1 Materials

Pnc-Si was supplied by SiMPore Inc., Rochester, NY. Supplemented Endothelial Growth Medium (EGM) (Lonza), Dulbecco's Modified Eagle Medium (DMEM), 0.25% Trypsin-EDTA, Fetal Bovine Serum (FBS), penicillin/streptomycin, glutamine, Liebovitz L-15 media were purchased from Invitrogen (Carlsbad, CA, USA). Sodium bicarbonate, sodium chloride, sodium hypochlorite, DTT, hydrogen peroxide, cloning rings (6.4 mm inner diameter x 8 mm height) were purchased from Sigma (St. Louis, MO, USA). Methanol (MeOH), ethanol (EtOH) and all tissue culture-treated polystyrene (TCPS) plasticware were purchased from VWR.

2.2.2 Cell Culture

Cell studies were performed with primary human umbilical vein endothelial cells (HUVEC, Microbiology & Immunology Lab, University of Rochester Medical Center, Rochester, NY, USA) and immortalized mouse embryo fibroblasts (3T3-L1, ATCC, Rockville, MD, USA). These cells were cultured in T25 flasks (BD Falcon) at 37°C in a 5% CO_2, humidified atmosphere. HUVEC were grown in EGM with 2% L-glutamine, 1% penicillin/streptomycin and 10% FBS, and 3T3-L1 were grown in DMEM with antibiotics and serum. Media was changed every other day. Cells were harvested after reaching 70-80% confluence by trypsinization with 0.25% trypsin-EDTA and subsequently seeded at appropriate densities. HUVEC and 3T3-L1 were used between passages 4-8 and 17-25, respectively to avoid using aged cells.

2.2.3 Pnc-Si Fabrication

Pnc-Si membranes were fabricated using standard semiconductor processes, as recently described (Figure 1.12) [7]. Thermal oxide, ranging from 1000-4500 Å, was grown on both sides of a (100) n-type silicon wafer. The backside of the wafer was patterned using photolithography in order to form an etch mask for the nanocrystalline membranes. During lithography, the front side oxide was removed. A 3-layer silicon dioxide (40 nm)/amorphous silicon (15 nm)/silicon dioxide (40 nm) film stack was then deposited onto the bare silicon wafer by RF magnetron sputtering. The deposition rates for the silicon dioxide and amorphous silicon layers are well-characterized [7]. A Surface Science Integration (Solaris 150) Rapid Thermal Processing (RTP) system (El Mirage, AZ) was used (850-1050°C) to transform the amorphous silicon to a nanocrystalline state. The membrane was exposed by etching the back side of the silicon wafer with a preferential silicon etchant, Ethylenediamine pyrocatechol (EDP). Due to its high silicon to oxide etch selectivity, the EDP etch terminated at the first protective oxide layer in the membrane film stack. Finally, the protective oxide layers were etched with buffered oxide

etchant (BOE), releasing the freely suspended porous nanocrystalline silicon membrane. The mask was designed to yield approximately 80 samples per silicon wafer. Each sample contained two approximately 2000 x 100 µm slits with freely suspended 15 nm thick pnc-Si membranes. This pattern can be altered and the active area can be changed according to need. Each pnc-Si chip has a 'well-side' and a 'membrane-side'. Well side is the side which is etched to expose the polynanocrystalline material and thus has trough-like features, whereas, membrane side is the coinciding planar side showing the membrane's face with slits containing the free standing membrane. The 'membrane side' has both supported as well as free standing pnc-Si material exposed unlike the 'well side' which just shows the free standing portion.

2.2.4 Post Production Rapid Thermal Processing

Typically, pnc-Si samples underwent an additional post-production thermal processing step in the Rapid Thermal Processing unit (SSI Solaris 150 Rapid Thermal Processing Unit) to enhance its stability. Samples were placed on a silicon carbide-coated graphite susceptor and exposed to Argon gas. The temperature was increased at 10°C/s to a steady state of 800°C. Samples were maintained at 800°C for 5 minutes, cooled to 25°C and used without further processing.

2.2.5 Pore Processing

Transmission electron microscopy (TEM) was used to determine if the rapid thermal processing changed the pore properties of pnc-Si. Specifically, plan-view transmission electron microscopy of untreated and thermally processed pnc-Si was performed in bright-field mode at 80 kV using a Hitachi H-7650. Images were acquired with an Olympus Cantega 11 megapixel digital camera. The digital images were then processed using a custom MATLAB script that calculated pore statistics (available for public download at *www.nanomembranes.org*). The MATLAB code identified pores in the TEM images based on a user-defined threshold that created a binary image. Equivalent pore diameters were calculated by extracting the radius of a circle that had

an area equal to the identified pore. Histograms of all identified pores were presented as a ratio of "contributed" pore area at a specific diameter to the total image area.

Atomic force microscopy (AFM) was used to measure pore characteristics and surface roughness over a time period for which the pnc-Si samples were incubated in serum free media (DMEM) @ 37°C in oven. Images were acquired entirely using high aspect ratio Olympus AC160 cantilevers (mean tip radius < 15 nm) in repulsive mode of Asylum Atomic Force Microscope. The image processing and control program (IGOR) for the AFM was used to select a linear region of interest on the height image and a cross-sectional height scan was used to estimate the pore diameter. Further, the images were inverted in ImageJ and then were processed using custom MATLAB script. Appropriate threshold was selected and pore statistics were calculated. The calibration for all AFM images was 0.55 pixels/nm.

2.2.6 Rhodamine Diffusion

To determine whether the post-production thermal processing of pnc-Si in the RTP unit affected molecular diffusion though nanoporous pnc-Si, the diffusion profile of rhodamine was measured. This was done because pores identified in TEM images may not have been open pores. Pnc-Si samples were attached to a PBS-coated glass cover slip with vacuum grease and 100 μM rhodamine 6G (Sigma) in 1X PBS was added to the backside of pnc-Si. Rhodamine diffusion through pnc-Si membranes was monitored by a Zeiss Axiovert 200M epifluorescent microscope for 20 minutes, and the time-lapse images were characterized using a customized MATLAB program. The MATLAB code was written to select a fixed rectangular region from the time-lapse images based on user-defined input parameters (width, length, and centroid). A line-scan of fluorescence intensities along the length of the rectangular region was obtained by averaging the fluorescence intensities across the width of that region. The averaging was performed to

reduce background noise. The line-scans from successive time-lapse images were then plotted along the temporal-axis to produce the diffusion profile.

2.2.7 Chemical Stability and Biodegradation

a) Discoloration and Bead Assay

To measure membrane stability, polystyrene cloning rings were attached to pnc-Si with vacuum grease (silicone) in order to isolate the pnc-Si samples and these samples were incubated at 25°C in serum-supplemented DMEM. A solution of 15 µm polystyrene beads (4 µl in 1.5 ml de-ionized H_2O) (FS07F, Bangs Laboratories) was then added to the DMEM contained within the cloning rings. The cloning rings prevent the beads from rolling off the pnc-Si chip surface. After allowing the beads to settle for ~20 minutes, images were captured for over 30 hours to monitor the membrane integrity *via* time-lapse phase contrast microscopy. Microscopy was performed with a 10X objective on an epifluorescent Nikon Eclipse TS-100F inverted microscope equipped with Cooke SensiCam cooled CCD camera. To measure discoloration, pnc-Si samples were sterilized with MeOH and then incubated in serum-supplemented DMEM under cell culture conditions or at 25°C. Once a day, samples were removed from the media, rinsed in de-ionized H_2O and 70% EtOH, imaged with a Canon PowerShot A650IS 12.1 megapixel digital camera, sterilized in MeOH and returned to culture plates. Pnc-Si membrane stability and chip discoloration were monitored for 7 days. To investigate whether cells affected discoloration and membrane stability, 3T3-L1 cells were seeded directly into wells with pnc-Si samples.

b) Pnc-Si in Media and Other Chemicals

For monitoring discoloration in non sterile conditions in different media, salts, buffers and other chemicals, samples were rinsed in de-ionized H_2O followed by 70% EtOH and dried to clean any debris off the surface. They were then incubated in the desired solution taken in tissue culture wells in oven at 37°C. Samples were removed from the solution at desired time points,

rinsed in de-ionized H_2O and 70% EtOH, imaged with a Canon PowerShot A650IS 12.1 megapixel digital camera and returned to culture plates.

c) Dissolution of Pnc-Si in Media

Pnc-Si samples were sterilized and incubated in serum-free DMEM in the oven @37°C. Samples were taken out at different time points (0, 90 min, 150 min, 6 h and 24 h). Individual samples were taken for respective time points. They were thoroughly rinsed in de-ionized H_2O and IPA followed by N_2 gas blow drying and then sent for TEM/AFM imaging.

d) Enhancing Stability of Pnc-Si by Liquid-Phase Silanization

Samples were treated in a UV-ozone chamber (Novascan PSD-UVT-UVOP) for 15 minutes at 30°C to clean and decontaminate any organic matter or impurities off the surface. This treatment also renders the samples oxidized before the silane deposition. 5 ml de-ionized H_2O was mixed with 4.8 ml MeOH in a petridish and kept covered. 2 ml of APTES (3-Aminopropyltriethoxysilane) was added to this solution followed by 40 µl of glacial acetic acid which helps in hydrolysis. The solution mixture was stirred properly and left covered for 10 minutes. The UV-ozone treated samples were dipped in the solution for 15 minutes. Vacuum grease (silicone) was used to anchor as well as lift the chips off the bottom so that both the sides are exposed to the silane solution. Samples were taken out and rinsed in de-ionized H_2O followed by running isopropyl alcohol (IPA) through the tweezers. After this they were dipped in Pentane for 10 seconds and dried using Nitrogen gas. They were then left to bake in the oven at 75°C for 30 minutes and the amino-silanized samples were ready for use.

2.3 Results and Discussion

2.3.1 Correlation between Pnc-Si Degradation and Discoloration

Porous silicon films dissolve in physiological media and produce soluble silicic acid compounds [5, 12]. In days-long cell proliferation experiments, the deposited silicon films were chemically attacked by cell culture media, and changes in the optical interference of these silicon layers were manifest as changes in pnc-Si color, as seen for P-Si [10]. In fact, this pnc-Si degradation was observed conveniently as color changes from native dark blue to purple-pink to yellow-gold to silver (Figure 2.1). For example, complete removal of the thin crystalline silicon film after ~1 day exposed the yellow color of the oxide-coated silicon wafer.

We investigated the mechanism of discoloration and its ramifications for cell culture. This was particularly important because of the ultrathinness of pnc-Si membranes. Chemically stable and intact pnc-Si membranes are imperative for co-cultures [2] and quantitative studies of cell-cell communication and drug permeability. However, less stable pnc-Si membranes are advantageous as biocompatible and biodegradable scaffolds for tissue engineering or controlled drug delivery applications [3, 4].

a) Microparticle Bead Assay as a Method to Visualize Pnc-Si Breakage

To correlate the membrane stability to qualitative color changes, a microparticle assay was developed. The free standing membrane is optically transparent in growth media and thus it is difficult to monitor its integrity through phase-contrast or fluorescence microscopy. For this assay, 15 μm polystyrene beads were allowed to settle on top of pnc-Si membranes and then viewed with an inverted microscope. The beads could be focused at the height of the membrane slit edges which showed that the free standing membrane is intact. When pnc-Si membranes broke, polystyrene beads dropped out of the focal plane, through the well volume at the backside of the chip and onto the bottom of the 6-well plates (Movie 1: Phase-contrast movie of

microparticle assay in Supplementary Compact Disk). Therefore, this assay detected pnc-Si membrane breakage as a change in microparticle focus. The pnc-Si membranes broke after 12-13 hours at 25°C in serum-supplemented DMEM (Figure 2.1). This time consuming assay clearly demonstrated membrane breakage, but a simpler indication of membrane integrity was desired. As the material dissolves in media, the layer thickness decreases causing optical interference or change in the wavelength of the reflected light off its surface. Therefore, pnc-Si chip color was closely tracked simultaneously with membrane breakage. Membrane breakage occurred as the chip started to discolor from blue to purple. Hence, pnc-Si chip discoloration directly correlated to membrane integrity, and tracking discoloration was much easier than visualizing the breakthrough of beads.
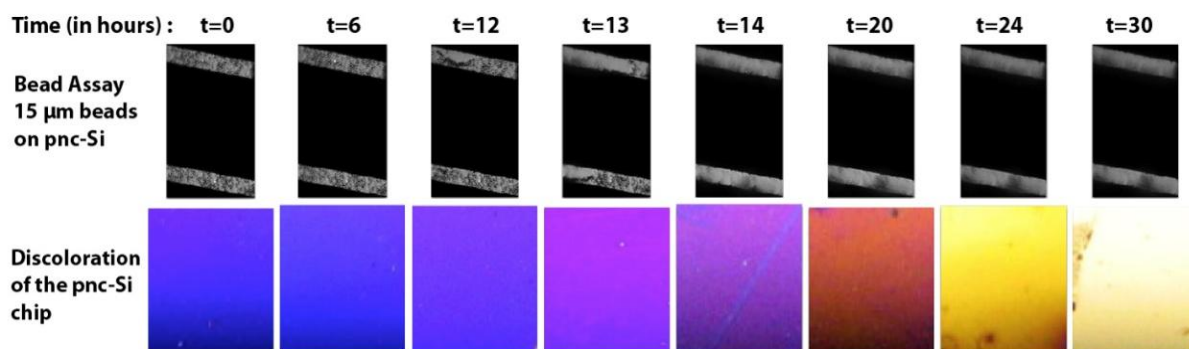

Figure 2.1 Correlation between pnc-Si membrane integrity and chip discoloration over 30 hours in serum-supplemented DMEM at 25°C. Top panels: 15 μm polystyrene beads settled on pnc-Si and were located *via* phase microscopy. At ~12 hours, the pnc-Si membrane broke and the polystyrene beads fell out of the focal plane. Bottom panels: pnc-Si chip discoloration showed a change in color from bright blue to gold over 30 hours. The initial transition from blue to purple closely matched the time point of membrane breakage.

These experiments showed that pnc-Si membranes were stable in serum-supplemented cell culture media for about 12 hours before significant membrane biodegradation occurred. Because long term stability is necessary for many applications, we questioned if surface modifications could promote pnc-Si stability in biological media. One of the steps in fabrication involved stripping of protective oxide layers to expose the pnc-Si [7]. It was observed that non-

stripped samples did not discolor in cell growth media for a long time. Our observation that the protective oxide stabilizes membranes motivated the hypothesis that densification of the spontaneously formed superficial native oxide (of ~1 nm thickness) on pnc-Si (after fabrication and oxide stripping) could leave the membrane film stable and protect it from chemical attack.

b) Post Production Rapid Thermal Processing of Pnc-Si

To investigate the ability of a densified native oxide to promote stability, pnc-Si samples underwent rapid thermal processing. Rapid thermal processing (RTP) provides thermal energy in a short period of time (few seconds) which induces a higher quality oxide layer. A rapid thermal processing step could also be densifying the native oxide layer formed spontaneously after the fabrication by getting rid of substantial amounts of sub-oxide species. After fabrication, porous silicon has a fairly disordered surface with random bridging oxygen atoms, lattice defects in the Si (imperfect grain boundaries), and random adsorbed water. This is a low-density layer that provides little protection. By heating the sample through RTP, enough energy is supplied so that some of these atoms can rearrange themselves, possibly creating a more continuous film. In addition, if there is any extra oxygen around while the membrane is heated, the oxide layer can actually grow in thickness as surface Si atoms get oxidized [21, 22, 24]. As an additional benefit, post production rapid thermal processing renders the surface similar to bioactive glass [36] [37].

After a post-production thermal processing step in the RTP unit was performed, discoloration experiments were conducted as described above. Untreated pnc-Si discolored from blue to gold within 1 day, which agreed with our previous experiments (Figure 2.1). By contrast pnc-Si with a densified surface oxide layer and/or stabilized grain boundaries *via* RTP discolored after 4 days (Figure 2.2). Therefore, post-production thermal processing significantly passivates the chemical attack on pnc-Si by cell culture media. The RTP temperature, time and ramp rate

could be used to regulate the life of pnc-Si membrane. In presence of 3T3-L1 cells, treated membranes were less stable (discoloration in 3 days), which was likely due to chemical or pH microenvironments created by growing cells. In other work with porous silicon [5], the growth of an oxide layer considerably slowed silicon degradation.
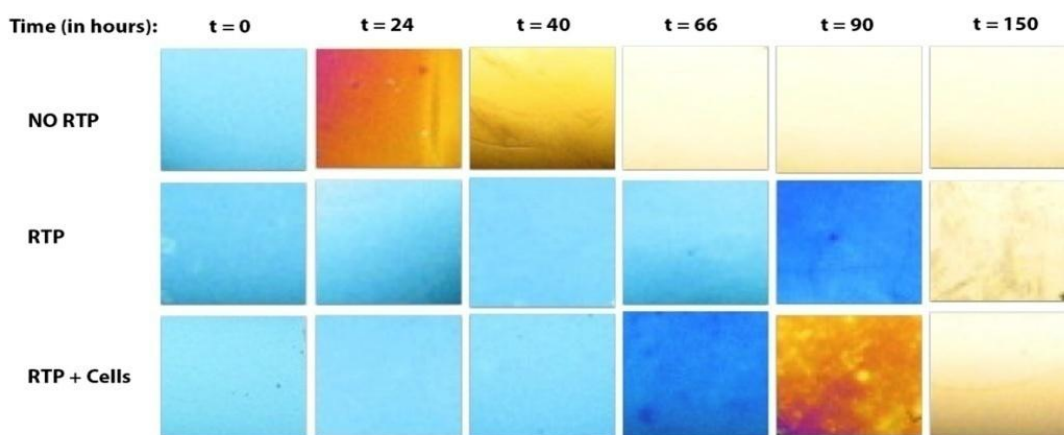

Figure 2.2 Effect of post-production thermal processing in the RTP on chip discoloration under cell culture conditions in serum-supplemented DMEM. Without post-production RTP, pnc-Si samples discolored from blue to gold within 1 day (top). RTP delayed discoloration by at least 4 days, with discoloration noted after ~7 days (middle). The presence of cells (3T3-L1) along with pnc-Si increased the rate discoloration, such that the color change from blue to gold occurred between three and four days (bottom).

c) Physical Effects of RTP on Pnc-Si

Post-production thermal processing in RTP enhanced chemical stability and lowered biodegradation rates but the physical effects (i.e., changes in pore size, porosity) of this processing were unknown. One concern was that the porosity of the membrane could be reduced by RTP. Therefore, pnc-Si samples were visualized with TEM before and after thermal treatment in the RTP. TEM micrographs showed no difference in pore diameter or porosity (calculated *via* custom MATLAB-based image processing, Figure 2.3 A) between untreated and annealed samples (Figure 2.3 B).
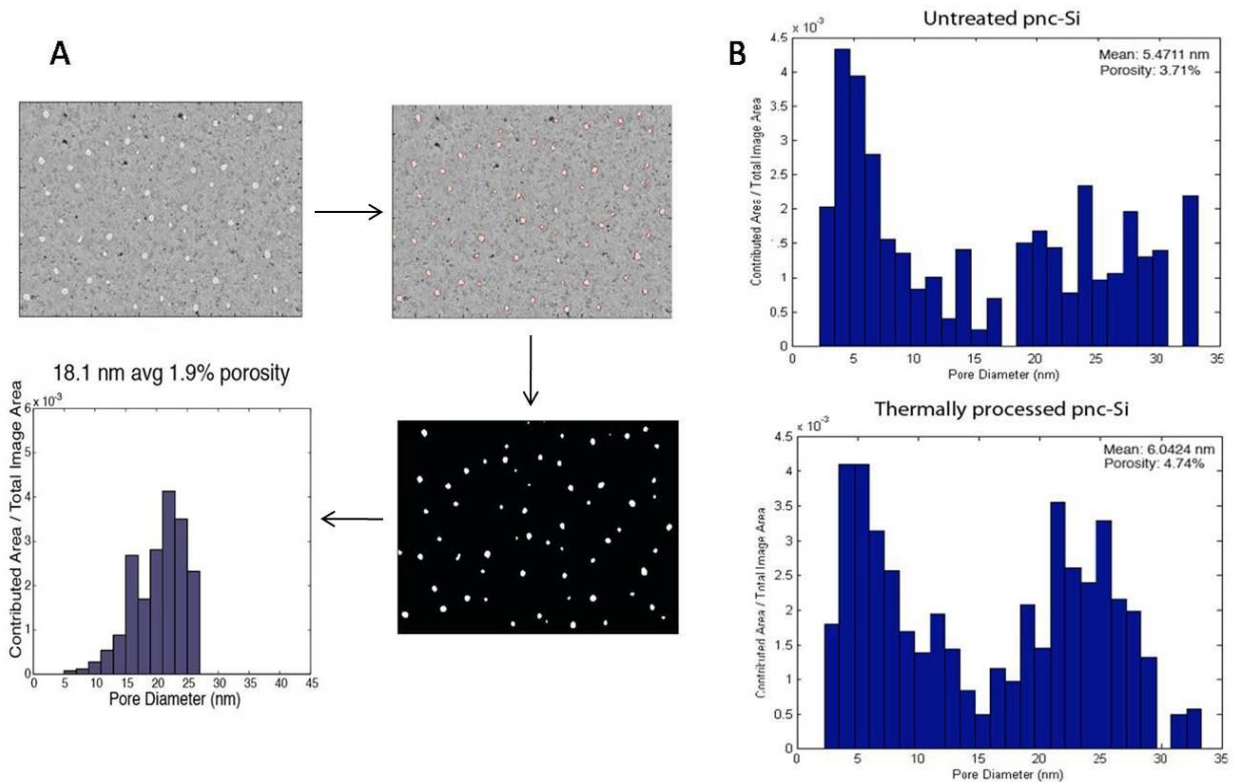
Figure 2.3 A) Pore size histograms of untreated and thermally processed pnc-Si were created from a customized MATLAB program that also determined mean pore size and porosity (calculated as the pore area/total image area), B) The untreated pnc-Si sample had a mean pore size of ~5.5 nm and porosity of ~3.7%. A thermally processed pnc-Si sample from the same manufacturing batch exhibited similar mean pore size (~6 nm) and porosity (~4.6%). The maximum pore sizes of these two samples were the same (~33 nm) and the pore size distributions were highly similar.

A more biologically relevant experiment was also performed to check if the pores were functional in which Rhodamine 6G diffusion was measured through pnc-Si membranes. Diffusion profiles of untreated and thermally-processed samples were not significantly different (Figure 2.4), which showed that post-production RTP did not alter the porosity or pore sizes of pnc-Si membranes. In the future, this test should be repeated using a larger dye molecule. Rhodamine 6G has molecular size of less than 1 nm, which is low to compare changes in sizes of similar order.
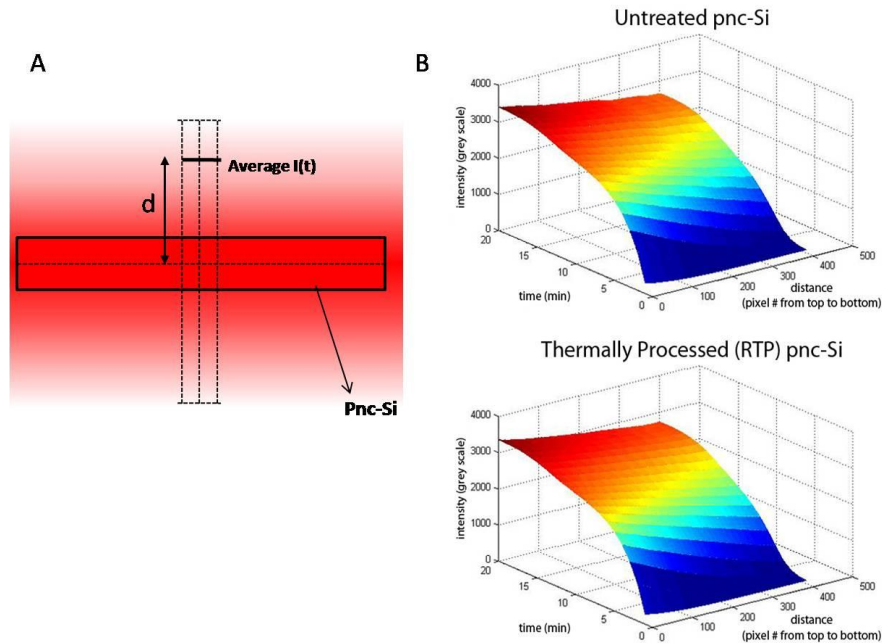
Figure 2.4 A) Schematic of rhodamine diffusion across pnc-Si and its measurement. Fluorescent intensities were measured along a line perpendicular to a pnc-Si membrane window for 20 minutes, B) Rhodamine diffusion profiles across untreated and thermally processed pnc-Si. Fluorescent intensities decreased with the distance from the window (distance axis) and increased with time. Importantly, the diffusion profiles of untreated and thermally processed pnc-Si were nearly identical.

d) Mechanism of Pnc-Si Degradation

Further understanding of the discoloration mechanism is an active area of research in the Nanomembrane Research Group. There are two hypotheses derived for the mechanism of pnc-Si membrane degradation and related discoloration (Figure 2.5).

i) Simultaneous degradation: The dense native silicon dioxide layer slowly dissolves under chemical attack from the media components to form orthosilicic acid. The dissolution takes place according to the given equation. At the same time, pnc-Si oxidizes to form silicon dioxide (oxidation takes place as media enters the pores from either side of the membrane). In combination these processes lead to continuous depletion of the membrane.

$$SiO_2 + 2H_2O \rightarrow H_4SiO_4$$
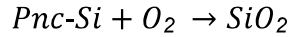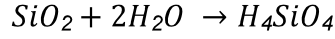
$$Pnc\text{-}Si + O_2 \rightarrow SiO_2$$

The SiO$_2$ layer depletes slowly at a rate equal to the difference between rate of formation (or rate of pnc-Si oxidation) and rate of degradation (or rate of orthosilicic acid formation). This hypothesis states that there is continuous depletion of pnc-Si and once pnc-Si is completely consumed, there is no further SiO$_2$ formation. Hence the remaining SiO$_2$ continues to degrade as orthosilicic acid leading to exposure of the bare silicon surface. At this point the color of the pnc-Si chip turns silver.
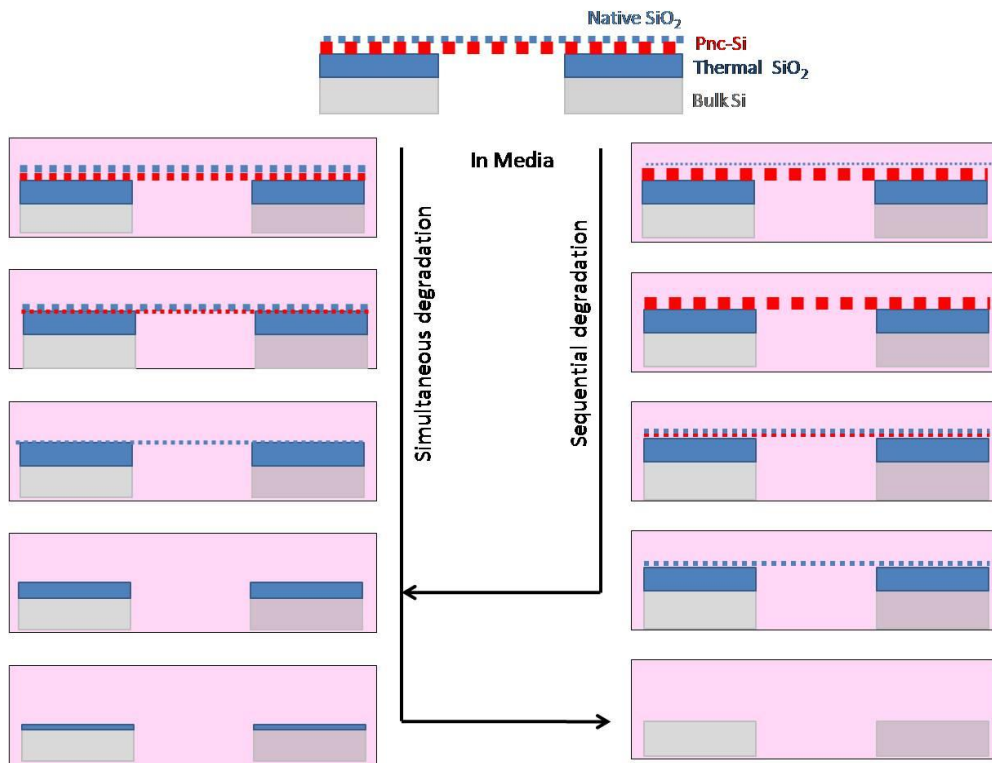
Figure 2.5 In simultaneous degradation mechanism, continuous depletion of the silicon dioxide and pnc-Si layer takes place. Silicon dioxide converts to orthosilicic acid and pnc-Si gets oxidized. In sequential degradation mechanism, silicon dioxide depletion completes to expose the pnc-Si. Exposed pnc-Si gets oxidized to form more silicon dioxide which further dissolves. Both degradation mechanisms lead to change in thicknesses of the layers and thus the color of the pnc-Si chip.

ii) Sequential degradation: Pnc-Si is protected by the oxide layer until the oxide completely depletes under the chemical attack to form orthosilicic acid.

$$SiO_2 + 2H_2O \rightarrow H_4SiO_4$$
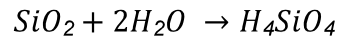
Once the oxide layer is gone, pnc-Si is exposed and undergoes oxidation forming SiO_2. This turns the membrane's yellowish tinge transparent (SiO_2).

$$Pnc\text{-}Si + O_2 \rightarrow SiO_2$$
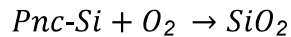
Now the new SiO_2 formed again dissolves in media as orthosilicic acid. After complete conversion of pnc-Si to SiO_2, followed by dissolution of SiO_2, bare Si is exposed resulting in silver pnc-Si chip color.

Both the hypotheses can be tested by characterization of surface layers using techniques such as ellipsometry, X-ray photoelectron spectroscopy, FTIR or Infrared absorption spectroscopy.

e) Analysis of Pnc-Si Dissolution

Both the flat pnc-Si membrane surface and the inner pore walls are attacked by the media. After fabrication, the pore edges are smooth and round. They become rough and irregular in shape as discoloration occurs in biological media, as evident from the TEM images (Figure 2.6 B). The AFM analysis supported the TEM data. It also showed an increase in the roughness (rms) of pnc-Si surface from 0.16 nm to 0.22 nm to 0.33 nm on incubation in serum-free media for 0, 90 and 150 minutes respectively (Figure 2.6 A). This may be attributed to the deposition of proteins and precipitates from the media [38-40] or due to the irregular erosion of the material from its surface.

The changes in cut-off pore sizes and porosity observed by TEM images are in agreement with the AFM images as well (Figure 2.6 C). After running the pore processing software for the TEM images, it was found that the mean pore diameter increased from ~13 nm to ~17 nm after incubation for 150 minutes in serum-free DMEM at 37°C in oven. Also the cut off diameter

increased from ~30 nm to ~40 nm. This is similar to the AFM images which showed increase in mean pore diameter from ~13 nm to ~23 nm over 150 minutes of incubation. From these tests, it is evident that dissolution of pnc-Si is taking place and not delamination or cracking and flaking of the material.
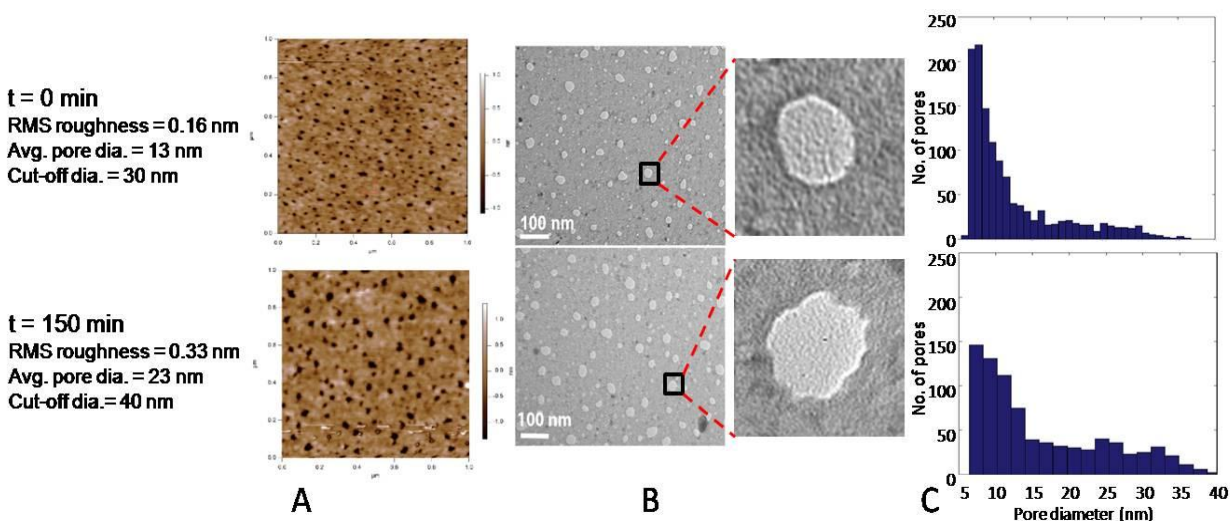
Figure 2.6 A) Atomic force microscopy on pnc-Si samples before and after incubation in serum-free DMEM (Image courtesy: Barrett J. Nehilla). Images show increase in roughness, mean pore size and cut-off diameter after 150 minutes of incubation, B) Transmission electron microscopy on the same pnc-Si samples show similar increase in mean pore size and change in shape of the pore edges (inset) (Image courtesy: David Fang), C) Histograms from pore processing program show increase in number of pores with bigger diameter and increase in cut-off diameter.

2.3.2 Other Influences on Pnc-Si and Its Dissolution

To understand which components of culture media were responsible for pnc-Si degradation, pnc-Si was exposed to a range of media and buffers and monitored for discoloration. Pnc-Si discolored in serum-supplemented cell growth media such as Dulbecco's Modified Eagle Medium (DMEM) and Endothelial Growth Medium (EGM) over time. However, it did not discolor in Leibovitz's L-15, a sodium bicarbonate free media used to support cell growth in non-CO_2 equilibrated environments (Figure 2.7). No discoloration in L-15 media suggests a role for

sodium bicarbonate in discoloration. Sodium bicarbonate is commonly used for buffering cell culture media in CO_2 equilibrated environments (5-10% CO_2). This non toxic buffer improves the pH control of media and provides cells with carbonate ions that are necessary for their metabolic functions.
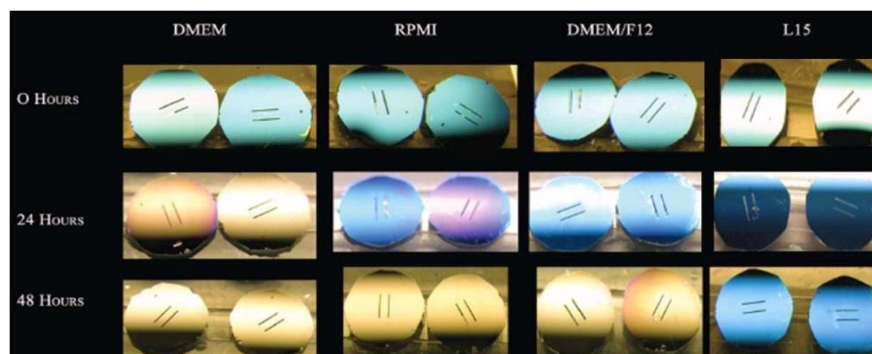
Figure 2.7 Discoloration does not take place in L-15 as it does in DMEM and RPMI media. Sodium bicarbonate-free L-15 media does not discolor pnc-Si over a span of at least 2 days under incubation. DMEM causes discoloration within a day followed by RPMI that discolors pnc-Si within two days. Both DMEM and RPMI constitute sodium bicarbonate and this implies its role in pnc-Si degradation (Courtesy: Barrett J. Nehilla)

The following set of chemical equations describes the mechanism in which sodium bicarbonate maintains pH levels in CO_2 equilibrated environments.

$$(1) \quad CO_2(l) + H_2O <=> H_2CO_3 <=> HCO_3^- + H^+$$

$$(2) \quad NaHCO_3 <=> HCO_3^- + Na^+$$
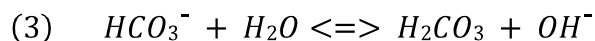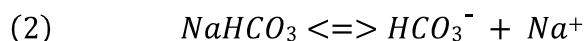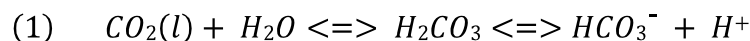
$$(3) \quad HCO_3^- + H_2O <=> H_2CO_3 + OH^-$$

$$From\ (2)\ and\ (3),\ \ NaHCO_3 + H_2O <=> H_2CO_3 + OH^- + Na^+$$

To investigate the role of sodium bicarbonate, discoloration of pnc-Si in different concentrations of sodium bicarbonate was monitored. It was found that with increasing concentrations of sodium bicarbonate, the rate of discoloration increased (Figure 2.8). Aqueous solutions of

sodium bicarbonate are mildly basic and are commonly used to elevate pH levels. Thus, high pH could be responsible for degradation and discoloration of pnc-Si. In addition, acidic conditions are used in the fabrication process of pnc-Si [7].
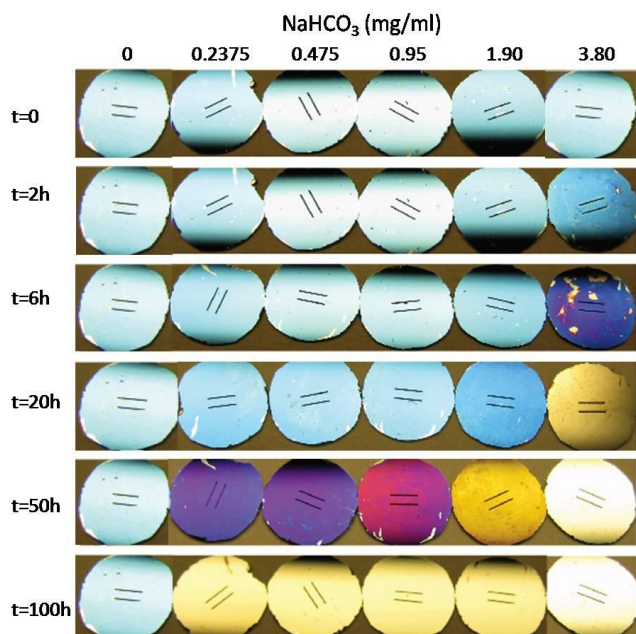
Figure 2.8 Sodium bicarbonate dose responses in the oven @ 37°C. Increase in concentrations of sodium bicarbonate resulted in increase in the discoloration rate. NaHCO$_3$ concentrations lower than 3.8 mg/ml caused comparatively slower discoloration, whereas 3.8 mg/ml appeared to be a threshold above which discoloration rates are much higher. This experiment was conducted in non-sterile conditions in the oven.

Interestingly, pnc-Si immersed in DMEM was found to be more stable in cell culture conditions (pCO$_2$ ~5%, relative humidity ~90%) than in the oven (pCO$_2$ < 0.1%, relative humidity ~60%) at the same temperature of 37°C (Figure 2.9 A). One important difference between the incubator and the oven is the pCO$_2$ level. Higher pCO$_2$ levels in the incubator leads to CO$_2$ acidification, thus decreasing the pH. This could explain the reason for pnc-Si stability in incubator but not in the oven. Also, with increase in the oven temperature the rate of discoloration increased, which is understandable from the dissolution reaction rate kinetics [12].

Biological media includes various other salts that could have a role in discoloration. To investigate this, sodium chloride, a sodium-based salt apart from sodium bicarbonate, was tested. Pnc-Si was immersed in increasing concentrations of NaCl at room temperature. It was found that higher concentrations of NaCl caused discoloration at a faster rate than lower concentrations (Figure 2.9 B).
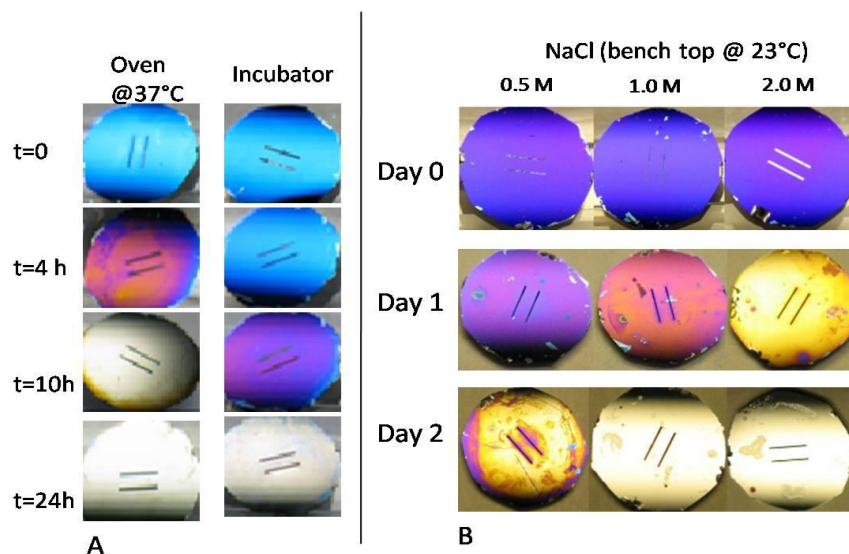
Figure 2.9 A) Comparison of discoloration rates in the oven and incubator with DMEM. Pnc-Si sample discolored completely in the oven after 10 hours, whereas, it took almost 24 hours in the incubator for pnc-Si to turn silver, B) Sodium chloride dose responses on bench top @ 23°C. Like sodium bicarbonate, discoloration rate of pnc-Si increased with the increase in the concentration of sodium chloride solution. The salt solutions used here are highly concentrated and thus the experiment was conducted at room temperature.

To incorporate effects of pH as well as salts and figure out the dominant factor amongst the two, solutions with different combinations of NaCl and $NaHCO_3$ concentrations were used. It was expected that the mixture with highest concentrations of both NaCl and $NaHCO_3$ would result in fastest discoloration and solution with lower concentrations will cause slower discoloration. Solutions with higher $NaHCO_3$ and lower NaCl were expected to cause discoloration due to higher pH of NaOH formed, whereas those with lower $NaHCO_3$ and higher NaCl were expected to discolor due to higher salt concentration. The difference in the discoloration rates due to solutions with different concentrations of NaCl and $NaHCO_3$ could help in determining the dominant factor. In several trials of this experiment, no clear trend for discoloration with sodium chloride and sodium bicarbonate was observed. Experiments are still going on to elucidate the exact mechanism involved.

Previous work in the lab showed that addition of a strong reducing agent, DTT (dithiothreitol-Cleland's reagent), did not prevent discoloration and that the addition of a strong oxidizing agent like hydrogen peroxide did not increase discoloration rate. On the other hand, oxidizing agent like sodium hypochlorite (bleach) with higher pH (pH~11) discolored pnc-Si to some extent. This indicates that the degradation mechanism is not just simple oxidation. From all the different experiments conducted, it suggests that there is interplay of pH changes, salt concentrations and pnc-Si characteristics that decide the life of this material in biological media.

Like other three dimensional tissue scaffolds or drug delivery system, dissolution of pnc-Si should also depend on its porosity and pore size [9, 12, 41]: once the pores get bigger or the porosity increases, the degradation process should accelerate because of increased internal surface area. To test this idea, samples of pnc-Si with different porosities were taken and tested in DMEM over a time period. As can be seen in figure 2.10, the sample having micro-size pinholes was found to completely discolor in 3 hours, whereas the sample with no pores did not start discoloring at this time point. There was not much of a difference between samples with porosities of 1.23% and 6.48%, but their discoloration rates were in between the highly porous and non-porous samples. It was evident that the rate of discoloration here increased with increase in total surface area or porosity of membranes.
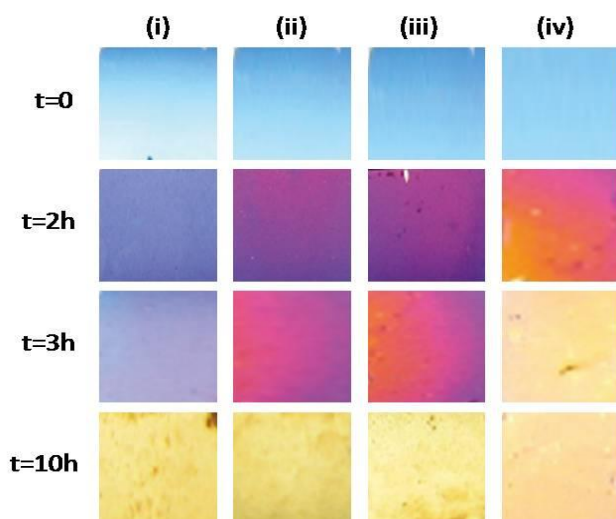
Figure 2.10 Discoloration is proportional to porosity of the membrane. Samples with different porosities were tested in serum-free DMEM in oven @ 37°C. Samples with (i) no visible pores, (ii) porosity of 1.23% and mean pore size of 6.7±1.9 nm, (iii) porosity of 6.48% and mean pore size of 8.1±2.7 nm, (iv) pin-holes (~10 µm in size) were used.

Degradation of membrane barrier can be helpful in creating stratified tissue or graft *in vitro.* Two different populations of cells can be cultured on either side of the membrane support, such as endothelial cells and smooth muscle cells, and co-join as the membrane dissolves [42].

2.3.3 Enhancing Stability of Pnc-Si

With the additional post production thermal processing step in RTP, the degradation of pnc-Si was prevented for 3-4 days (Figure 2.2). This sustainability needs to be further increased for conventional applications of pnc-Si in the fields of co-culture and drug permeability assays. Different surface treatments are known to increase stability of porous silicon in physiological conditions. These treatments could be applied to a novel material like pnc-Si to further delay its dissolution without hampering the biocompatibility. In the same way that a dense oxide layer provides protection to underlying pnc-Si, other surface chemistries might enhance stability without compromising the cell culture applications [13, 32]. Silane coupling agents that contain three inorganic reactive groups (ethoxy in case of 3-aminopropyl triethoxy silane) bond well to the metal hydroxyl groups on inorganic substrates like silicon (Figure 2.11).
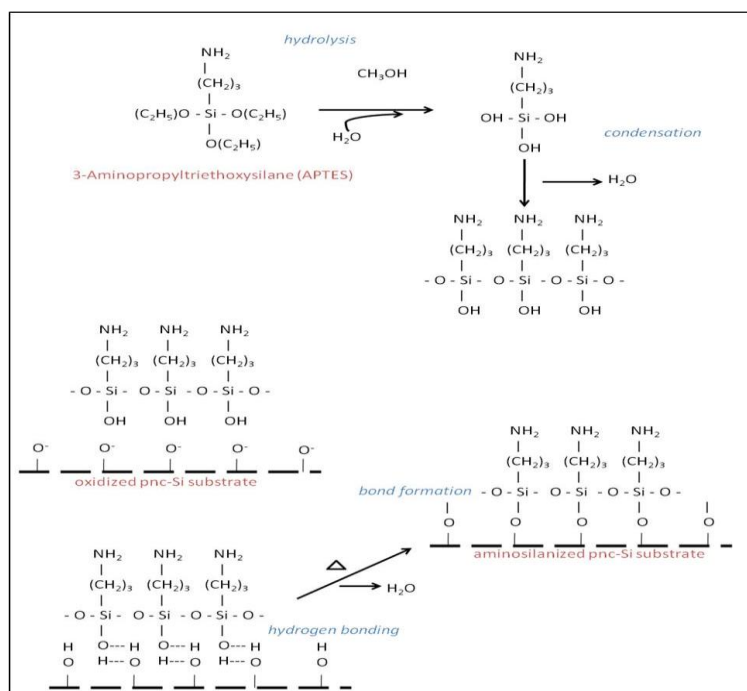
Figure 2.11 The alkoxy groups on silicon in APTES hydrolyze and self assemble to form silanols, either through the addition of water or from residual water on the inorganic surface. The silanols coordinate with metal hydroxyl groups on the inorganic surface to form an oxane bond and eliminate water. Silane molecules also react with each other to give a multimolecular structure of bound silane coupling agent on the surface [43].

Liquid-phase amino-silanization was used to provide a protective amino-silane layer on the pnc-Si surface to help prolong its discoloration. UV-ozone treatment of pnc-Si renders the surface hydrophilic and oxidized/hydroxylized for the amino-silane to bond. As can be seen in the figure 2.12, when incubated in serum-free DMEM, the amino-silanized sample discolored after 12 hours in comparison to non-silanized sample which almost turned gold after 7 hours. A combination of RTP and silanization worked better than just RTP (< 12 hours) and provided stability for ~28 hours.
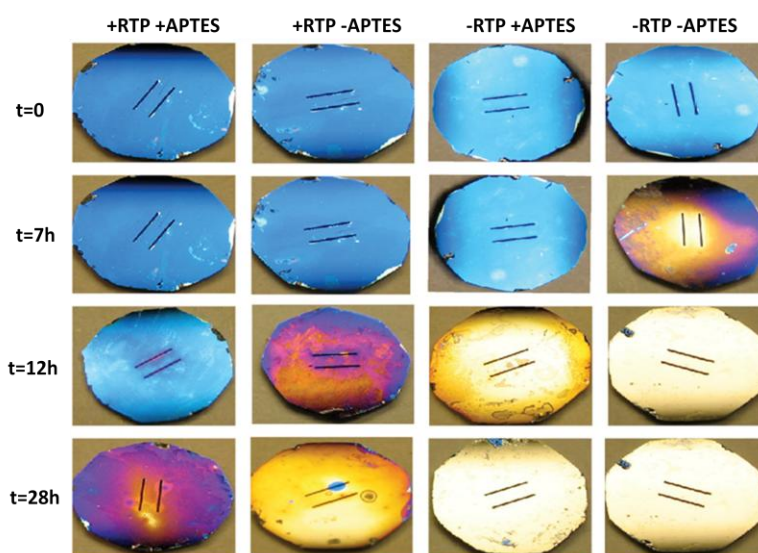
Figure 2.12 Pnc-Si samples after RTP and APTES treatment were tested for chemical stability in serum-free DMEM in oven @ 37°C. The non-treated sample started discoloring after 7 hours followed by amino-silanized sample (< 12 hours). RTP treated sample (< 28 hours) showed better protection than APTES. Sample with RTP as well as APTES treatment started discoloring after 28 hours. (The experiment was carried in an oven to speed up the discoloration for faster results)

Amino terminal ends of silane groups could eventually be exploited for common silicon surface modifications by adding polyethylene glycol or any other linker chemistry to control cell adhesion [44]. Additionally, thermal carbonization alters the surface chemistry and also helps in stabilizing porous silicon [31]. Studies examining improvement in stability of pnc-Si due to thermal carbonization are in progress.

2.4 Conclusion

This chapter shows that, like porous silicon, pnc-Si undergoes dissolution in cell culture media rather than delaminating and cracking or flaking. Pnc-Si was found to be stable in low pH and low salt concentrations, but there is interplay of pH changes, salt concentrations and pnc-Si characteristics that decide the life of this material. Qualitative visual color changes of pnc-Si chip were directly correlated to nanoporous membrane stability and its biodegradation *in vitro* through a microparticle assay. The change in the color is due to variation in optical interference of the silicon layers deposited on pnc-Si. As the thicknesses of the deposited layers deplete, the wavelength of the light reflected from its surface shifts resulting in a visual color change. The rate of substrate degradation was controlled through post production rapid thermal processing and it is hypothesized to densify the spontaneously formed native oxide layer or form a superior quality oxide layer rendering the surface glass-like. The biodegradation rates of pnc-Si were further slowed down for some long-term cell culture applications by surface treatments like UV-ozone oxidation followed by amino-silanization, but short-term experiments were immediately possible after RTP alone. Biodegradation also creates an opportunity to create stratified tissue *in vitro* by culturing different cell types on either side of pnc-Si membranes and allowing the two populations to co-join as the membrane dissolves.

2.5 References

1. Agrawal, A.A., Nehilla, B.J., Reisig, K.V., Gaborski, T.R., Fang, D.Z., Striemer, C.S., Fauchet, P.M., and McGrath, J.L. (2009). Porous nanocrystalline silicon membranes as highly permeable and molecularly thin substrates for cell culture. ACS Nano (submitted).

2. Zhang, S.F., Xia, L., Kang, C.H., Xiao, G.F., Ong, S.M., Toh, Y.C., Leo, H.L., van Noort, D., Kan, S.H., Tang, H.H., et al. (2008). Microfabricated silicon nitride membranes for hepatocyte sandwich culture. Biomaterials *29*, 3993-4002.

3. Anglin, E.J., Cheng, L., Freeman, W.R., and Sailor, M.J. (2008). Porous silicon in drug delivery devices and materials. Adv Drug Deliv Rev *60*, 1266-1277.

4. Salonen, J., Kaukonen, A.M., Hirvonen, J., and Lehto, V.P. (2008). Mesoporous silicon in drug delivery applications. J Pharm Sci *97*, 632-653.

5. Low, S.P., Williams, K.A., Canham, L.T., and Voelcker, N.H. (2006). Evaluation of mammalian cell adhesion on surface-modified porous silicon. Biomaterials *27*, 4538-4546.

6. Freshney, R.I. (2000). Culture of animal cells: A Manual of Basic Technique, (New York: Wiley-Liss).

7. Striemer, C.C., Gaborski, T.R., McGrath, J.L., and Fauchet, P.M. (2007). Charge- and size-based separation of macromolecules using ultrathin silicon membranes. Nature *445*, 749-753.

8. Canham, L.T. (1997). Properties of Porous Silicon, Volume 18, (INSPEC PUBLICATION).

9. Canham, L.T. (1995). Bioactive silicon structure fabrication through nanoetching techniques. Advanced Materials *7*, 1033.

10. Stewart, M.P., and Buriak, J.M. (2000). Chemical and biological applications of porous silicon technology. Advanced Materials *12*, 859-869.

11. Whitehead, M.A., Fan, D., Mukherjee, P., Akkaraju, G.R., Canham, L.T., and Coffer, J.L. (2008). High-porosity poly(epsilon-caprolactone)/mesoporous silicon scaffolds: calcium phosphate deposition and biological response to bone precursor cells. Tissue Eng Part A *14*, 195-206.

12. S. H. C. Anderson, H.E., D. J. Wallis, L. T. Canham, J. J. Powell, (2003). Dissolution of different forms of partially porous silicon wafers under simulated physiological conditions. physica status solidi (a) *197*, 331-335.

13. Low, S.P., Voelcker, N.H., Canham, L.T., and Williams, K.A. (2009). The biocompatibility of porous silicon in tissues of the eye. Biomaterials *30*, 2873-2880.

14. Reffitt, D.M., Jugdaohsingh, R., Thompson, R.P., and Powell, J.J. (1999). Silicic acid: its gastrointestinal uptake and urinary excretion in man and effects on aluminium excretion. J Inorg Biochem *76*, 141-147.

15. Canham, L.T., Reeves, C.L., Newey, J.P., Houlton, M.R., Cox, T.I., Buriak, J.M., and Stewart, M.P. (1999). Derivatized mesoporous silicon with dramatically improved stability in simulated human blood plasma. Advanced Materials *11*, 1505.

16. M. Björkqvist, J.S., E. Laine, L. Niinistö, (2003). Comparison of stabilizing treatments on porous silicon for sensor applications. physica status solidi (a) *197*, 374-377.

17. Salonen, J., and Lehto, V.P. (2008). Fabrication and chemical surface modification of mesoporous silicon for biomedical applications. Chemical Engineering Journal *137*, 162-172.

18. Salonen, J., Lehto, V.P., and Laine, E. (1997). The room temperature oxidation of porous silicon. Applied Surface Science *120*, 191-198.

19. Salonen, J., Lehto, V.P., and Laine, E. (1997). Thermal oxidation of free-standing porous silicon films. Applied Physics Letters *70*, 637-639.

20. Petrova-Koch, V., Muschik, T., Kux, A., Meyer, B.K., Koch, F., and Lehmann, V. (1992). Rapid-thermal-oxidized porous Si - The superior photoluminescent Si. Applied Physics Letters *61*, 943-945.

21. Kobeda, E., Kellam, M., and Osburn, C.M. (1991). Rapid Thermal Annealing of Low-Temperature Chemical Vapor-Deposited Oxides. Journal of the Electrochemical Society *138*, 1846-1849.

22. Yu, J.J., and Lu, Y.F. (2000). Effects of rapid thermal annealing on ripple growth in excimer laser-irradiated silicon-dioxide/silicon substrates. Applied Surface Science *154*, 670-674.

23. Jenn-Gwo Hwu, M.J.J. (1998). Method for making a silicon dioxide layer on a silicon substrate by pure water anodization followed by rapid thermal densification H01L 21316 Edition. (National Science Council).

24. Choi, W.K., Choo, C.K., Han, K.K., Chen, J.H., Loh, F.C., and Tan, K.L. (1998). Densification of radio frequency sputtered silicon oxide films by rapid thermal annealing. Journal of Applied Physics *83*, 2308-2314.

25. Lucovsky, G., Manitini, M.J., Srivastava, J.K., and Irene, E.A. (1987). Low-Temperature Growth of Silicon Dioxide Films - a Study of Chemical Bonding by Ellipsometry and Infrared-Spectroscopy. Journal of Vacuum Science & Technology B *5*, 530-537.

26. Chao, S.C., Pitchai, R., and Lee, Y.H. (1989). Enhancement in Thermal-Oxidation of Silicon by Ozone. Journal of the Electrochemical Society *136*, 2751-2752.

27. Baunack, S., and Zehe, A. (1989). A Study of Uv Ozone Cleaning Procedure for Silicon Surfaces. Physica Status Solidi a-Applied Research *115*, 223-227.

28. Cui, Z.J., Madsen, J.M., and Takoudis, C.G. (2000). Rapid thermal oxidation of silicon in ozone. Journal of Applied Physics *87*, 8181-8186.

29. Thompson, W.H., Yamani, Z., Hassan, L.H.A., Greene, J.E., Nayfeh, M., and Hasan, M.A. (1996). Room temperature oxidation enhancement of porous Si(001) using ultraviolet-ozone exposure. Journal of Applied Physics *80*, 5415-5421.

30. Kern, W. (1993). Handbook of Semiconductor wafer cleaning technology.

31. Torres-Costa, V., Martin-Palma, R.J., Martinez-Duart, J.M., Salonen, J., and Lehto, V.-P. (2008). Effective passivation of porous silicon optical devices by thermal carbonization. Journal of Applied Physics *103*, 083124.

32. Li, H.-L., Fu, A.-P., Xu, D.-S., Guo, Gui, L.L., and Tang, Y.-Q. (2002). In Situ Silanization Reaction on the Surface of Freshly Prepared Porous Silicon. Langmuir *18*, 3198-3202.

33. Arroyo-Hernández, M., Martín-Palma, R.J., Torres-Costa, V., and Martínez Duart, J.M. (2006). Porous silicon optical filters for biosensing applications. Journal of Non-Crystalline Solids *352*, 2457-2460.

34. Torres-Costa, V., Agulló-Rueda, F., Martín-Palma, R.J., and Martínez-Duart, J.M. (2005). Porous silicon optical devices for sensing applications. Optical Materials *27*, 1084-1087.

35.	Chan, S., Li, Y., Rothberg, L.J., Miller, B.L., and Fauchet, P.M. (2001). Nanoscale silicon microcavities for biosensing. Materials Science and Engineering: C *15*, 277-282.

36.	Chin, V., Collins, B.E., Sailor, M.J., and Bhatia, S.N. (2001). Compatibility of primary hepatocytes with oxidized nanoporous silicon. Advanced Materials *13*, 1877.

37.	el-Ghannam, A., Ducheyne, P., and Shapiro, I.M. (1997). Formation of surface reaction products on bioactive glass and their effects on the expression of the osteoblastic phenotype and the deposition of mineralized extracellular matrix. Biomaterials *18*, 295-303.

38.	Coen, M.C., Lehmann, R., Groning, P., Bielmann, M., Galli, C., and Schlapbach, L. (2001). Adsorption and Bioactivity of Protein A on Silicon Surfaces Studied by AFM and XPS. J Colloid Interface Sci *233*, 180-189.

39.	Sharma, S., Popat, K.C., and Desai, T.A. (2002). Controlling nonspecific protein interactions in silicon biomicrosystems with nanostructured poly(ethylene glycol) films. Langmuir *18*, 8728-8731.

40.	Bowen, W.R., Doneva, T.A., and Stoton, J.A.G. (2003). Protein deposition during cross-flow membrane filtration: AFM studies and flux loss. Colloids and Surfaces B-Biointerfaces *27*, 103-113.

41.	Herino, R., Bomchil, G., Barla, K., Bertrand, C., and Ginoux, J.L. (1987). Porosity and Pore-Size Distributions of Porous Silicon Layers. Journal of the Electrochemical Society *134*, 1994-2000.

42.	Wu, H.C., Wang, T.W., Kang, P.L., Tsuang, Y.H., Sun, J.S., and Lin, F.H. (2007). Coculture of endothelial and smooth muscle cells on a collagen membrane in the development of a small-diameter vascular graft. Biomaterials *28,* 1385-1392.

43.	Corning, D. (2005). A Guide to Silane solutions.

44.	Faucheux, N., Schweiss, R., Lutzow, K., Werner, C., and Groth, T. (2004). Self-assembled monolayers with different terminating groups as model substrates for cell adhesion studies. Biomaterials *25,* 2721-2730.

Chapter 3

Pnc-Si Biocompatibility: Cell culture in a Two Dimensional Format[*] [1]

3.1 Introduction

Porous nanocrystalline silicon (pnc-Si) membranes [2] can be used for various cell culture related applications if they are biocompatible and stable enough for the cells to adhere, spread, proliferate and remain viable for a suitable period of time. As seen in the previous chapter, work on porous silicon (P-Si) provides insight into newly discovered pnc-Si. Pnc-Si is stable in physiological conditions for at least 3-4 days after post production rapid thermal processing which should be sufficient for short term cell culture experiments. Pnc-Si life could further be extended for long term cell culture experiments (over several weeks) through additional treatments like silanization, carbonization, protein coatings, etc. In this chapter, pnc-Si is established as a viable cell culture substrate with the help of cell cultures of two distinct cell lines. To verify that pnc-Si is a suitable substrate for cell culture, different cell growth metrics such as cell viability, adhesion, spreading and proliferation of distinct cell lines (mouse embryo fibroblasts 3T3-L1 and primary human umbilical vein endothelial cells) are investigated. 3T3-L1 is an immortalized and robust cell line, whereas HUVEC is an environmentally sensitive primary cell line, which makes both of these cell types extremely distinct to test pnc-Si for a wide range of cell cultures possible.

Cells are known to be sensitive to topological, chemical and electrical properties of substrates on which they are grown [3]. Cells cultivated on microstructures made by semiconductor technology grow normally on silicon surfaces covered with microelectrode arrays, as well as on microperforated silicon membranes with square pores [4, 5]. The size of the pores in porous

---

[*] The material in this chapter is prepared for a manuscript and at the time of writing it is ready for submission to Journal of *American Chemical Society - Nano*.

silicon (P-Si) does not present a problem to cell growth, demonstrating that cells can be cultivated on a nanoporous topology [5]. Surface modifications can also be done to promote or hinder cell adhesion [6, 7]. For example, an amino-silanized substrate can promote or hinder cell attachment, depending on the silane monolayer's terminal functional group [8, 9].

As the first stage in mammalian cell proliferation *in vitro*, cell adhesion is an important parameter in determining a surface's potential as a cell culture substrate [10, 11]. Anchorage-dependent cells adhere optimally on wettable surfaces like tissue culture polystyrene, glass and polycarbonate [12]. Pnc-Si membrane surfaces are likely "coated" by a thin silicon dioxide layer after production due to air exposure which is then densified in the post production rapid thermal processing step (see Chapter 2). Therefore, although pnc-Si is a novel nanomaterial, its surface properties are similar to glass which should be favorable for cell adhesion [13]. The work presented in this chapter directly compares cell adhesion on pnc-Si to common hydrophilic cell culture substrates like glass and tissue culture grade polystyrene.

In the next stage after adhesion, cells start producing their extracellular matrix and spread across the culture substrates [14]. It is possible that the nanoporous topography of pnc-Si facilitated rapid maturation after cell adhesion since other nanotopographies affected cell behavior *in vitro* [15-18]. The two cells lines used in this study, namely, 3T3-L1 and HUVEC are expected to have normal cell adhesion and proliferation on nanoporous pnc-Si membranes since a variety of cell types have been cultured on much thicker nanoporous silicon substrates [19-21]. Hence, the surface properties and nanoporous topography of pnc-Si should not hinder its use as a cell culture substrate. Proper spreading demonstrates the ease at which the cells get used to the material's surface and produce extra cellular matrix. Pnc-Si is expected to support normal cell spreading and morphology in a similar manner as glass. After adhesion and spreading, a cell culture substrate promotes cell proliferation. Cell proliferation is measured as

per capita growth rate i.e. number of cell divisions per cell per hour and it approximately corresponds to one cell division per day.

The cell culture tests in this chapter are carried in a 'two dimensional' format, in which the pnc-Si chip is laid flat on the bottom of the culture well with the 'membrane side' facing up. Vacuum grease is applied to keep the chip anchored as well as keep both sides of the membrane completely immersed. Cells can be plated on the membrane side of the chip with the help of cloning rings that prevent the cells from rolling off the surface and inverted microscope can be used for easy visualization. Though a facile configuration, two dimensional format is not the ideal format for regular experimental use. Transwell system of pnc-Si or so called the 'three dimensional' configuration is the commercial format for carrying out actual drug permeability and cellular co-culture experiments, and is discussed in the next chapter.

3.2 Material and Methods

3.2.1 Materials

Pnc-Si supplied by SiMPore Inc., Rochester, NY. Dulbecco's Modified Eagle Medium (DMEM), 0.25% Trypsin-EDTA, Fetal Bovine Serum (FBS), penicillin/streptomycin, glutamine, Liebovitz L-15 media, CellTracker Green 5-chloromethylfluorescein diacetate (CMFDA) and the Live/Dead Viability/Cytotoxicity Kit (Calcein AM and EthD-1) were purchased from Invitrogen (Carlsbad, CA, USA). AlexaFluor dyes were purchased from Invitrogen-Molecular Probes. Cloning rings (6.4 mm inner diameter x 8 mm height) and poly-l-lysine (PLL) for cell culture were purchased from Sigma (St. Louis, MO, USA). Methanol (MeOH), ethanol (EtOH), $22mm^2$ glass cover slips and all tissue culture-treated polystyrene (TCPS) plasticwares (24-well culture plates, petridishes, and BD Falcon T25/75 tissue culture flasks) were purchased from VWR.

3.2.2 Cell Culture: HUVEC and NIH 3T3-L1

Cell studies were performed with primary human umbilical vein endothelial cells (HUVEC, Microbiology & Immunology Lab, University of Rochester Medical Center, Rochester, NY, USA) and immortalized mouse embryo fibroblasts (3T3-L1, ATCC, Rockville, MD, USA). These cells were cultured in 0.1% gelatin coated T25/T75 flasks (BD Falcon) at 37°C in a 5% CO_2, humidified atmosphere. HUVEC were grown in EGM (Lonza) with 2% L-glutamine, 1% penicillin/streptomycin and 10% FBS, and 3T3-L1 were grown in DMEM (Invitrogen) supplemented with antibiotics and serum. Media was changed every other day. Cells were harvested after reaching 70-80% confluence by trypsinization with 0.25% trypsin-EDTA and subsequently seeded at appropriate densities. HUVEC and 3T3-L1 were used between passages 4-8 and 17-25, respectively.

3.2.3 Cell Adhesion

HUVEC and 3T3-L1 were separately seeded within cloning rings on each of the five substrates: poly-L-Lysine (PLL) coated tissue culture polystyrene, tissue culture polystyrene (TCP), glass cover slips, teflon-fluorinated ethylene propylene (Integument Technologies, Inc.,Tonawanda, NY) and pnc-Si (Figure 3.1). After seeding, cells were incubated for 5-6 hours in serum-supplemented media to allow attachment and then stained with CMFDA. In detail, cells were gently rinsed in PBS to remove non-adhered cells, and the media was replaced with 6 µM CMFDA in serum-free media. After 45 minutes at 37°C, CMFDA solution was replaced with serum-free media, and cells were incubated for another 30 minutes. For the pnc-Si samples, the cloning rings were removed and the chips were flipped over for imaging. Microscopy was performed with a 10X objective on an epifluorescent Nikon Eclipse TS-100F inverted microscope equipped with a Cooke SensiCam cooled CCD camera. Microscope control and image acquisition was achieved with customized MATLAB scripts. Cells were counted with a

MATLAB script, and the percent adhesion was determined by comparing the MATLAB-counted cell density to the original seeding density.

3.2.4 Cell Spreading

To measure cell spreading, HUVEC and 3T3-L1 cells were seeded inside cloning rings and onto either glass cover slips or pnc-Si samples. An open perfusion microincubator (Harvard Apparatus) was used to maintain cells at 37°C and mineral oil was floated on top of the media to minimize evaporation. To account for lower ambient CO_2 concentrations outside the incubator, sodium bicarbonate-free Liebovitz L-15 with 10% FBS was added (1:1, v/v) to normal cell media. Cell attachment and spreading was monitored over 5 hours by acquiring images *via* time lapse phase contrast imaging on the Nikon/Cooke system described above.
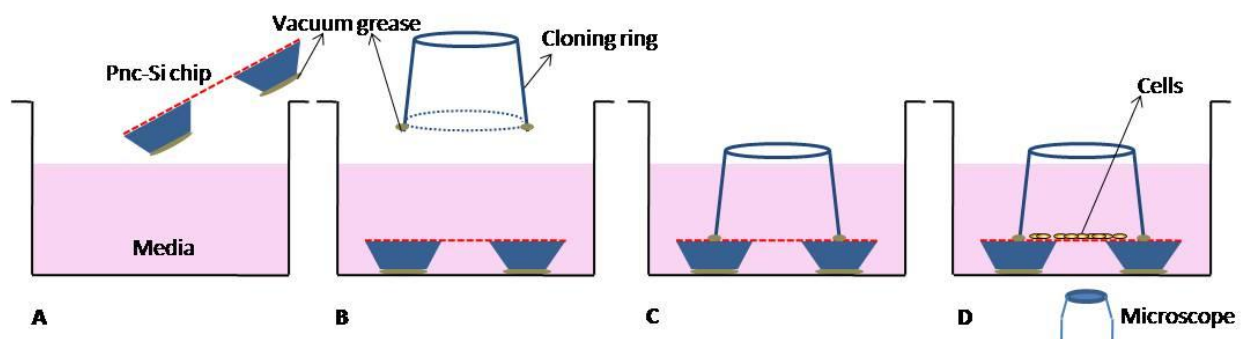
Figure 3.1 Two dimensional configuration of pnc-Si: A) vacuum grease is applied to the base of the pnc-Si chip and it is immersed into the media full culture well at an angle to prevent the membrane from breaking, B) the pnc-Si chip is anchored to the base of the well and vacuum grease is applied to the base of a cloning ring, C) the cloning ring is placed carefully on the chip, and, D) cells are plated inside the cloning ring and can be viewed through the slits using an inverted microscope.

3.2.5 Cell Proliferation

For growth kinetics experiments, HUVEC and 3T3-L1 cells were first grown to 70-80% confluence in media with or without serum. Cells were then seeded onto tissue culture polystyrene, glass or pnc-Si in two dimensional format at low densities. To control the culture

area between polystyrene, glass and pnc-Si, cloning rings were attached *via* vacuum grease to these substrates. Cell proliferation was monitored over 4-5 days by staining cells with CMFDA and counting stained cells using the MATLAB script. Multiple images were taken with the Nikon microscope, and cell densities were obtained for each substrate on each day. For pnc-Si, the cloning rings were removed and samples were flipped over for imaging. At least three trials with triplicate measurements were carried out for each study. The data was graphed according to following exponential growth kinetics,

$$\frac{N}{N_o} = e^{rt}$$

where, 'N/N_0' is the cell density normalized to the cell density on day one, 'r' is the *per capita* growth rate (slope of semi-log plot) and 't' is time.

3.2.6 Cell Viability

For cell viability experiments, HUVEC and 3T3-L1 were seeded onto glass cover slips or pnc-Si samples in two dimensional format, and the culture area was constrained by cloning rings. After incubation in serum-supplemented media for 2 days, the live/dead cytotoxicity assay was used to stain cells. In detail, growth media was replaced with 2 µM calcein AM and 4 µM EthD-1 in PBS. Cells were stained in this solution for 45 minutes at 25°C and subsequently imaged with the Nikon microscope. After imaging, a control experiment was conducted by adding 70% EtOH to cells for two hours and then repeating the live/dead assay. For pnc-Si, cloning rings were removed and samples were flipped over for imaging.

3.2.7 Cell Counting from Fluorescent Images via MATLAB

For cell adhesion and growth kinetics data (Figures 3.2, 3.4 and 3.5), cells on different substrates were stained and then counted with a custom-designed, MATLAB-based cell

counting program (available for public download at *www.nanomembranes.org*). The MATLAB code employed a user-defined fluorescence intensity threshold to mask fluorescent cell images into binary black and white images. The white image objects thus were then counted as cells only if their areas were within a user-defined range of pixels. To verify the accuracy of the cell counting program, the centroid of each counted white image object (i.e., each "cell") was labeled with an identification number on the original fluorescent images. Any mismatches between the counted centroids and the actual cell centroids were then identified and selected for removal. The final MATLAB output included the total number of cells counted per image.

3.2.8 Data Analysis: Data was reported as the mean ± standard error. All post-acquisition image processing (overlays, pseudocolor) was conducted with ImageJ. Statistical analysis was performed using SPSS software (SPSS, Inc. Chicago, IL, USA). For ANOVA, either a Kruskal-Wallis or Dunn's post-hoc analysis was performed. For all tests, significance was determined to be $p < 0.05$.

3.3 Results and Discussion

3.3.1 Cell Adhesion

Optimal proliferation and spreading of anchorage-dependent cells *in vitro* requires thorough attachment to culture substrates [22]. Anchorage-dependent HUVEC and 3T3-L1 cells were used to explore the suitability of pnc-Si as a cell culture substrate. As the first stage in mammalian cell proliferation *in vitro* [10, 11], cell adhesion is an important parameter in determining the potential of a surface as a viable culture substrate. Anchorage-dependent cells adhere optimally on wettable surfaces like tissue culture polystyrene, polycarbonate and glass, but hydrophobic materials like teflon are inferior culture substrates [12] because cells do not adhere to hydrophobic surfaces and instead remain rounded and eventually die.

100

Fluorescence microscopy was used to investigate the cell adhesion properties of pnc-Si and other common cell culture surfaces. After five hours *in vitro*, adhered cells were stained with CMFDA (5-chloromethylfluorescein diacetate). CMFDA is a chloromethyl derivative of fluorescein that freely diffuses through the membranes of live cells. Once inside the cell, chloromethyl group of CMFDA reacts with thiols, probably *via* a ubiquitous glutathione S-transferase-mediated reaction, to form a cell-impermeant fluorescent dye. CMFDA has a relatively low pKa, which ensures that it will exhibit bright, green fluorescence (ex/em λ ~495 nm/~515 nm) in the cytoplasm at all physiological pH levels for at least a few cell generations. After staining, viable cells were counted *via* MATLAB-based scripts and then cell adhesion values were obtained by normalizing to the original cell seeding density. For pnc-Si, counts were acquired from both supported and free-standing pnc-Si membrane areas since the topographical properties of these areas are identical. There was no significant difference between HUVEC (50.45±5.70%, 64.27±1.26%, 65.97±10.93%) or 3T3-L1 (65.14±7.57%, 65.78±4.39%, 74.53±9.04%) adhesion to pnc-Si, glass and tissue culture plastic, respectively (p<0.05) (Figure 3.2). High cell adhesion to poly-L-lysine-coated tissue culture plastic (80.51±6.32% for HUVEC, 92.31±3.48% for 3T3-L1) was expected since PLL is a commonly-used and highly-charged polymer that improves initial cell adhesion before cells produce their own extracellular matrix [23, 24]. PLL was used as a posititve control for this experiment. Since teflon (teflon-FEP) is a poorly wettable substrate with low cell adhesion strengths [25], it was used as a negative control and showed low adhesion (17.72±2.12% for HUVEC, 32.53±3.04% for 3T3-L1) (Figure 3.2). For all substrates, 3T3-L1 adhesion was greater than that of HUVEC because this immortalized cell line is more robust than primary HUVEC. These results showed that cell adhesion to pnc-Si was comparable to common cell culture substrates. Normal cell adhesion was expected because pnc-Si is likely "coated" by a superficial thin, native oxide layer after production. Therefore, the silicon dioxide layer makes pnc-Si surface properties similar to glass and thus favorable for cell adhesion.
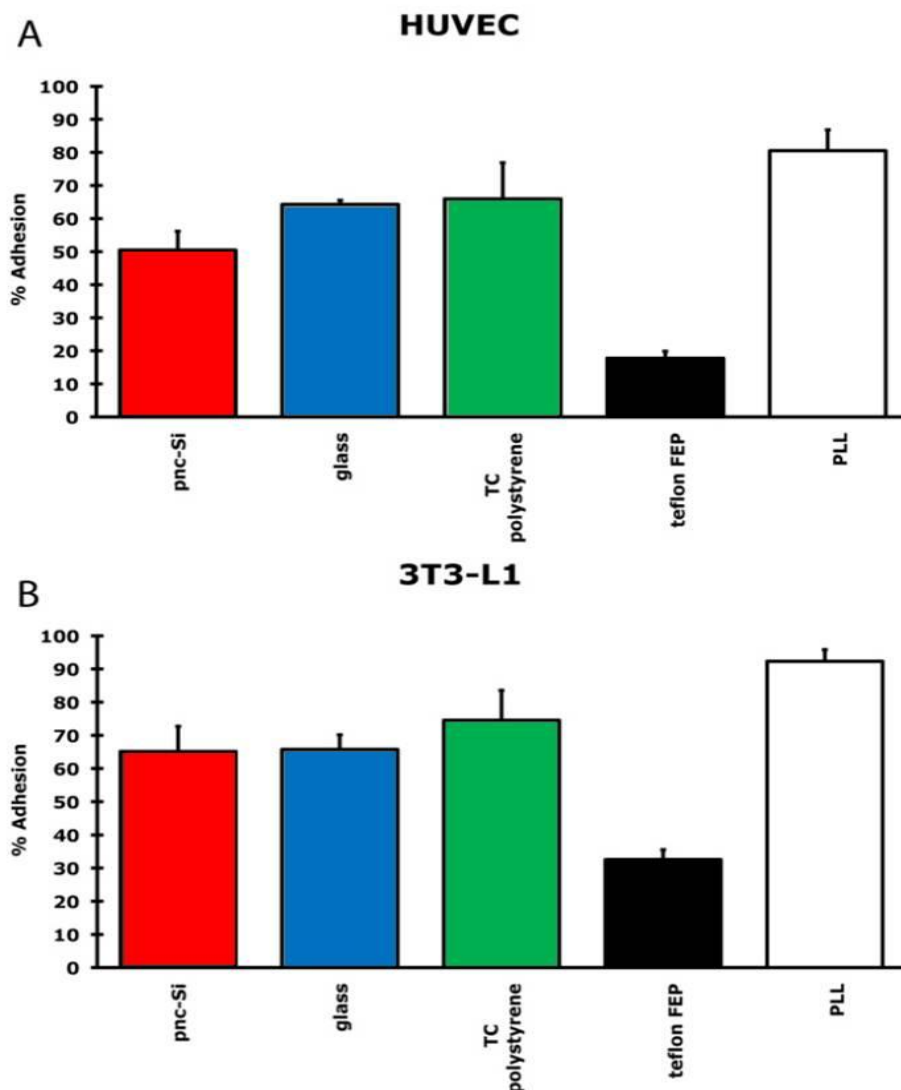
Figure 3.2 Cell Adhesion: Percent adhesion of HUVEC (A) and 3T3-L1 (B) cells on pnc-Si, glass and tissue culture polystyrene after 5 hours of cell culture. Teflon and PLL-coated glass were included as negative and positive controls, respectively. (n >= 3 with triplicate measurements). One-way ANOVA found differences in attachment of 3T3-L1/HUVEC to pnc-Si, glass, and plastic to be insignificant (p > 0.05). Significant differences were observed for the control experiments.

Additional treatments of pnc-Si with serum or extracellular matrix proteins may further enhance cell adhesion [6] in future studies. Also, the terminal amino group of silanized pnc-Si surfaces can be exploited with functional chemistry to enhance cell adhesion.

3.3.2 Cell Spreading

After adhesion, cells spread across culture substrates [14]. Since pnc-Si and glass are optically transparent and have similar silicon dioxide surface properties, we compared 3T3-L1 and HUVEC cell spreading on these surfaces with time-lapse phase contrast microscopy (Figure 3.3).
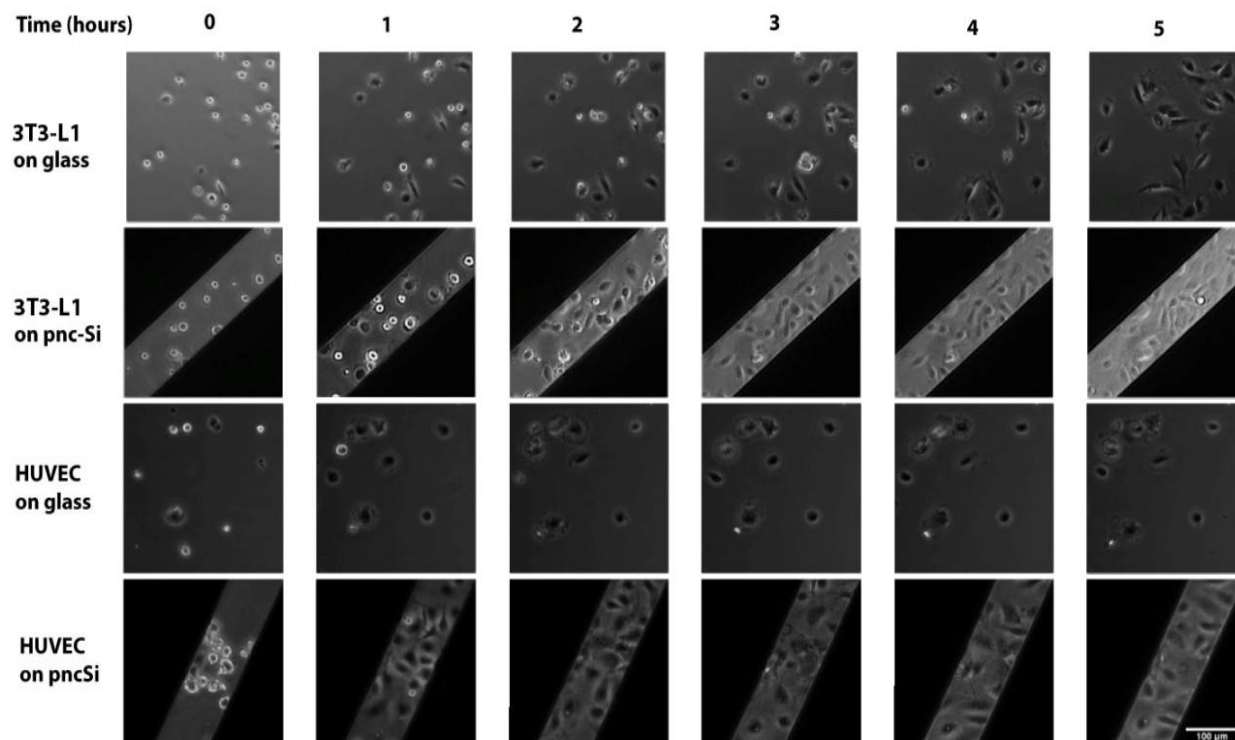
Figure 3.3 Cell spreading: Phase contrast images from time-lapse movies (Movies 2-5) of 3T3-L1 (top 2 rows) and HUVEC (bottom 2 rows) on glass and pnc-Si over 5 hours. Both cell types adhered and spread equally well on pnc-Si and glass. Cell morphology was also normal. The 100 µm scale bar applies to all images.

 Immediately after plating, both cell types had settled (0 hours) but not adhered or spread on the surface as they exhibited spherical morphologies. Over next 2 hours, cells adhered and spread across the substrate. After 5 hours, both 3T3-L1 and HUVEC cells appeared fully spread and show movements on both glass and pnc-Si. 3T3-L1 maintained elongated fibroblast-like morphology especially on pnc-Si and HUVEC exhibited cobblestone morphology which is typical

of confluent HUVEC monolayers [26]. The HUVEC maturation to cobblestone morphology was noticeable on pnc-Si but delayed on glass. It is possible that the nanoporous topography of pnc-Si facilitated rapid maturation after cell adhesion. Importantly, both 3T3-L1 and HUVEC spread across nearly the entire free-standing pnc-Si membrane after 5 hours. The rapidity with which 3T3-L1 and HUVEC spread on pnc-Si suggests that these membranes will facilitate the formation of high integrity monolayers on pnc-Si. Cell spreading in time-lapse phase contrast movies for both cell types on glass and pnc-Si are available as supplementary data (Movies 2-5 in Supplementary Compact Disk).

3.3.3 Cell Proliferation

Pnc-Si clearly supported cell adhesion and spreading, so cell proliferation was investigated next. To quantify cell proliferation, cells were grown for 4-5 days on different substrates, fluorescent cell counts were acquired daily and per capita growth rates (number of cell divisions per cell per hour) were calculated. Growth in serum-free media was used as a control to show that the assay was sensitive to less favorable growth conditions. Figure 3.4 shows that HUVEC proliferated faster on pnc-Si (per capita growth rate: 0.0296±0.0055 divisions/cell-hour) than on glass (0.0198±0.0024 divisions/cell-hour) and tissue culture polystyrene (0.0223±0.0036 divisions/cell-hour). 3T3-L1 cells showed statistically similar per capita growth rates on pnc-Si, glass and tissue culture plastic (0.0302±0.0066, 0.0318±0.0077, 0.0365±0.0051 divisions/cell-hour, respectively). These values correspond to approximately 1 cell division per day for both HUVEC and 3T3-L1 on pnc-Si. The values for 3T3-L1 data are in agreement with our prior work [27]. The serum starved cells had significantly low per capita growth rates.
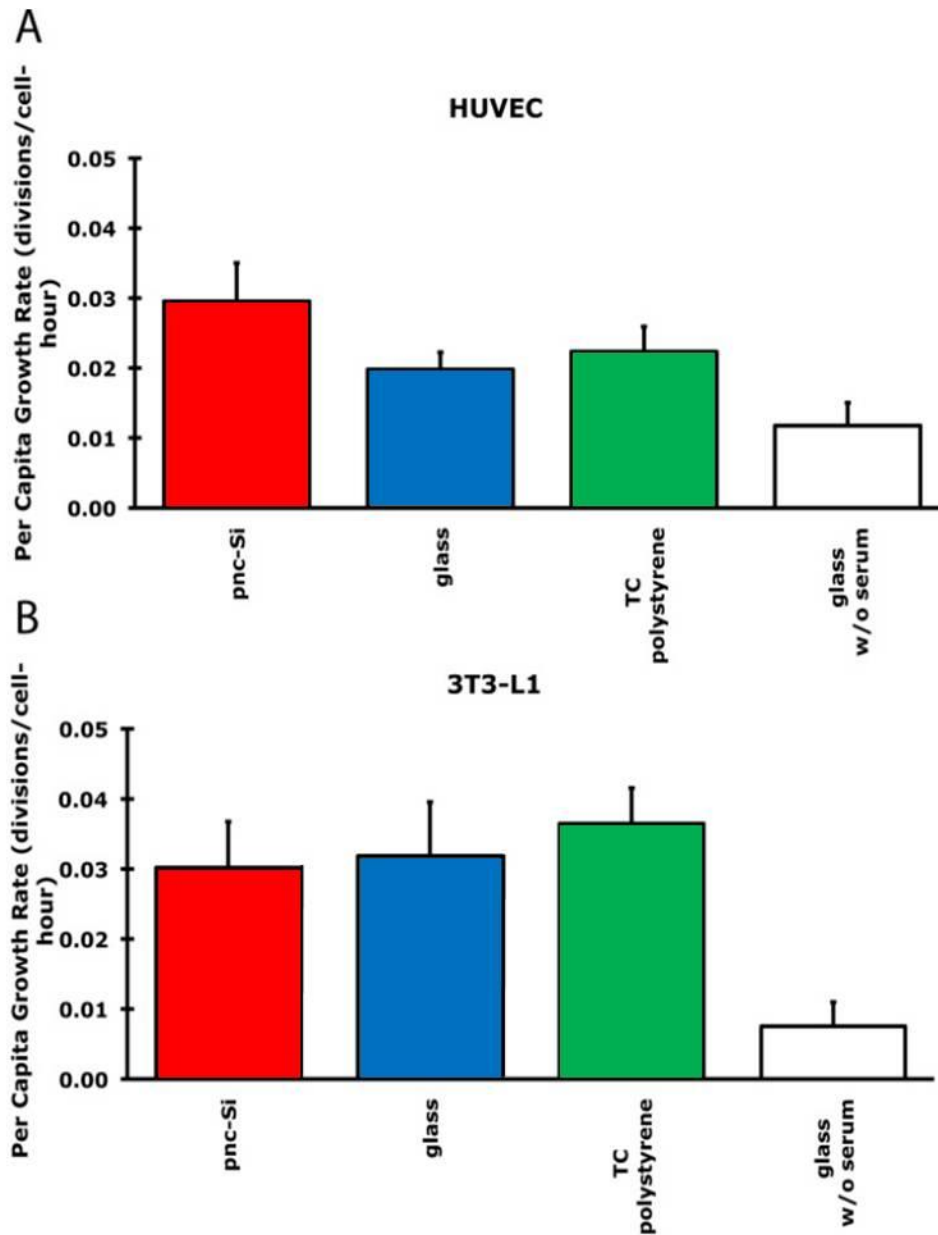
Figure 3.4 Cell growth kinetics: Per capita growth rate (number of cell divisions per cell per hour) of HUVEC (A) and 3T3-L1 (B) on glass, pnc-Si and tissue culture polystyrene over 5 days. Serum starved cells were used as a control and showed low per capita growth in both cell types. Per capita growth rates of 3T3-L1 on all 3 substrates were not significantly different ($p > 0.05$). Per capita growth of HUVEC on pnc-Si was significantly greater than on glass and plastic.

The increase in HUVEC growth rate could derive from differences in surface topology or the profile of bound proteins from serum. Also, the access to nutrients through the pnc-Si

membrane nanopores from apical as well as basal sides could have enhanced the sensitive HUVEC growth. In the future, non-porous pnc-Si material having similar surface properties but no functional pores can be used to cut off nutrient access from one side and investigate these possibilities. On much thicker nanoporous silicon substrates, a variety of cell types have been successfully cultured [19-21, 28, 29]. Therefore, it is not surprising that the nanoporous topography and the superficial oxide surface properties of pnc-Si membranes do not interfere with 3T3-L1 and HUVEC cell adhesion and proliferation over 4-5 days.

3.3.4 Effects of Pnc-Si Degradation on Cell Proliferation

Chapter 2 showed that pnc-Si is biodegradable in cell growth media and that the pnc-Si chip discolored over the course of time. As pnc-Si discolored from blue to gold in cell media over 1-3 days, its surface properties also changed. Therefore, it was possible that these changes in the pnc-Si surface affected cell proliferation. Although the degradation byproducts of porous silicon were found non-toxic to primary hepatocytes in another study [6], we have not established that P-Si and pnc-Si degrade by the same mechanism and so it was important to characterize the potential toxicity of nanocrystalline silicon biodegradation with 3T3-L1 and HUVEC. To investigate the biocompatibility of pnc-Si degradation byproducts, per capita growth rates for the first 2 days of cell culture were compared to growth rates for the next 2 days of culture (Figure 3.5). HUVEC and 3T3-L1 growth rates in first two days of culture (0.0344 ± 0.0117 divisions/cell-hour, 0.0314 ± 0.0007 divisions/cell-hour, respectively) were not statistically different from the next two days of culture (0.0269 ± 0.0073 divisions/cell-hour, 0.02718 ± 0.0042 divisions/cell-hour, respectively). Since pnc-Si degraded over 1-3 days in cell culture media (Chapter 2), cells in the second two days of culture were certainly exposed to pnc-Si degradation compounds. Therefore, even though the underlying pnc-Si membrane surface chemistry changed during cell growth experiments and degradation byproducts were released into the growth media, the processes had no observable effect on cell proliferation rates of immortalized and primary cells.
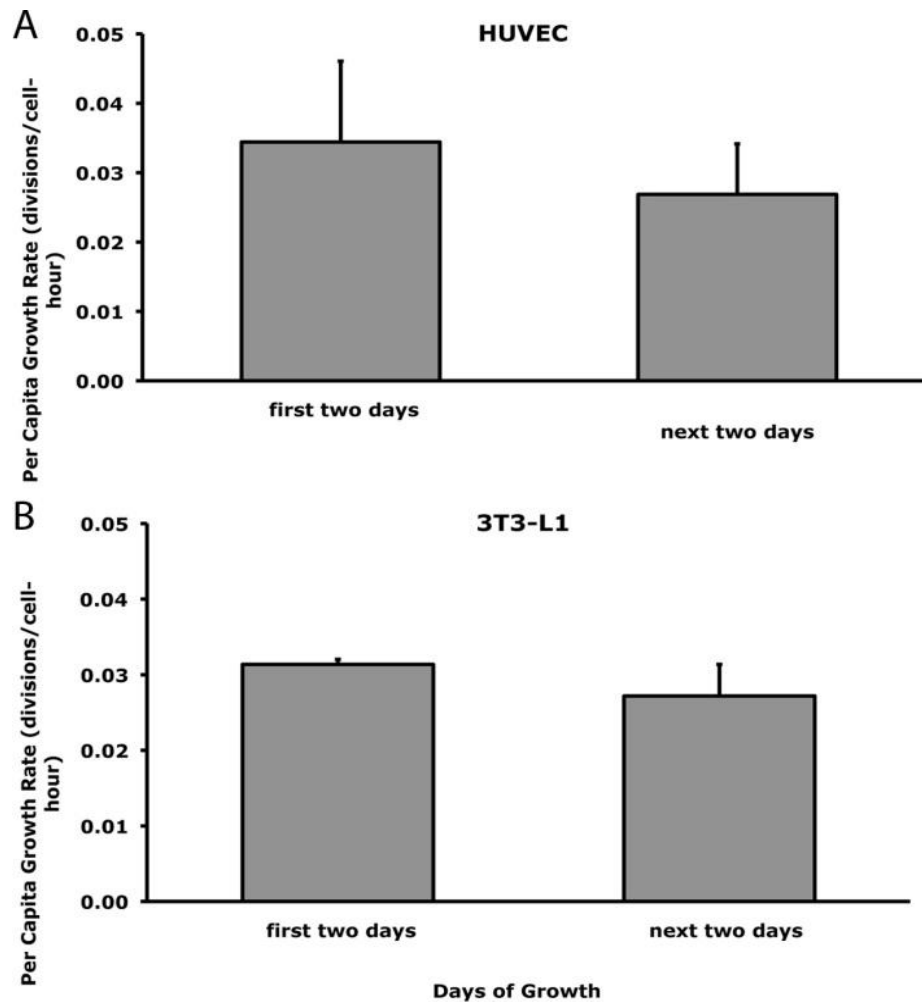
Figure 3.5 Effects of pnc-Si degradation on cell proliferation: Comparison of per capita growth rate of HUVEC (A) and 3T3-L1 (B) during first 2 days and the next 2 days of culture. Cell counts were normalized to the initial cell seeding density to determine the rate for the first 2 days. During next 2 days, the cell counts were normalized to the density on the third day. No significant difference was observed between the growth rate on the first 2 days to the next 2 days of culture for both HUVEC and 3T3-L1 cells (p < 0.05).

3.3.5 Cell Viability

Although the cell adhesion, spreading and proliferation data suggested that pnc-Si was a favorable cell culture substrate and not acutely cytotoxic, cell viability was directly measured to confirm the biocompatibility of pnc-Si. In detail, cell viability on glass and pnc-Si was tested with

a cell viability assay consisting of green calcein AM (live) and red EthD-1 (dead) fluorescent stains (Figure 3.6).
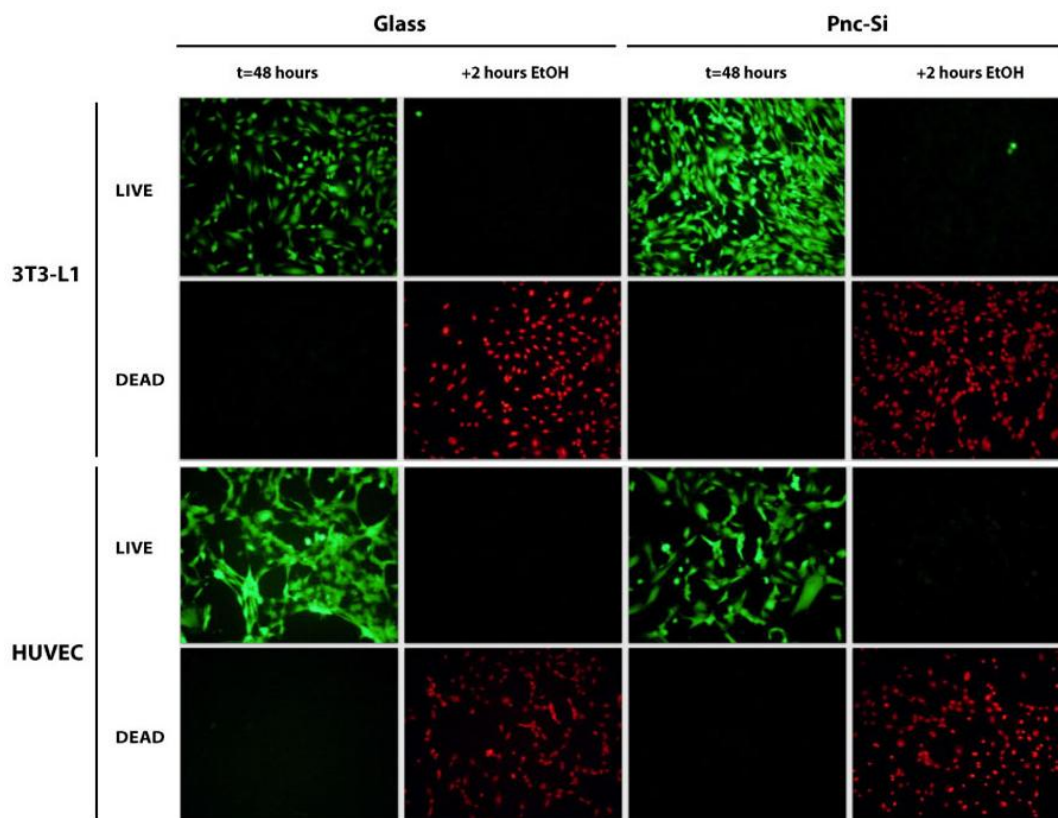
Figure 3.6 Cell viability of primary and immortalized cell lines on glass and pnc-Si: 3T3-L1 and HUVEC viability on glass and pnc-Si after 2 days *in vitro*, as measured by the Live/Dead Cell Viability Assay (Invitrogen). Robust green fluorescence showed nearly 100% viability of both 3T3-L1 and HUVEC after 2 days. After 2 hours in 70% EtOH (positive control to kill cells), both cell types stained red by EthD-1, the dead cell stain.

Live cells are distinguished by the presence of ubiquitous intracellular esterase activity. This enzyme converts a virtually non-fluorescent, cell-permeant and uncharged ester, calcein acetoxymethyl (AM), to intensely fluorescent and charged calcein. Once inside the cell, the lipophilic groups of ester are hydrolytically cleaved by non-specific esterases, resulting in a charged form that leaks out of cells much slowly than its parent compound. The polyanionic

calcein dye is well retained within live cells, producing an intense uniform green fluorescence (ex/em λ ~495 nm/~515 nm). EthD-1 enters cells with damaged membranes and undergoes nearly 40-fold enhancement of fluorescence upon intercalating with nucleic acids, thereby producing a bright red fluorescence in dead cells (ex/em λ ~495 nm/~635 nm). A microscopy-based cell viability assay was chosen because other work showed that certain colorimetric viability assays of cells on porous silicon were unreliable [9]. After 2 days in vitro, both 3T3-L1 and HUVEC were 100% viable on both glass and pnc-Si (Figure 3.6).

Furthermore, cell morphologies in the nearly confluent monolayer appeared normal. EtOH-killed cells stained completely red, which confirmed the specificity of this assay. The lack of background fluorescence in these images shows that autofluorescence of the pnc-Si substrate is negligible at least at these wavelengths. This experiment validated the accuracy of our previous microscopy-based cell adhesion and growth studies and showed that pnc-Si was comparable to glass as a biocompatible cell culture substrate manifesting no acute cytotoxicity.

3.4 Conclusion

This chapter demonstrated that nanoporous pnc-Si membranes are viable cell culture substrates in two dimensional format. To that end, the adhesion, spreading, growth kinetics and viability of immortalized 3T3-L1 and primary HUVEC were compared on pnc-Si, glass and tissue culture plastic. Pnc-Si performed comparably to the common cell culture substrates in each of these metrics. Importantly, pnc-Si biodegradation exerted no cytotoxic effects even after its own degradation over the culture period.

The thinness of pnc-Si should enable the development of more physiologically relevant *in vitro* tissue models. Compared to conventional polymeric track-etched membranes for cell culture, pnc-Si membranes are orders-of-magnitude more permeable, optically transparent and only 15 nm thick. Therefore, pnc-Si is a new biomaterial that should find many uses in the study of cell biology and physiology (e.g., monolayer transport assays, cellular co-cultures) and is a potential biodegradable scaffold for three-dimensional tissue constructs. The two dimensional format is not ideal for regular experimental use. Pnc-Si's silicon planer geometry can be exploited to use it in more desirable formats for transwell and microfluidic applications. A transwell system of pnc-Si or the "three dimensional configuration" is introduced in the next chapter. This format is the commercial format used for carrying drug permeability and cellular co-culture experiments.

3.5 References

1. Agrawal, A.A., Nehilla, B.J., Reisig, K.V., Gaborski, T.R., Fang, D.Z., Striemer, C.S., Fauchet, P.M., and McGrath, J.L. (2009). Porous nanocrystalline silicon membranes as highly permeable and molecularly thin substrates for cell culture. ACS Nano (submitted).

2. Striemer, C.C., Gaborski, T.R., McGrath, J.L., and Fauchet, P.M. (2007). Charge- and size-based separation of macromolecules using ultrathin silicon membranes. Nature *445*, 749-753.

3. Curtis, A.S., Casey, B., Gallagher, J.O., Pasqui, D., Wood, M.A., and Wilkinson, C.D. (2001). Substratum nanotopography and the adhesion of biological cells. Are symmetry or regularity of nanotopography important? Biophys Chem *94*, 275-283.

4. Canham, L.T. (1995). Bioactive silicon structure fabrication through nanoetching techniques. Advanced Materials *7*, 1033.

5. Bayliss, S.C., Heald, R., Fletcher, D.I., and Buckberry, L.D. (1999). The culture of mammalian cells on nanostructured silicon. Advanced Materials *11*, 318-321.

6. Chin, V., Collins, B.E., Sailor, M.J., and Bhatia, S.N. (2001). Compatibility of primary hepatocytes with oxidized nanoporous silicon. Advanced Materials *13*, 1877.

7. Moxon, K.A., Hallman, S., Aslani, A., Kalkhoran, N.M., and Lelkes, P.I. (2007). Bioactive properties of nanostructured porous silicon for enhancing electrode to neuron interfaces. J Biomater Sci Polym Ed *18*, 1263-1281.

8. Faucheux, N., Schweiss, R., Lutzow, K., Werner, C., and Groth, T. (2004). Self-assembled monolayers with different terminating groups as model substrates for cell adhesion studies. Biomaterials *25*, 2721-2730.

9. Low, S.P., Williams, K.A., Canham, L.T., and Voelcker, N.H. (2006). Evaluation of mammalian cell adhesion on surface-modified porous silicon. Biomaterials *27*, 4538-4546.

10. Freshney, R.I. (2000). Culture of animal cells: A Manual of Basic Technique, (New York: Wiley-Liss).

11. Guo, M., Chen, J., Zhang, Y., Chen, K., Pan, C., and Yao, S. (2008). Enhanced adhesion/spreading and proliferation of mammalian cells on electropolymerized porphyrin film for biosensing applications. Biosens Bioelectron *23*, 865-871.

12. Koenig, A.L., Gambillara, V., and Grainger, D.W. (2003). Correlating fibronectin adsorption with endothelial cell adhesion and signaling on polymer substrates. J Biomed Mater Res A *64*, 20-37.

13. el-Ghannam, A., Ducheyne, P., and Shapiro, I.M. (1997). Formation of surface reaction products on bioactive glass and their effects on the expression of the osteoblastic phenotype and the deposition of mineralized extracellular matrix. Biomaterials *18*, 295-303.

14. Voger, E.A., and Bussian, R.W. (1987). Short-term cell-attachment rates: a surface-sensitive test of cell-substrate compatibility. J Biomed Mater Res *21*, 1197-1211.

15. Bayliss, S.C., Buckberry, L.D., Harris, P.J., and Tobin, M. (2000). Nature of the silicon-animal cell interface. Journal of Porous Materials *7*, 191-195.

16. Ainslie, K.M., Tao, S.L., Popat, K.C., and Desai, T.A. (2008). In vitro immunogenicity of silicon-based micro- and nanostructured surfaces. ACS Nano *2*, 1076-1084.

17. Lechleitner, T., Klauser, F., Seppi, T., Lechner, J., Jennings, P., Perco, P., Mayer, B., Steinmuller-Nethl, D., Preiner, J., Hinterdorfer, P., et al. (2008). The surface properties of nanocrystalline diamond and nanoparticulate diamond powder and their suitability as cell growth support surfaces. Biomaterials *29*, 4275-4284.

18. Bayliss, S.C., Harris, P.J., Buckberry, L.D., and Rousseau, C. (1997). Phosphate and cell growth on nanostructured semiconductors. Journal of Materials Science Letters *16*, 737-740.

19. Ma, S.H., Lepak, L.A., Hussain, R.J., Shain, W., and Shuler, M.L. (2005). An endothelial and astrocyte co-culture model of the blood-brain barrier utilizing an ultra-thin, nanofabricated silicon nitride membrane. Lab Chip *5*, 74-85.

20. Harris, S.G., and Shuler, M.L. (2003). Growth of endothelial cells on microfabricated silicon nitride membranes for an in vitro model of the blood-brain barrier. Biotechnology and Bioprocess Engineering *8*, 246-251.

21. Alvarez, S.D., Derfus, A.M., Schwartz, M.P., Bhatia, S.N., and Sailor, M.J. (2009). The compatibility of hepatocytes with chemically modified porous silicon with reference to in vitro biosensors. Biomaterials *30*, 26-34.

22. Alberts, B., Wilson, J.H., and Hunt, T. (2008). Molecular biology of the cell, 5th Edition, (New York: Garland Science).

23. Lakard, S., Herlem, G., Propper, A., Kastner, A., Michel, G., Valles-Villarreal, N., Gharbi, T., and Fahys, B. (2004). Adhesion and proliferation of cells on new polymers modified biomaterials. Bioelectrochemistry *62*, 19-27.

24. Quirk, R.A., Chan, W.C., Davies, M.C., Tendler, S.J., and Shakesheff, K.M. (2001). Poly(L-lysine)-GRGDS as a biomimetic surface modifier for poly(lactic acid). Biomaterials *22*, 865-872.

25. van Kooten, T.G., Schakenraad, J.M., van der Mei, H.C., and Busscher, H.J. (1992). Influence of substratum wettability on the strength of adhesion of human fibroblasts. Biomaterials *13*, 897-904.

26. Jaffe, E.A., Nachman, R.L., Becker, C.G., and Minick, C.R. (1973). Culture of human endothelial cells derived from umbilical veins. Identification by morphologic and immunologic criteria. J Clin Invest *52*, 2745-2756.

27. Bindschadler, M., and McGrath, J.L. (2007). Sheet migration by wounded monolayers as an emergent property of single-cell dynamics. Journal of Cell Science *120*, 876-884.

28. Salonen, J., and Lehto, V.P. (2008). Fabrication and chemical surface modification of mesoporous silicon for biomedical applications. Chemical Engineering Journal *137*, 162-172.

29. Sun, W., Puzas, J.E., Sheu, T.J., Liu, X., and Fauchet, P.M. (2007). Nano- to microscale porous silicon as a cell interface for bone-tissue engineering. Advanced Materials *19*, 921.

Chapter 4

Pnc-Si Transwell Hybrid: Cell Culture in Three Dimensions

4.1 Introduction

The previous chapter demonstrated pnc-Si as a short term cell culture substrate for HUVEC and 3T3-L1 fibroblasts in a two dimensional format. The goal in this chapter is to establish the usefulness of pnc-Si for cell culture experiments. To accomplish this, cell culture is extended to three dimensions using custom-designed pnc-Si transwell devices, the configuration in which nanoporous membranes are used in commercial applications (see *www.millipore.com*). The transwell is created by assembling pnc-Si chips in a SepCon^{TM}, which is a polypropylene cup-like housing. With the addition of a flange, this assembly forms a 'pnc-Si transwell hybrid' that closely resembles the shape and dimensions of the commercial transwell inserts for 24-well plates. In transwells, the porous membrane divides the well into two chambers: an upper and a lower chamber (apical/donor and basolateral/receiver chambers respectively) (Figure 4.1). The transwell system creates an *in vitro* cellular microenvironment for testing.

Membrane-based cell culture incorporates unique design features to improve flexibility, allowing researchers discrete access to both the apical and basolateral cell surfaces for experimental design. *In vitro* models of cellular systems can be set up for analyzing various cellular interaction mechanisms as well as to monitor cell monolayer permeability to drugs, toxins, etc [1-3]. Long term *in vitro* transwell culture models offer a number of ethical and economic advantages, helping understand a biological process much sooner apart from offering a viable alternative to live animal testing. The combination of lower-cost and higher throughput using such devices can help bring products to the market faster.
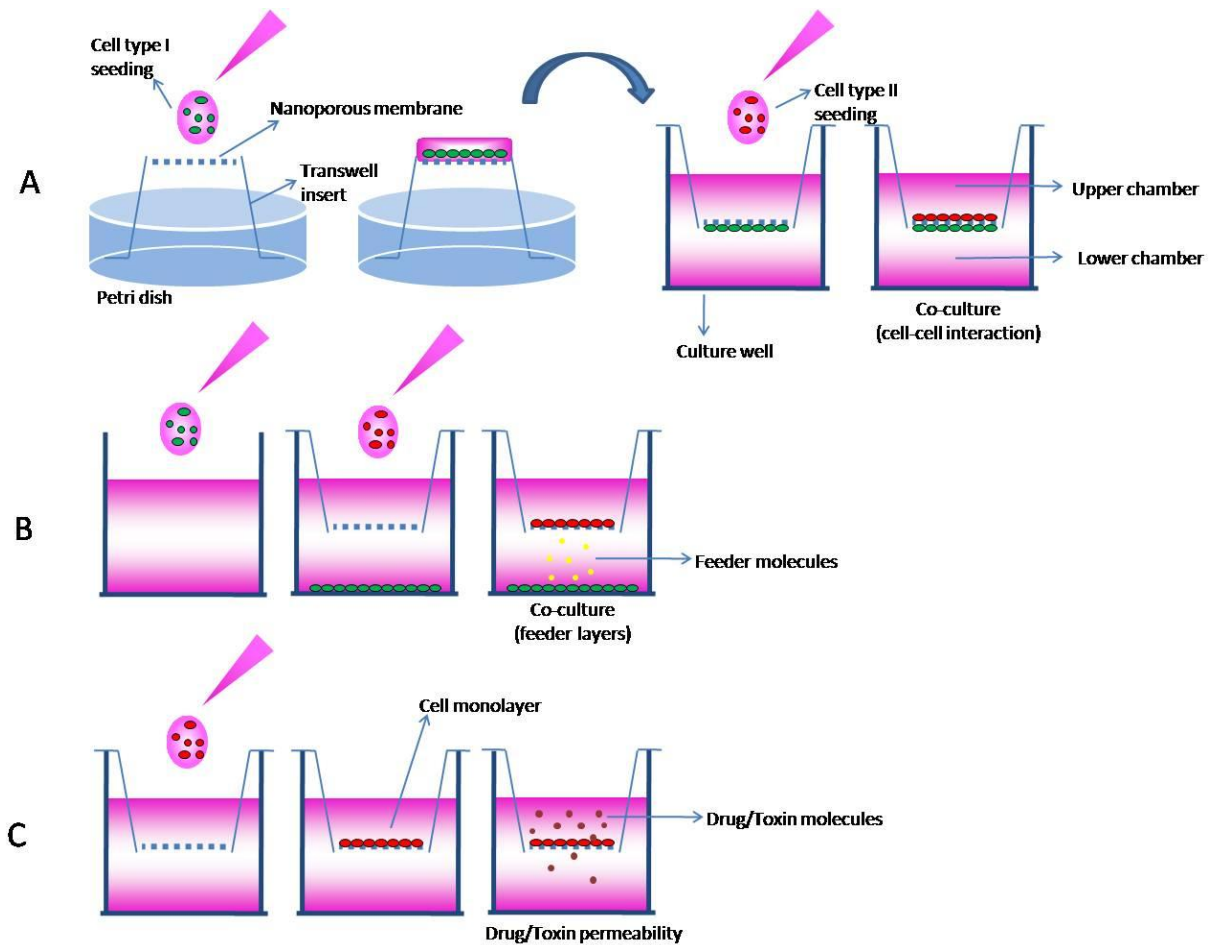
Figure 4.1 Three dimensional cell culture methods: A) cell type I is seeded on bottom side of the membrane of an inverted transwell insert, which is inserted in a 24-well plate after the cells adhere, followed by seeding of cell type II on the other side of membrane, B) cell type I is plated on the bottom of a 24-well plate, followed by seeding of cell type II on the upper side of a membrane insert, C) cells are allowed to form a monolayer after seeding on upper side of a membrane insert, and drug/toxin molecules allowed to permeate across to the bottom chamber of the transwell.

Transwells are used for two major types of cell culture applications. First, the transwell membranes serve as semi-permeable substrates in assays of cell monolayer barrier function. In these applications, cells are grown to confluence on upper side of the transwell membrane (Figure 4.2). The ability of cell monolayers to regulate transport between chambers is determined with electrical resistance measurements or by measuring the flux of small,

115

fluorescent- or radio-labeled molecules. For accurate measurement of barrier function, the membrane filter that separates the two chambers must have significantly less resistance to transport than the confluent cell monolayer [4]. For example, the diffusive permeability of track etched (TE) membranes is limiting for some monolayer permeability studies and in these instances the high permeability of pnc-Si should offer new opportunities. Caco-2 monolayers are routinely used as *in vitro* model for small intestinal villus epithelium because drug transport through properly differentiated Caco-2 monolayers correlates directly with drug adsorption rates *in vivo* [5]. So, pnc-Si has the potential to extend the limits of *in vitro* drug permeability models featuring Caco-2 monolayers. Pnc-Si membranes should also be helpful for *in vitro* studies of vascular permeability. These studies examine the ability of inflammatory signals and leukocytes to regulate the permeability of endothelial monolayers [6]. The high resistance of track-etched membranes severely limits the dynamic range of vascular permeability assay. By extending the dynamic range of these assays by an order-of-magnitude or more, pnc-Si membranes should enable more detailed studies of the kinetics and concentration dependence of inflammatory agents *in vitro*.
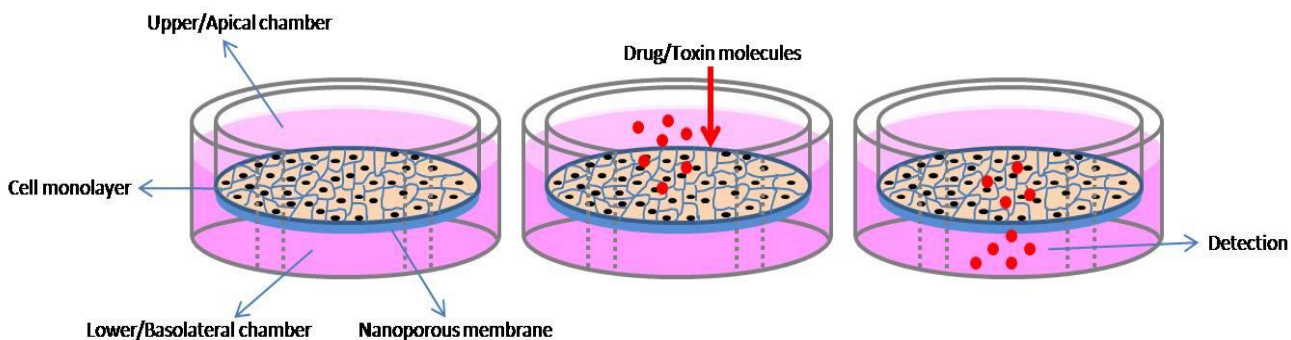

Figure 4.2 Cell monolayer barrier function assay: A confluent cell monolayer is formed on apical side of the nanoporous membrane, across which drug/toxin molecules are allowed to permeate to reach the lower chamber, where they can be detected to examine the cell monolayer barrier function. Influence of inflammatory signals can regulate the permeability of the endothelial monolayers.

In the second application of transwell devices, membrane filters are used to physically separate different cell types in a cellular co-culture. Such arrangements are employed in the study of cell-cell communication, for three-dimensional tissue models and in the creation of bioreactors requiring 'feeder' cells to support the growth of a second cell type [7]. Transwell systems are often used to examine the ability of one cell type to influence the activities of another (Figure 4.3). Such studies occasionally find that cells separated by transwell devices do not display the same signaling known to occur *in vivo*, while cells plated together on the same side of the surface do [1, 2, 8, 9]. An apparent conclusion from such results is that intercellular signaling is mediated by cell-cell contacts. However, this conclusion could be misleading because an alternative possibility is that signaling can be mediated by diffusible factors that are rendered ineffective by the current transwell set-up.

Given that the cell types of interest are typically co-localized *in vivo*, it is reasonable that diffusing molecules responsible for cell-cell communication are produced in small quantities and only effective near cells where concentrations are high. Used as high permeability, ultrathin membranes separating two cell types, pnc-Si membranes appear uniquely suitable for investigations of cell-cell communication mechanisms. For example, the paradox related to transwell experiments involving the suppression of T-cells by T-regulatory cells (T-regs). *In vivo* data has established that T-regs suppress the response of T-cells to immune complexes [10]. The current transwell experiments fail to reconstitute this regulation *in vitro*, whereas, the cell cultures that permit contact between the cell types can [11]. There are many other instances of communication systems between cell types *in vivo* that are modeled by transwell devices *in vitro*. In embryonic development, secreted signaling molecules known as morphogens drive embryonic tissue differentiation, and in neuronal development, endothelial cells are thought to drive the differentiation of neural progenitors using signaling molecules that act at short distances [8].
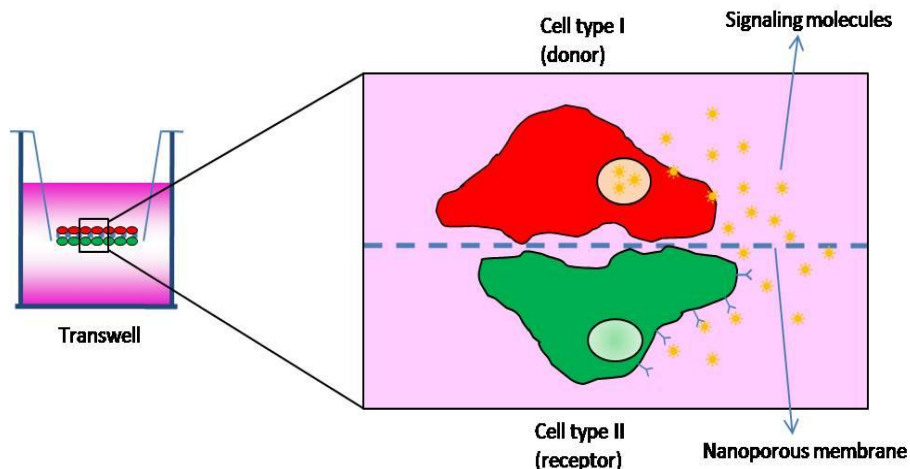
Figure 4.3 Cell to cell communication: Signaling molecules from cell type I reach the receptors on cell type II after diffusing across the nanoporous membrane. The nanoporous membrane separates the two cell types but still allows them to interact through diffusive signaling molecules.

For both classes of transwell experiments, formation of a confluent cell monolayer is imperative. The morphology and physical integrity of cell-cell junctions can be visualized by fluorescent staining of junction proteins. The functional integrity of these monolayers on pnc- Si can then be assessed with trans-epithelial or trans-endothelial electrical resistance (TEER) and albumin transport experiments [12]. TEER measurements are used to rapidly and conveniently track monolayer integrity *via* changes in ion flux resistance as a measure of tight junction integrity [13].

In order to employ pnc-Si in transwell applications, it is important to first examine the stability and biocompatibility of pnc-Si in the transwell format. To test this, studies similar to those in Chapter 2 and 3 were carried out in this chapter. As the first step towards complete characterization of transwell biocompatibility and cell proliferation, we examined HUVEC adhesion with pnc-Si transwells. Maximum stability of treated pnc-Si in three dimensional format was also investigated for long term cell culture applications.

4.2 Material and Methods

4.2.1 Materials

Pnc-Si membranes were supplied by SiMPore Inc., Rochester, NY. SepCon™ polypropylene tubes and rings (Harbec Plastics, Ontario, NY) were purchased. Endothelial Growth Media (EGM) was purchased from Lonza, and Dulbecco's Modified Eagle Medium (DMEM), 0.25% Trypsin-EDTA, Fetal Bovine Serum (FBS), penicillin/streptomycin, glutamine, Liebovitz L-15 media, CellTracker Green 5-chloromethylfluorescein diacetate (CMFDA) and the Live/Dead Viability/Cytotoxicity Kit (Calcein AM and EthD-1) were purchased from Invitrogen (Carlsbad, CA, USA). APTES (3-aminopropyl triethoxy silane) was purchased from Sigma (St. Louis, MO, USA). Methanol (MeOH), ethanol (EtOH), all tissue culture-treated polystyrene (TCPS) plasticware (24-well culture plates, petridishes, and BD Falcon T25/75 tissue culture flasks) were purchased from VWR.

4.2.2 Cell Culture: HUVEC

Cell studies were performed with primary human umbilical vein endothelial cells (HUVEC, Microbiology & Immunology Lab, University of Rochester Medical Center, Rochester, NY, USA). These cells were cultured in 0.1% gelatin coated T25/T75 flasks (BD Falcon) at 37°C in a 5% CO_2, humidified atmosphere. HUVEC were grown in EGM (Lonza) with 2% L-glutamine, 1% penicillin/streptomycin and 10% FBS. Media was changed every other day. Cells were harvested after reaching 70-80% confluence by trypsinization with 0.25% trypsin-EDTA and subsequently seeded at appropriate densities. HUVEC were used between passages 4-8.

4.2.3 Pnc-Si Transwell Assembly

The pnc-Si transwell insert is composed of the bottom half of a SepCon™ and the top flange of a commercial transwell device. Flange from Corning transwell insert was cut using a Dremel tool

and conveniently matched the diameter of the SepCon™. These hybrid SepCon™ transwells fitted perfectly in the 24-well plates. Pnc-Si chips were assembled in the SepCon™ tube using rubber o-ring followed by a plastic retention ring (Figure 4.4). Pnc-Si chip was placed such that the membrane side of the chip was facing down/out. This assembly reduces the frontal exposed surface area of pnc-Si from ~0.33 cm^2 to 0.22 cm^2. The SepCon™ pnc-Si assembly was autoclaved for sterilization, whereas the transwell insert flange was soaked in 70% ethanol for about 20 minutes before being used for cell culture or chemical stability experiments. The flange melts in the high temperature of autoclave, hence was treated differently.
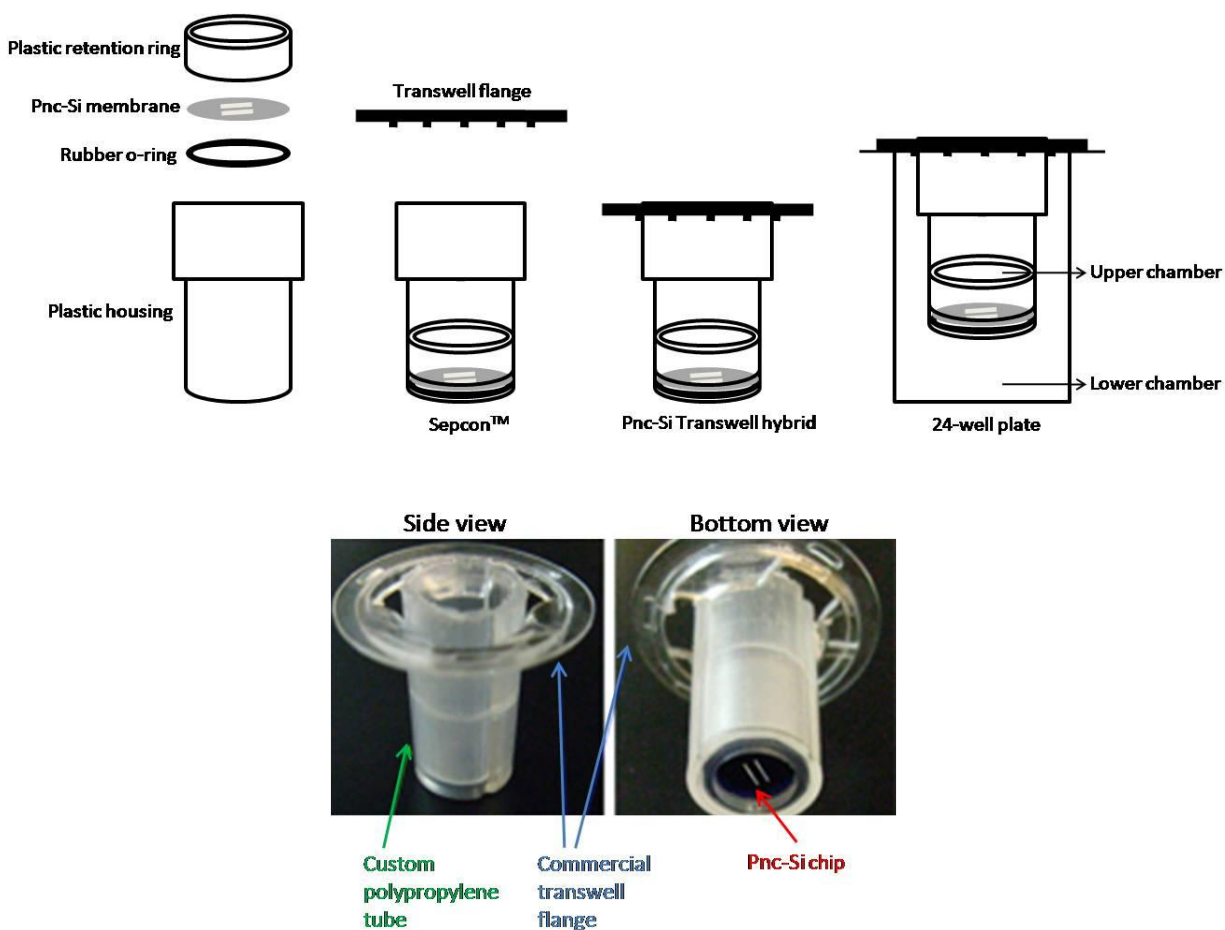

Figure 4.4 Pnc-Si transwell assembly: Pnc-Si membrane chip is assembled in the plastic housing by clamping it in between a rubber o-ring and a plastic retention ring. A transwell flange is attached to the assembled SepCon™ to form the pnc-Si transwell device. (Image courtesy: Barrett J. Nehilla)

4.2.4 Chemical Stability

To monitor discoloration as a measure of chemical stability, pnc-Si tranwells were sterilized and then incubated in serum-supplemented DMEM under cell culture conditions or at 37°C in dry heat oven. Once a day, samples were removed from the media, rinsed in de-ionized H_2O and 70% EtOH, imaged with a Canon PowerShot A650IS 12.1 megapixel digital camera, sterilized in MeOH and returned to culture plates. Pnc-Si chip discoloration was monitored for several days. Care was taken to ensure that there was no air trapped around the pnc-Si chip so that it was completely immersed in media.

4.2.5 Post Production Rapid Thermal Processing

Typically, pnc-Si samples underwent an additional post-production thermal processing step in the Rapid Thermal Processing unit (SSI Solaris 150 Rapid Thermal Processing Unit) to enhance their chemical stability in cell growth media. Samples were placed on a silicon carbide-coated graphite susceptor and exposed to Argon gas. The temperature was increased at 10°C/s to a steady state of 800°C. Samples were maintained at 800°C for 5 minutes, cooled to 25°C and used without further processing.

4.2.6 Liquid-Phase Silanization

Pnc-Si samples were treated in a UV-ozone chamber (Novascan PSD-UVT-UVOP) for 15 minutes at 30°C to clean and decontaminate the surface from any organic matter or impurities. This treatment also renders the surface oxidized before the amino-silane deposition. 5 ml de-ionized H_2O was mixed with 4.8 ml MeOH in a petridish and kept covered. 2 ml of APTES (3-aminopropyltriethoxysilane) was added to this solution followed by 40 µl of glacial acetic acid which helps in hydrolysis. The solution mixture was stirred properly and left covered for 10 minutes. The treated samples were dipped in the solution for 15 minutes. Vacuum grease (silicone) was used to anchor as well as lift the chips from the bottom so that both the sides are

exposed to the amino-silane solution. Samples were taken out and rinsed in de-ionized H_2O followed by running isopropyl alcohol (IPA) through the tweezers. After this they were dipped in pentane for 10 seconds and dried using N_2 gas. They were then left to bake in oven at 75°C for 30 minutes and the amino-silanized samples were ready for use.

4.2.7 Cell Adhesion

HUVEC were seeded on the membrane side of treated and untreated pnc-Si samples assembled in SepCon™ transwell hybrids. For this, the transwell inserts were flipped over to rest on the flanges in a petridish and the cells were seeded onto the exposed pnc-Si surface. After seeding, cells were incubated for 5-6 hours in serum-supplemented media to allow attachment and then stained with CMFDA. In detail, cells were gently rinsed in PBS to remove non-adhered cells, and the media was replaced with 6 µM CMFDA in serum-free media. After 45 minutes at 37°C, the CMFDA solution was replaced with serum-free media, and cells were incubated for another 30 minutes. For imaging, the pnc-Si transwell inserts with cells were flipped back into the 24-well plates containing media. Microscopy was performed with a 10X objective on an epifluorescent Nikon Eclipse TS-100F inverted microscope equipped with Cooke SensiCam cooled CCD camera used to capture images. Microscope control and image acquisition was achieved with customized MATLAB scripts. Cells were counted with a MATLAB script, and the percent adhesion was determined by normalizing the MATLAB-counted cell density to the original seeding density.

4.2.8 Contact Angle Study

Contact angles were measured for non-silanized and silanized samples, with or without incubation in EGM (+ 10%FBS) (serum-supplemented Endothelial growth media). After being silanized, the samples were incubated in media for 25 minutes. They were then rinsed gently with HBSS followed by IPA and left to dry on benchtop. 4 µl of de-ionized H_2O was put on each

surface and imaged carefully keeping the surface horizontal and in same plane as the camera focus. The contact angles were approximately measured using ImageJ.

4.2.9 Cell Morphology and Viability

After cells were seeded on the flipped pnc-Si transwell inserts, they were returned to the incubator in serum-supplemented media to allow proper attachment and spreading. Cells were stained with calcein AM. Growth media was replaced with 2 μM calcein AM and 4 μM EthD-1 in PBS taken in 24-well plates. Cells were stained in this solution for 45 minutes at 25°C and subsequently imaged with the Nikon microscope. After imaging, the transwell inserts with cells were again incubated in 24-well plates containing media. Correspondingly, images were taken at different days to monitor HUVEC viability and morphology.

4.2.10 Cell Counting from Fluorescent Images via MATLAB

For cell culture data, cells were stained and then counted with a custom-designed, MATLAB-based cell counting program (available for public download at *www.nanomembranes.org*). The MATLAB code employed a user-defined fluorescence intensity threshold to mask fluorescent cell images into binary black and white images. The white image objects were then counted as cells only if their areas were within a user-defined range of pixels. To verify the accuracy of the cell counting program, the centroid of each counted white image object (i.e., each "cell") was labeled with an identification number on the original fluorescent images. Any mismatches between the counted centroids and the actual cell centroids were then identified and selected for removal. The final MATLAB output included the total number of cells counted per image.

4.3 Results and Discussion

4.3.1 Chemical Stability and Biodegradation

As discussed before in Chapter 2, pnc-Si was observed to discolor from its native dark blue color to purple-pink to yellow-gold to silver in days-long cell culture experiments. Previous experiments also showed that untreated pnc-Si membranes in two dimensional format discolored in serum-supplemented cell culture media within a day, whereas pnc-Si with a densified surface oxide layer and/or stabilized grain boundaries *via* post production rapid thermal processing discolored after 4 days (Figures 2.1, 2.2).

Interestingly, untreated pnc-Si was found to be more stable in the three dimensional format, lasting for almost a week in typical cell culture conditions that degrade membranes in just a day in the two dimensional format. None of the following hypotheses were found to be true after conducting preliminary experiments:

i) *Hypothesis:* The bulk silicon on 'well' side of pnc-Si chip catalyzes the degradation of the pnc-Si on the 'membrane' side. In the three dimensional format, a separation of these two sides of the chip is provided by the SepCon™ and hence pnc-Si is more stable. To test this, two-slit samples with both intact slits, one intact slit, both broken slits and no slits (blank chip) were used to regulate the passage of the catalytic reaction. It was expected that the sample with no slits would undergo slowest discoloration followed by samples with both intact slits, one intact slit and both broken slits, but no such trend was observed.

ii) *Hypothesis:* The extrinsic stress characteristics of the free standing membrane play a role in its chemical vulnerability. Clamping pnc-Si in a SepCon™ format increases film stresses which in turn increase stability in comparison to a non-clamped flat sample in two dimensional format. To investigate this, samples with different clamping stresses,

such as, samples clamped with thicker o-ring, with no o-ring and with vaccum grease in place of o-ring were used. The results did not show any particular order for discoloration rates with respect to the clamping stresses.

iii) *Hypothesis:* The attacking components from the media adhere to the polypropylene tube or rubber o-ring in the three dimensional format and this prevents their effect on the pnc-Si membrane, keeping it stable for longer. To test this hypothesis, SepCon[TM] and o-ring pieces were incubated in media along with pnc-Si sample in two dimensional format. We observed that the discoloration was still faster in two dimensional format as compared to transwell format.

iv) *Hypothesis:* The edges have an exposed pnc-Si sandwiched between the oxide layers that catalyze the membrane collapse. These edges are unexposed to media in case of three dimensional format. To investigate this, the edges of a pnc-Si chip were coated with 'nail polish' polymer (nitrocellulose in ethyle acetate) to simulate the three dimensional format and compared to actual three dimensional format, but still the discoloration rate in coated chip was found to be faster.

v) *Hypothesis:* Overall less surface area is exposed to biological media in the three dimensional SepCon[TM] arrangement as compared to the two dimensional format (0.22 cm^2 compared to 0.33 cm^2). We analyzed this by coating different areas of pnc-Si chip in two dimensional format with 'nail polish' to reduce the surface area exposed. It was observed that the coated area did not discolor, however the discoloration of exposed area was faster than the sample in three dimensional format.

Maximum Stability of Pnc-Si

Apart from post production rapid thermal processing of pnc-Si, surface treatments like liquid amino-silanization further delayed membrane degradation. Amino-silanization provided a protective amino-silane layer on the pnc-Si surface (Figure 2.12). As in the two dimensional

format, thermal and amino-silane treatments should also enhance the chemical stability of pnc-Si in the three dimensional format. To investigate this, samples underwent RTP and amino-silane treatments and were assembled in three dimensional format before incubating in DMEM. In this long term study, samples were imaged at least once in a week after rinsing in de-ionized water followed by 70% ethanol and then returned to incubator.

As seen in figure 4.5, the untreated samples in two dimensional format discolored first (< 2 days) and then the untreated transwell samples discolored next (< 7 days). After 2 weeks, the APTES-treated samples completely discolored. This showed that APTES alone offered no benefit over RTP. At week 2, the RTP and RTP+APTES samples began to discolor. After 3 weeks, the RTP samples were completely discolored, and the RTP+APTES samples were close behind.
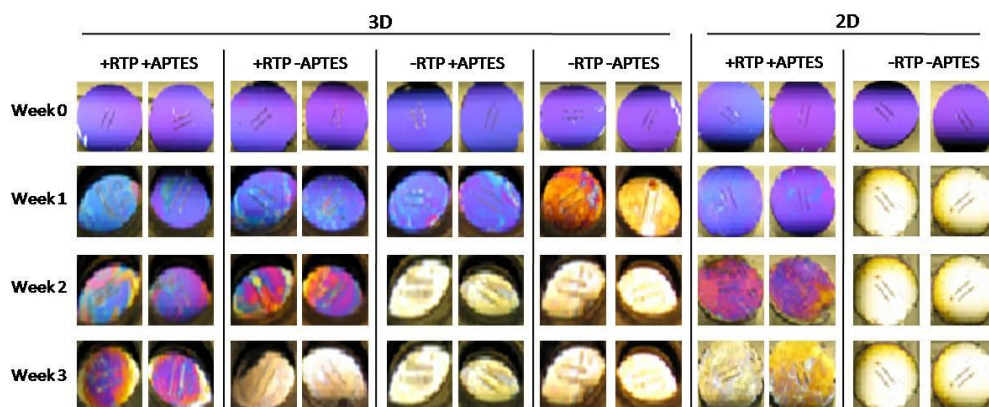

Figure 4.5 Maximum stability of pnc-Si in cell culture conditions. Pnc-Si samples with or without RTP and APTES treatment were autoclaved and incubated in DMEM in transwell as well as two dimensional format. Two samples for each condition were used. RTP+APTES treatment provided maximum passivation with no discoloration until third week (< 3 weeks), whereas non-treated samples in 3D format almost discolored in one week. In 2D format, RTP+APTES provided stability for more than a week (< 2 weeks) and the non-treated samples discolored in less than a week (< 2 days). (Courtesy: Barrett J. Nehilla)

A similar experiment using samples from a different wafer was carried out (Figure 4.6). It was observed that the untreated sample in three dimensional format discolored first (< 7 days) and

the amino-silanized (APTES) sample in the transwell format was completely discolored by second week. Samples that were only treated with amino-silane (< 2 weeks) did not fare as well as samples that were only RTP treated (< 9 weeks). A combination of RTP and APTES worked even better and provided stability over a period of 9 weeks. After 9 weeks of monitoring discoloration, this study was stopped. Additionally, samples that were steam sterilized in autoclave for cell culture use were also more stable. It is known that autoclaving of porous silicon substrates gives rise to increased silicon oxide and also to some Si-OH bonding [14, 15].
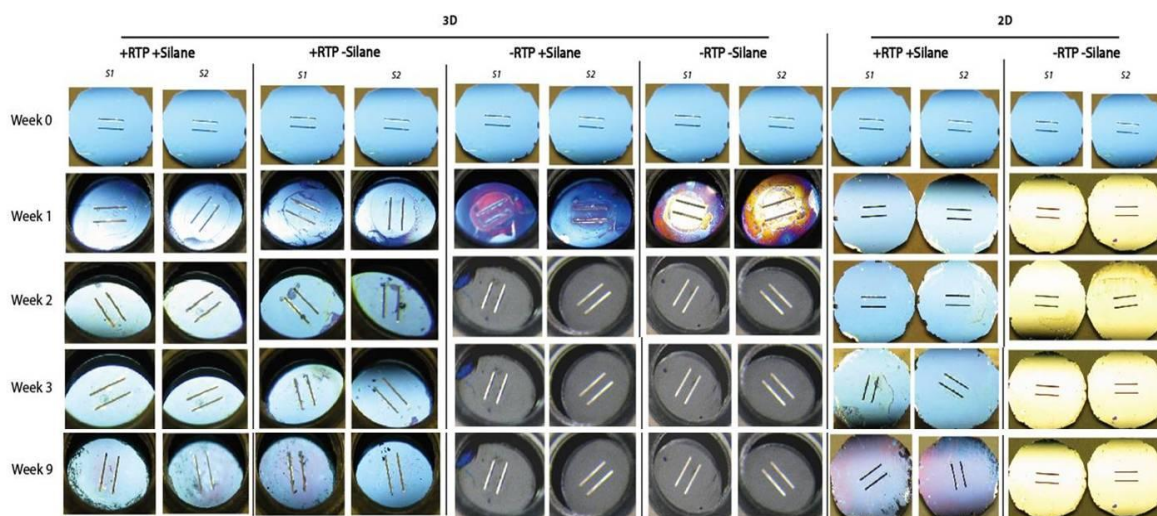

Figure 4.6 Maximum stability test of pnc-Si from a different wafer showed RTP+APTES samples to last for over 9 weeks without discoloring in cell culture conditions. RTP only samples also showed no discoloration until the ninth week, whereas the non-treated samples and APTES only samples discolored within one and two weeks respectively. In two dimensional format, RTP+APTES showed increased stability and started discoloring after 9 weeks.

In combination, pnc-Si samples when assembled in transwell format, after post production rapid thermal processing followed by amino-silanization and autoclaving, did not discolor till 9 weeks in serum-supplemented DMEM under incubator conditions (37°C, pCO_2 ~5%, relative humidity ~90%). Such stability is ideal for long term cell culture applications. The second trial differed from the first experiment. The difference could be due to material variation as the two

experiments were performed using samples from different wafers manufactured over a period when fabrication methods and supplies underwent few alterations. Chemically stable and intact pnc-Si membranes are imperative for membrane-based co-cultures [16] and quantitative studies of cell-cell communication and drug permeability. However, less stable pnc-Si membranes are advantageous as biocompatible and biodegradable scaffolds for tissue engineering or controlled drug delivery applications [17, 18].

4.3.2 Contact Angles and Cell Adhesion

After long term stability was established for pnc-Si transwells with treatments like post production rapid thermal processing and amino-silanization, it was important to see if cells in pnc-Si transwells were as normal as they were in case of the two dimensional format (Figures 3.2-3.6). It is known that anchorage-dependent cells like HUVEC adhere optimally on wettable surfaces like tissue culture polystyrene, polycarbonate and glass, while hydrophobic materials like teflon make inferior culture substrates [19]. Silanization of pnc-Si raised the concern that it would render pnc-Si hydrophobic. While an amino-silane monolayer should be hydrophilic in nature due to its exposed amino-terminal groups, the hydrophobic silane groups might dominate thick or semi-inverted monolayers formed due to liquid-phase silanization [20]. To investigate this, contact angles were measured for both treated and untreated pnc-Si surfaces by placing 40 µl of water on them. The angle between the water surface and pnc-Si surface was estimated from the image taken after keeping the focus in same plane as the surface. We found that, amino-silanization significantly increased the contact angle of pnc-Si from ~37° to ~72°. The contact angles are close to the values found in a recent study comparing liquid-phase and gas-phase amino-silanization of silicon substrates [20]. This hydrophobicity could lead to improper cell adhesion on the amino-silanized pnc-Si. Interestingly, after the treated samples were incubated in biological media for 25 minutes, contact angles again decreased and were similar to the non-treated samples (Figure 4.7). This result likely arose from the adsorption of serum

128

proteins from the media onto the treated surface to passivate the amino-silane layer. Another possibility is that the components of the media reacted with the surface to remove any non-covalently attached silanes.
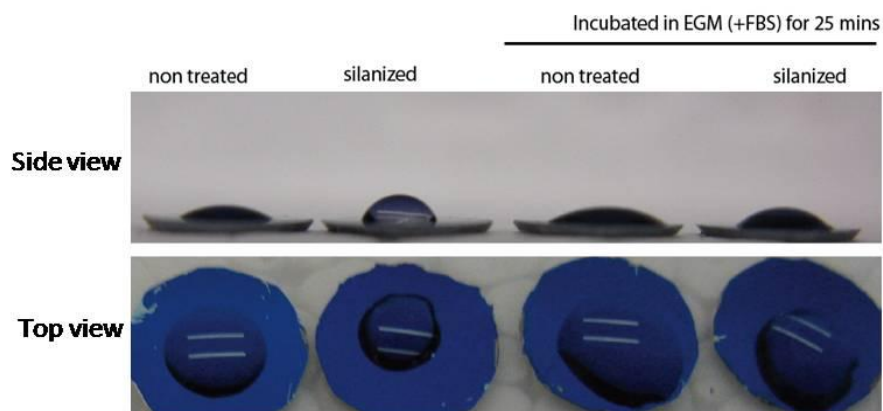
	Non-Silanized	Silanized	Non-Silanized (pre-incubated in media)	Silanized (pre-incubated in media)
Contact Angle	37.5 ± 2.5°	72.5 ± 2.5°	27.5 ± 2.5°	37.5 ± 2.5°

Figure 4.7 Contact angle measurements of treated and non-treated pnc-Si. Images were taken after keeping the focal plane close to the plane of the pnc-Si surface. The contact angle between 40 µl water and pnc-Si surface was estimated using ImageJ. The table gives a range of values of contact angles for the pnc-Si surfaces before and after incubation in biological media. Contact angle of silanized surface was nearly reduced to half after the media incubation.

As the contact angles of amino-silanized pnc-Si were found to be similar to non-treated pnc-Si after pre-incubation in media, cell adhesion was investigated next. To examine this, suspensions of cells were plated on treated as well as non-treated pnc-Si surfaces of inverted transwell inserts (Figure 4.1). The transwells were kept inverted in a petridish because placing the transwell inserts back into the 24-well plate before cell attachment would have allowed cells to fall from the pnc-Si surface to the bottom of the 24-well plate. The cells were allowed to

adhere for 4-5 hours of incubation. After five hours of attachment and spreading, cells were stained with CMFDA and fluorescent imaging was done. During staining and imaging, the transwells were placed back into the 24-well plates containing media. Cells were counted *via* MATLAB-based scripts and cell adhesion values were obtained by normalizing to the original cell seeding density. For pnc-Si, cell counts were acquired from both supported and free-standing pnc-Si membrane areas since the topographical properties of these areas are identical. From the cell adhesion study, we found no significant difference between HUVEC adhesion on pnc-Si and amino-silanized pnc-Si (61.14±7.72% and 54.68±14.44%, respectively. The cell adhesion value for non-treated pnc-Si agrees with the cell adhesion data in two dimensional format reported in Chapter 3. Other studies have shown normal cell attachment after such treatments [21], and additional treatments of pnc-Si with serum or extracellular matrix proteins (like collagen, fibronectin) may further enhance cell adhesion [22] in the future studies. Also, amino-terminal group of silanized pnc-Si surfaces might used in conjunction with functional linker chemistries to regulate cell adhesion.

4.3.3 Cell Morphology

The morphology of anchorage-dependent cells is an indicator of their health and thus the biocompatibility of the substrate environment. To test the ability of cells to spread on pnc-Si in three dimensional format, a cell suspension was plated on non-treated pnc-Si surface of inverted transwell insert. The cells were allowed to adhere and spread for 4-5 hours of incubation after which they were stained with calcein AM and imaged through fluorescence microscopy. During staining and imaging, the transwells were placed back into the 24-well plates containing media. After imaging, the transwells were returned to the incubator for observations at later time points. In this experiment, we found that after 4-5 hours of cell plating, the morphologies of the adhered and stained cells on pnc-Si in transwell format were abnormal (Figure 4.8). The cells exhibited rounded morphology or had plenty of spindle processes.

However, the green fluorescence due to the live stain proved that most cells were viable. It took ~2 days for HUVEC to elicit a normal morphology. On day 4, the spreading and cell density was higher than on day 2, and cells looked ~60% confluent. At this time point, most of the HUVEC exhibited characteristic cobblestone morphology. Since cells exhibit normal morphology within 2 days of cell seeding and proliferate normally, short term morphological abnormalities do not seem to affect overall cell health.

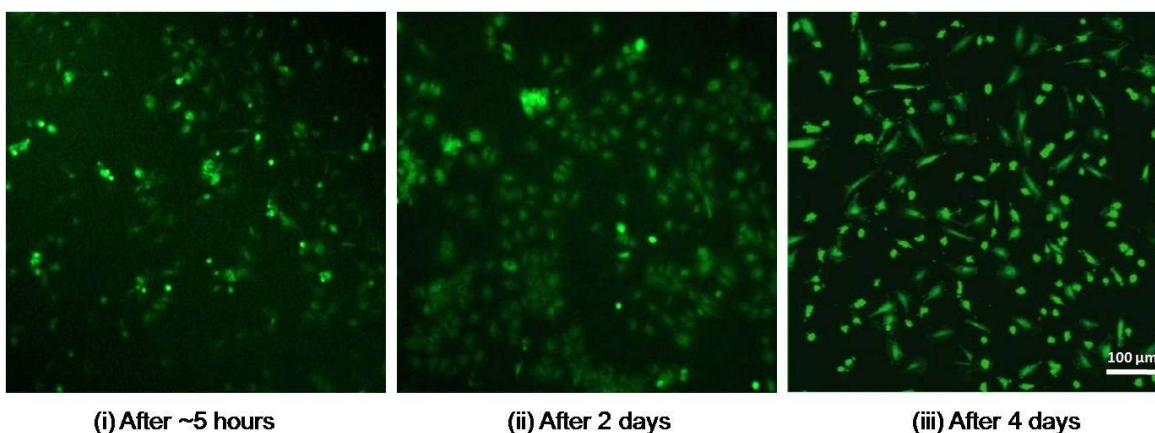(i) After ~5 hours   (ii) After 2 days   (iii) After 4 days

Figure 4.8 HUVEC morphology on pnc-Si in transwell format. Fluorescent images of live stained cells on pnc-Si surface after (i) 5 hours, (ii) 2 days and (iii) 4 days. The cell morphology after 4-5 hours of plating was found to be abnormal, but improved over the course of two days. On day 4, the cells were well spread and exhibited characteristic morphology. The 100 µm scale bar applies to all the images.

Preliminary results showed that 12-13 hours long adhesion assays with inverted transwells resulted in normal morphology. The low volume of media on inverted transwells started evaporating in this time frame and should be replenished. In the future, a longer incubation period in this experiment could confirm whether all the cells subsequently attain normal morphology and proliferate to form a healthy monolayer.

After 4-5 hours of incubation for cell adhesion on a substrate, rounded cell morphology with no projections implies a less favorable surface for cell culture. However, occasionally cells show morphology with spindle processes and rounded shapes immediately after attachment, but they

recover over time to exhibit characteristic morphology. This delay could either take place because of the cells getting accustomed to the substrate topography and surface chemistry or may be the stress induced due to surrounding forces acting on the cells [23]. Since the studies in two dimensional format showed normal HUVEC morphology, pnc-Si topography or surface chemistry is unlikely to cause the delay in morphological recovery in the three dimensional format. Another possible reason for the delay could be the stress induced in the cells because of hanging from the pnc-Si in a transwell format.

HUVEC morphology could also depend on the plating density. It is possible that very high seeding density permitted "normal" cell adhesion but then prevented cells still in suspension from adhering to the surfaces and instead lead to formation of clumps or cell aggregates. Hence, the plating density should be optimized for pnc-Si transwell seeding. The change in substrate properties due to different sterilization techniques could also affect the cell behavior, depending on whether the substrate was autoclaved (steam sterilized) or rinsed in 70% ethanol. Traces of alcohol are bound to hinder cell spreading, whereas autoclaving could render the surface oxidized and make it a favorable surface. It is known that autoclaving of porous silicon substrates gives rise to increased silicon oxide and also to some Si-OH bonding [14, 15]. Another possibility is the deposition of any contaminants from the SepCon[TM] plastic pieces on the pnc-Si surface during autoclaving that could hinder cell spreading. Additionally, change in the pnc-Si material properties over time with varying fabrication conditions and supplies could have affected its biocompatibility to some extent.

4.4 Conclusion

The work in this chapter established that pnc-Si can be used in three dimensional format which makes it applicable in different co-culture and drug permeability experiments. The transwell format changes the configuration of pnc-Si making it possible to directly replace commercially available 24-well inserts in applications. To form pnc-Si transwells, pnc-Si was assembled in a SepCon^{TM} tube by clamping in between a rubber o-ring and a plastic retention ring. The transwell format was found to enhance pnc-Si stability in biological media which was further improved with surface treatments like post production rapid thermal processing and amino-silanization. The transwell format did not seem to hinder HUVEC cell adhesion, but a delay in recovery from abnormal cell morphology was observed. This delay should not affect the overall cell health and lead to formation of a cell monolayer because short term morphological abnormalities can be overcome by increasing the incubation period after cell plating on inverted transwells. After accomplishing nine weeks long chemical stability and biocompatibility, long term cell culture applications should now be possible using pnc-Si in a transwell format.

4.5 References

1. Kornyei, Z., Szlavik, V., Szabo, B., Gocza, E., Czirok, A., and Madarasz, E. (2005). Humoral and contact interactions in astroglia/stem cell co-cultures in the course of glia-induced neurogenesis. Glia *49*, 430-444.

2. Ahn, S.E., Kim, S., Park, K.H., Moon, S.H., Lee, H.J., Kim, G.J., Lee, Y.J., Cha, K.Y., and Chung, H.M. (2006). Primary bone-derived cells induce osteogenic differentiation without exogenous factors in human embryonic stem cells. Biochem Biophys Res Commun *340*, 403-408.

3. Artursson, P., and Karlsson, J. (1991). Correlation between oral drug absorption in humans and apparent drug permeability coefficients in human intestinal epithelial (Caco-2) cells. Biochem Biophys Res Commun *175*, 880-885.

4. Avdeef, A., Artursson, P., Neuhoff, S., Lazorova, L., Grasjo, J., and Tavelin, S. (2005). Caco-2 permeability of weakly basic drugs predicted with the double-sink PAMPA pKa(flux) method. Eur J Pharm Sci *24*, 333-349.

5. Hubatsch, I., Ragnarsson, E.G., and Artursson, P. (2007). Determination of drug permeability and prediction of drug absorption in Caco-2 monolayers. Nat Protoc *2*, 2111-2119.

6. Gautam, N., Hedqvist, P., and Lindbom, L. (1998). Kinetics of leukocyte-induced changes in endothelial barrier function. Br J Pharmacol *125*, 1109-1114.

7. Kim, S., Ahn, S.E., Lee, J.H., Lim, D.S., Kim, K.S., Chung, H.M., and Lee, S.H. (2007). A novel culture technique for human embryonic stem cells using porous membranes. Stem Cells *25*, 2601-2609.

8. Ichijo, H., and Bonhoeffer, F. (1998). Differential withdrawal of retinal axons induced by a secreted factor. J Neurosci *18*, 5008-5018.

9. Schramm, C.A., Reiter, R.S., and Solursh, M. (1994). Role for short-range interactions in the formation of cartilage and muscle masses in transfilter micromass cultures. Dev Biol *163*, 467-479.

10. Sojka, D.K., Huang, Y.H., and Fowell, D.J. (2008). Mechanisms of regulatory T-cell suppression - a diverse arsenal for a moving target. Immunology *124*, 13-22.

11. Pandiyan, P., Zheng, L., Ishihara, S., Reed, J., and Lenardo, M.J. (2007). CD4+CD25+Foxp3+ regulatory T cells induce cytokine deprivation-mediated apoptosis of effector CD4+ T cells. Nat Immunol *8*, 1353-1362.

12. Villasante, A., Pacheco, A., Ruiz, A., Pellicer, A., and Garcia-Velasco, J.A. (2007). Vascular endothelial cadherin regulates vascular permeability: Implications for ovarian hyperstimulation syndrome. J Clin Endocrinol Metab *92*, 314-321.

13. Tavelin, S., Grasjo, J., Taipalensuu, J., Ocklind, G., and Artursson, P. (2002). Applications of epithelial cell culture in studies of drug transport. Methods Mol Biol *188*, 233-272.

14. Bayliss, S.C., Heald, R., Fletcher, D.I., and Buckberry, L.D. (1999). The culture of mammalian cells on nanostructured silicon. Advanced Materials *11*, 318-321.

15. Jay, T., Canham, L.T., Heald, K., Reeves, C.L., and Downing, R. (2000). Autoclaving of porous silicon within a hospital environment: Potential benefits and problems. Physica Status Solidi a-Applied Research *182*, 555-560.

16. Zhang, S.F., Xia, L., Kang, C.H., Xiao, G.F., Ong, S.M., Toh, Y.C., Leo, H.L., van Noort, D., Kan, S.H., Tang, H.H., et al. (2008). Microfabricated silicon nitride membranes for hepatocyte sandwich culture. Biomaterials *29*, 3993-4002.

17. Anglin, E.J., Cheng, L., Freeman, W.R., and Sailor, M.J. (2008). Porous silicon in drug delivery devices and materials. Adv Drug Deliv Rev *60*, 1266-1277.

18. Salonen, J., and Lehto, V.P. (2008). Fabrication and chemical surface modification of mesoporous silicon for biomedical applications. Chemical Engineering Journal *137*, 162-172.

19. Koenig, A.L., Gambillara, V., and Grainger, D.W. (2003). Correlating fibronectin adsorption with endothelial cell adhesion and signaling on polymer substrates. J Biomed Mater Res A *64*, 20-37.

20. Fiorilli, S., Rivolo, P., Descrovi, E., Ricciardi, C., Pasquardini, L., Lunelli, L., Vanzetti, L., Pederzolli, C., Onida, B., and Garrone, E. (2008). Vapor-phase self-assembled monolayers of aminosilane on plasma-activated silicon substrates. Journal of Colloid and Interface Science *321*, 235-241.

21. Low, S.P., Williams, K.A., Canham, L.T., and Voelcker, N.H. (2006). Evaluation of mammalian cell adhesion on surface-modified porous silicon. Biomaterials *27*, 4538-4546.

22. Chin, V., Collins, B.E., Sailor, M.J., and Bhatia, S.N. (2001). Compatibility of primary hepatocytes with oxidized nanoporous silicon. Advanced Materials *13*, 1877.

23. Freshney, R.I. (2000). Culture of animal cells: A Manual of Basic Technique, (New York: Wiley-Liss).

Chapter 5

Conclusion and Future Directions

5.1 Conclusion

This thesis investigates the feasibility of porous nanocrystalline silicon (pnc-Si) as a molecularly thin and highly permeable substrate for cell culture experiments. Pnc-Si is a novel nanoporous membrane material with relatively inexpensive manufacturing and sufficient strength for use in laboratory devices. The work in this thesis has established that cell adhesion and growth on pnc-Si is equivalent to that on tissue culture grade plastic and glass. We also discovered methods to control the biodegradation of pnc-Si in its two dimensional as well as three dimensional formats. Though the two dimensional format showed short term stability, pnc-Si assembled as a transwell device showed optimal stability and biocompatibility for long term cell cultures. Such a viable cell culture substrate will be useful in membrane-based cell biology research, drug delivery and tissue engineering applications. Pnc-Si can be utilized to create improved *in vitro* models of cellular systems that match the *in vivo* dimensions with a degree of control unattainable with current transwell technologies. Enhanced *in vitro* models will enable more accurate pharmacological screening of therapies and permit more relevant investigations in developmental biology and pathology.

Pnc-Si was observed to undergo dissolution in cell culture media similar to porous silicon. Qualitative visual color changes of pnc-Si chip were directly correlated to nanoporous membrane stability and its biodegradation *in vitro* through a microparticle assay. The change in color was hypothesized to occur due to the variation in optical interference of the silicon layers deposited on pnc-Si. As the thickness of the stack depletes, it results in the change in wavelength of the light reflected off its surface. The biodegradation was discovered to be

controllable and non-cytotoxic. The rate of substrate degradation was controlled through post production rapid thermal processing (RTP), which is hypothesized to densify the spontaneously formed native oxide layer or form a superior quality oxide layer and render the surface glass-like. The biodegradation rates of pnc-Si were further slowed down for additional chemical stability by surface treatments like UV-ozone oxidation followed by amino-silanization (APTES).

Pnc-Si membranes were observed to be a viable cell culture substrate in the two dimensional format. Short term cell culture experiments were carried out to assess the biocompatibility of pnc-Si. These short term experiments were possible after post production rapid thermal processing to enhance chemical stability. To test biocompatibility, the adhesion, spreading, growth kinetics and viability of immortalized fibroblasts (3T3-L1) and primary human umbilical vein endothelial cells (HUVEC) were investigated on pnc-Si membranes and compared to glass coverslips and tissue culture grade polystyrene. Pnc-Si performed comparably to these common cell culture substrates in each of these metrics and showed convincing values for cell adhesion percentages and per capita growth rates. However, the two dimensional format is only applicable for limited short term experiments. Fortunately, pnc-Si's silicon planer geometry can be exploited to use it in more desirable formats such as transwells.

Using pnc-Si in transwell formats opens application to co-culture and drug permeability experiments. To form pnc-Si transwell hybrids, pnc-Si was assembled in a SepCon^{TM} tube that can replace commercially available 24-well cell culture inserts. The transwell format enhanced pnc-Si stability in biological media which was further improved with surface treatments like post production rapid thermal processing and amino-silanization. Pnc-Si stability is suitable for long term cell culture applications in the transwell format. The three dimensional configuration and surface treatments did not affect cell adhesion, but the transwell format did increase the time required for HUVECs to obtain normal cell morphology. Cell culture applications are now

possible for longer periods by using pnc-Si in a three dimensional environment rather than two dimensional.

5.2 Future directions

The unique characteristics of pnc-Si predict numerous advantages in studies related to cellular co-cultures, monolayer barrier functions and tissue engineering. As the next step towards being an enabling technology for such applications, the characterization of pnc-Si transwell biocompatibility should be completed by inspecting cell proliferation kinetics. These experiments should be conducted over the time scale of long cell culture research (typically, 6-8 weeks) and compared to commercial transwells. In addition, cells could be cultured on pnc-Si with larger free standing area for better assay sensitivity and visualization.

Further treatments can be carried out to ensure a consistent growth surface providing enhanced cell attachment and maximum yield. Comparisons should be made amongst surfaces coated with extracellular matrix proteins like collagen or fibronectin, which promote cell adhesion and healthy monolayer formation. Terminal silane molecules of amino-silanized pnc-Si can be exploited with carbodiimide linker chemistry to regulate protein adsorption. Surface treatments like thermal carbonization can be incorporated for further increase in pnc-Si stability.

Even though a correlation between the pnc-Si degradation was made with the discoloration of the pnc-Si chip, the exact mechanism of degradation is not fully understood. Recent study in the lab involving ammonium molybdate based colorimetric assay showed that pnc-Si degrades as orthosilicic acid. This degradation resembles the degradation of porous silicon. Moreover, the scope of techniques used to characterize surface chemistry such as ellipsometry, FTIR (Fourier transform infrared) spectroscopy, ICPOES (Inductively coupled plasma optical emission spectrometry) or other optical techniques should be investigated. An observation that was made

138

but not pursued completely was the increased stability of pnc-Si in three dimensional transwell format. Different hypotheses that were rejected should be validated again.

After the above goals are met, work in three dimensional cell culture can be further extended with sophisticated experiments establishing pnc-Si as an enabling technology for cellular co-culture and monolayer studies. In both these classes of experiments, pnc-Si should offer unique advantages of high permeability, sensitivity and low sample loss over current membrane-based culture devices featuring 1000 times thicker membranes.

In a proof of principle experiment, we recently demonstrated the potential of pnc-Si as a co-culture substrate[1*]. In this experiment, different populations of neutrophils (with red and green fluorescent tags respectively) were adhered to opposite sides of the nanoporous membrane and easily imaged *via* fluorescence microscopy (Figure 5.1). The 8 μm difference in focal planes closely matched neutrophil diameters (~8-9 μm), and demonstrated that the "red neutrophils" were separated from the "green neutrophils" by an invisible and ultrathin (15 nm) pnc-Si membrane. Therefore, pnc-Si membranes supported cell co-cultures and facile fluorescent examination.

The ability of pnc-Si to support more physiologically relevant cellular co-cultures should be investigated next. For example, signaling between T-cells and T-regulatory cells in the immune system could be elucidated. Pnc-Si can be used to test the ability of T-regs to suppress T-cell activation *via* soluble factors that diffuse short distances. Other co-cultures that require cells to be in spatial arrangement matching *in vivo* conditions could also be investigated. For example, the human vascular endothelial cell-smooth muscle cell co-culture that emulates *in vivo* vascular

---

* This information is available in a manuscript and at the time of writing the manuscript is ready for submission to Journal of *American Chemical Society - Nano*.
Agrawal, A.A., Nehilla, B.J., Reisig, K.V., Gaborski, T.R., Fang, D.Z., Striemer, C.S., Fauchet, P.M., and McGrath, J.L. (2009). Porous nanocrystalline silicon membranes as highly permeable and molecularly thin substrates for cell culture. ACS Nano (submitted).

architecture or functional brain microvascular endothelial cell-astrocyte co-culture as an *in vitro* model of the blood brain barrier, are possible with pnc-Si.
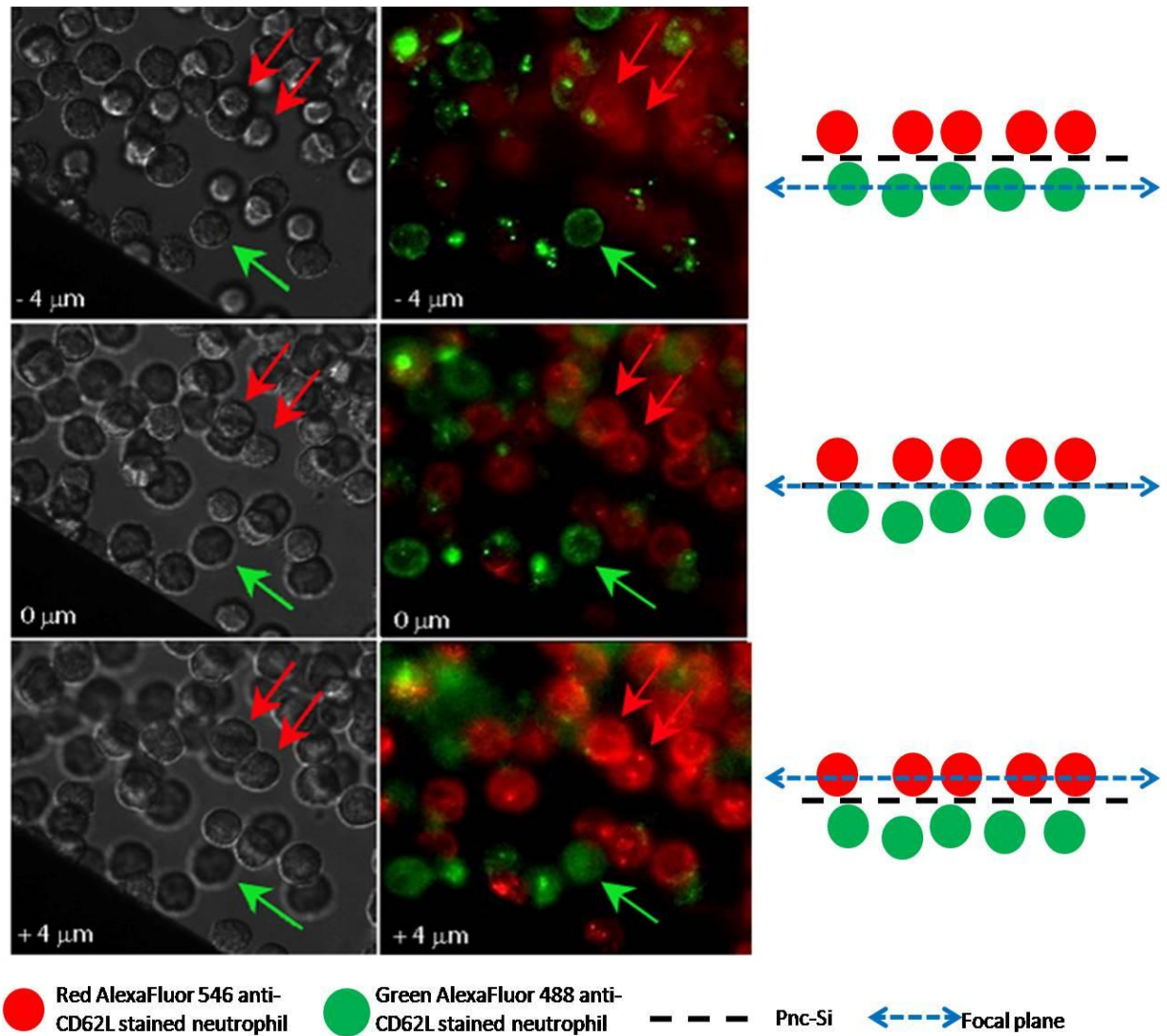

Figure 5.1 Neutrophil co-culture: Ultrathin pnc-Si membranes are suitable for cellular co-culture and transparent for fluorescence microscopy. Two human neutrophil populations were stained with either green AlexaFluor 488 anti-CD62L or red AlexaFluor 546 anti-CD62L. Differential interference contrast (DIC; left panels) and wide-field fluorescent (right panels) images were captured at -4, 0 and +4 μm, where 0 was estimated to be the membrane focal plane. Green cells on the bottom of the membrane are in focus at -4 μm (single green arrow) and red cells on the top of the membrane are in focus at +4 μm (double red arrows). (Image Courtesy: Thomas Gaborski)

Co-culture on ultrathin pnc-Si membrane should help elucidate mechanisms at the level of membrane-protein to membrane-protein interaction between two cell types across its nanopores. Pnc-Si based *in vitro* model system can be applied to tissue engineering as well. The biodegradation of pnc-Si creates an opportunity to construct stratified tissue *in vitro* by culturing different cell types on either side of pnc-Si membranes and allowing the two populations to conjoin and directly interact as the membrane dissolves after several days of co-culture.

As the biocompatibility of pnc-Si is established, it should provide a consistent growth surface with optimal cell attachment and proliferation. The growth of healthy vascular endothelial monolayers with expression of mature cell-cell adhesion complexes and low macromoleculer permeability should be demonstrated on a pnc-Si support. The presence of adheren junctions, tight junctions and gap junctions could be verified by immunofluorescence. Also, endothelial barrier function could be quantitatively monitored with trans-endothelial electrical resistance (TEER) or albumin flux. These parameters should be directly compared to monolayers grown in commercial transwell devices. Further, dose and kinetic responses to inflammatory signals (from drugs like histamine and thrombin) could be measured through the change in endothelial permeability.

The successful completion of the future work along with the foundation of work presented in the thesis will establish pnc-Si as a platform for answering questions that cannot be addressed with current commercial devices.